CHAPTER IV
RESULTS AND DISCUSSION

The results of the study entitled "**Enhancing *In vitro* Propagation Efficiency and Exploring Wound Healing Therapeutic Potential of *Rauvolfia tetraphylla* L.: A Multifaceted Approach**" with results and discussion are presented in this chapter.

4.1. Surface Sterilization of Seeds

The effect of surface sterilization on *R. tetraphylla* seeds using 1% sodium hypochlorite ($NaHCl_3$) and 0.1% mercuric chloride ($HgCl_2$) were investigated. Surface sterilization is a crucial step in seed germination to eliminate any potential contaminants, microorganisms and to ensure successful seed germination.

Seeds were treated with 10 min of $NaHCl_3$ and 1 min of $HgCl_2$, approximately 84.11% of the sterile plantlets were obtained. These results indicated that the surface sterilization process was effective surface microbial contamination. Increased time for 15 mins of $NaHCl_3$ and 2 mins of $HgCl_2$, the percentage of sterile plantlets 91.55% were obtained. Subsequently time increased upto 20 min $NaHCl_3$ and 3 min of $HgCl_2$, results highest percentage of sterile plantlets at 98.44%. Standardized the protocol for sterilization time for different sterilizing agents yielded the most successful sterilization and the production of sterile plantlets from *R. tetraphylla* seeds (Table 1) and subsequent growth, ensuring the production of healthy and viable plants.

Bharti *et al*. (2018) investigated the effectiveness of specific concentrations and durations of $NaHCl_3$ on tomato plants and it established that the maximum survival rates in *in vitro* were achieved using 10% $NaHCl_3$ for 8 minutes on true leaf (77.08%) and epicotyl (66.66%), 10 minutes on hypocotyl (74.30%), and 6 minutes on cotyledon (61.80%). Similarly, Al Ghasheem *et al*. (2018) evaluated the sterilization of peach plants and exhibited the maximum effectiveness at a concentration of 15% $NaHCl_3$ for 5 minutes resulted in a 50% survival rate, while a concentration of 10% $NaHCl_3$ for 10 minutes achieved a higher survival rate of 60%. It emphasizes the critical role of optimizing the concentration and duration of $NaHCl_3$ for successful culturing techniques.

Furthermore, Ramandi *et al*. (2019) investigated the *C. roseus* (L.) and it is emphasized the importance of specific concentrations and durations of $NaHCl_3$ and $HgCl_2$. A combination of

5% $NaHCl_3$ for 10 minutes and 0.3% $HgCl_2$ for 6 minutes resulted in significantly lower contamination percentages (14.66%) compared to the control group (94.66%). Darkazanli and Kiseleva (2021) analysed the impact of different concentrations of $NaHCl_3$ on the germination rate of *Phaseolus vulgaris*, and *Pisum sativum* seeds. At 20% $NaHCl_3$ for 5 minutes produced 100% germination of the seeds.

Neema *et al*. (2022) analysed the surface sterilization of coconut plants and examined different combinations such as $NaHCl_3$, $HgCl_2$, tween-20, and flame sterilization. The optimized combination consisting of 20% $NaHCl_3$ with 250 µL tween for 10 minutes, followed by tap water wash, 0.1% $HgCl_2$ for 3 minutes, 20% $NaHCl_3$ for 5 minutes, and flame sterilization resulted in significantly lower contamination (26.67%). It demonstrated the importance of optimizing the concentration and duration of $NaHCl_3$ and $HgCl_2$ for successful surface sterilization. These specific treatments effectively reduce microbial contamination, increase the percentage of sterile plant materials, and promote successful *in vitro* culture and isolation of endophytic bacteria.

4.2. *In vitro* Seed Germination

To overcome germination hindrance of *R. tetraphylla* seeds is very difficult way of conventional germination techniques. Hence, pretreatment with seed coat were removed at one end of the seed to facilitate the germination. Uncut seeds were used for control. Prior to cutting the seeds endured a cold treatment at 4°C for 2-3 days. The cold-treated, pre-cut seeds were inoculated on MS basal medium without any PGRs. The germination percentage of precut seeds were 83.33% (Table 2) on the 7^{th} day of inoculation. In contrast, the uncut seeds did not germinate due to the presence of the hard seed coat. Figure 1 depicts various stages of *in vitro* seed germination and the development of plantlets.

The cold treatment played a crucial role in breaking seed dormancy and facilitated germination percentage by overcoming the barrier imposed by the hard seed coat. In a similar manner, Hoque *et al*. (2020) studied the *in vitro* seed germination of *R. tetraphylla* and revealed that 78.00% cold-treated pre-cut seeds were germinated on MS basal medium without any PGRs. Interestingly in our study, a higher germination rate of 88.00% was achieved using MS basal

medium without the need for any hormone supplements, comparatively the germination percentage was more than 10% higher than previous research.

Hesami *et al*. (2018) explored germination of *Ficus religiosa* L. seeds and revealed that the maximum seed germination percentage 83.33% was observed when using a one-tenth strength of MS medium under controlled condition. Haruna *et al*. (2024) determined the *in vitro* seed germination of *Vitex doniana* and maximum percentage 87% was obtained when seeds were treated with pre-treatment at 25 - 35℃, which germinated on filter paper. Tanga *et al*. (2024) investigated seed germination of *Saussurea veitchiana* J.R.Drumm. & Hutch in maximum 54% germination were acquired by gibberellic acid (200 μM) at 20℃ pretreatments, it broke the seed dormancy partially and enhance the germination rate.

According to previous research on seed dormancy of *R. tetraphylla* but apparently seed coat hinders the germination and in our study, it was proved that pre-cut seeds had better germination over uncut seeds. Vernalization further improved seed germination leads to development of plantlets.

4.3. Callus Induction of *Rauvolfia tetraphylla*

Explants were collected from *in vitro* seedlings, callus induced from leaf, node, internode, and root explants. All the explants were inoculated on MS medium supplemented with various growth hormones such as IAA, IBA, 2,4-D, BAP, KIN, and combination of these hormones at different concentrations. Untreated control explants produced phenolic compounds at the excised ends and these compounds were not allow cell division leads to the explants ultimately succumbed. However, MS medium supplemented with growth hormone exhibited initial response observed at 7^{th} days of culture, which was characterized by curling and swelling of the explants. Subsequently, after two-weeks callus initiation was observed, explants were characterized by dedifferentiation and multiplication of parenchymatous cells and formation of mass of undifferentiated cells under the controlled conditions. Interestingly, a diverse range of callus induction frequencies was observed across various concentrations (0.5, 1.0, 1.5, 2.0, 2.5 mg/L) of PGRs. After callus induction, calli were subcultured within 20-28 days of interval on the fresh media for further proliferation. Various explants had different stages of development and hence their response to growth regulators was varied.

4.3.1. Development of Callus from Leaf Explants of *Rauvolfia tetraphylla*

Development of callus from the leaves of *R. tetraphylla* were obtained presents in (Table 3: Fig. 2). When IAA was applied at concentrations gradually increased from 0.5 to 2.5 mg/L, for callus development. In lowest concentration (0.5 mg/L), 22% callus formation but in the highest concentration (2.5 mg/L) 51% callus formation were observed. Correspondingly, IBA promoted callus formation in leaf explants, percentage of callus formation ranged from 19% to 41%. In the case of 2,4-D, callus formation in leaf explants displayed a steady increase as the concentration increased, 34% callus formation was observed from 0.5 mg/L while 2.5 mg/L resulted in 67% callus formation. BAP induced callus formation was relatively higher compared to other hormones, with percentages ranging from 25% (0.5 mg/L) to 58% (2.5 mg/L).

The combined application of hormones, such as IAA+IBA, IAA+2,4-D, IAA+BAP, IBA+2,4-D, and 2,4-D+BAP, influenced callus formation from leaf explants and enhanced callus induction compared to individual hormones. The maximum callus formation of 88% was observed on MS medium with 2,4-D+BAP (2.5 mg/L each). Specific hormone combinations and concentrations significantly influenced the callus formation in leaf explants of *R. tetraphylla*. Related to our study, Nabi *et al*. (2018) analysed leaf explants of *Spilanthes acmella* L. on MS medium with 2,4-D (1.5 mg/L) and BAP (0.5 mg/L) induced a maximum callus formation of 70%, resulting in dark green and fragile callus formation. In this study, the maximum callus induction was observed on MS medium with 2,4-D + BAP (2.5 mg/L).

Correspondingly, Copeland *et al*. (2020) investigated callus formation in leaf explants of *Crinum americanum* L. The formation of callus was initiated on 10^{th} day. The highest callogenesis rate 71.67% were observed on MS medium augmented with 2,4-D (2.5 mg/L) and BAP (10 mg/L). The effectiveness of 2,4-D as an auxin in stimulating and improving callogenesis *in vitro* is well-established. Similarly, 2,4-D (2.5 mg/L) on callogenesis in leaf explants of *R. tetraphylla*, observed highest percentage 67.22% of callus development on MS medium.

Nurwahyuni *et al*. (2020) evaluated the callus culture of *Styrax benzoin* Dryand and maximum 76.25% callus formation was achieved in young leaf explants on MS medium with BAP and NAA (3 mg/L). Dar *et al*. (2021) analysed callus formation in leaf explants of *Atropa acuminata* Royle ex Lindl. using three different combinations of phytohormones: MS media +

BAP + NAA, MS media + Kn + 2,4-D, and MS + 2,4-D + NAA. All three combinations resulted in callus formation, with maximum callus induction obtained in BAP +NAA (1 mg/L each). Furthermore, Yeasmin *et al*. (2022) established callus induction in leaf explants of strawberry, with the maximum callus formation 77.1% obtained on MS medium fortified with BAP (2.0 mg/L) + IBA (0.5 mg/L).

4.3.2. Development of Callus from Nodal Explants of *Rauvolfia tetraphylla*

The table 3 depicts the percentage (%) of callus induction observed in nodal explants of *R. tetraphylla* when treated with different PGRs at various concentrations. The results (Fig. 3) demonstrated the effect of PGRs on development of callus in nodal explants.

When IAA was applied callus formation in nodal ex plants showed an increase, at the lowest concentration (0.5 mg/L) 11.37%, while the highest concentration (2.5 mg/L) 23.44% callus formation was obtained. Similarly, IBA showed callus formation ranged from 8.44% to 26.58%. In the case of 2,4-D alone produced callus in nodal explants displayed a gradual increase as the concentrations from 0.5 mg/L (22.40%) callus to 2.5 mg/L (46.55%). BAP influenced callus formation and percentages ranged from 26.55% to 55.51%.

When different hormone combinations were applied, such as IAA+IBA, IAA+2,4-D, IAA+BAP, IBA+2,4-D, and 2,4-D+BAP exhibited varying effects on callus formation in nodal explants. These combinations generally enhanced callus induction compared to individual hormone treatments. The highest callus formation of 83.45% were obtained from node explants on MS medium with 2,4-D+BAP (2.5 mg/L each). Wani *et al*. (2018) examined the effect of callus induction of *Lavatera cashmeriana* Camb. on different PGRs and showed 100% callus regeneration on leaves, while nodes exhibited an 86.5% callus regeneration rate on MS medium with 2,4-D (2.0 mg/L). Auxins proved to be the most effective in inducing development of callus. In this study, MS medium with 2,4-D (2.5 mg/L) resulted in a callus formation percentage of 46.55% in the nodes of *R. tetraphylla*.

Nurokhman *et al*. (2020) analysed the impact of PGRs on leaf, internode, node, and petiole explants of *Gynura procumbens* (Lour.) Merr. at different concentrations on MS medium with 2,4-D (0.1 mg/L) + BAP (0.1 mg/L), 2,4-D (0.5 mg/L) + Kinetin (1.0 mg/L), NAA (0.5 mg/L) + BAP (0.5 mg/L), 2,4-D (5.0 mg/L) + BAP (0.5 mg/L), and 2,4-D (0.1 mg/L) + IAA (0.1 mg/L). Among these concentrations maximum callus induction was observed on MS medium

with 2,4-D (0.1 mg/L) + BAP (0.1 mg/L) in leaf explants. The combination of 2,4-D + BAP (0.1 mg/L) resulted in high callus fresh weight, and all explants successfully formed callus. The combination of 2,4-D and BAP demonstrated significant effectiveness as growth regulators in *R. tetraphylla* and exerted a remarkable influence.

4.3.3. Development of Callus in Internode Explants of *Rauvolfia tetraphylla*

The results established a detailed relationship between the specific hormone concentrations and the formation of callus in internode explant (Table 3; Fig. 4). The hormone IAA has a distinct effect on callus formation, with increasing callus formation ranging from 5.51% to 28.08%. This concentration-dependent effect suggests that higher levels of IAA promote a more robust callus formation response. The hormone IBA exhibited a positive correlation with callus formation from 3.94% to 30.16%. It highlights the importance of IBA concentration in stimulating callus formation in internode explant. 2,4-D demonstrated a callus formation from 43.44% to 65.14%, indicating a strong positive response between 2,4-D concentration and callus formation. Correspondingly, the hormone BAP showed a concentration-dependent effect on callus formation from 38.46% to 62.40%, underlining the role of BAP concentration in promoting callus formation.

When these hormones were combined, the results were intriguing. Combinations of 2,4-D + BAP (2.5+2.5 mg/L) exhibited significant synergistic effects, resulting in a remarkable callus formation percentage of 79.66%. These results emphasized the complexity of hormone interactions and their collective influence on callus formation.

The factors influencing callogenesis from *F. religiosa* L. and investigated the effects of the interaction of these factors with PGRs (2,4-D, BAP, IBA, NAA) on callogenesis across various explant (leaf, petiole, root, internode) (Hesami *et al*. 2018). It revealed that a combination of 2,4-D (0.5 mg/L) and BAP (0.05 mg/L) consistently promoted the maximum callus across all explants, highlighting the importance of PGRs concentrations in callogenesis. In the research by Nurokhman *et al*. (2019) analysed the callus induction from *G. procumbens* (Lour.) Merr, at various combinations (2,4-D, IAA, NAA, BAP, KIN) of PGRs to determine their impact on callus formation. The combination of NAA + BAP (0.5 mg/L) on MS medium showed

highest callus development (100%) in petiole and provides valuable guidance for optimizing the callus induction process.

Asmono (2020) assessed the growth response of internode and leaf explants from *Stevia rebaudiana* Bertoni under varying concentrations of BAP (2, 3, and 4 ppm). It revealed that both leaf and internode explants exhibited a remarkable percentage for callus formation (100%). The synergy between 2,4-D and BAP proved highly effective growth regulators in the internode of *R. tetraphylla*, enhancing the percentage of callus formation in comparison to alternative combinations. The detailed analysis of hormone concentrations and their effects on callus formation in internode tissues offers valuable insights into the plant propagation.

4.3.4. Development of Callus from Root Explants of *Rauvolfia tetraphylla*

Development of callus observed in root explants of *R. tetraphylla* when treated with different PGRs at varying concentrations showed in table 3. It shed light on the impact of these hormones on callus induction in root explants (Fig. 5). When IAA was treated the percentage of callus formation in root explants showed an increasing trend from 2.40% to 16.55%. Similarly, IBA showed percentage of callus formation ranged from 1.45% to 15.58%. In the case of 2,4-D alone responsible for increase as the concentration increased from 13.44% to 22.41% callus formation. The hormone BAP showed a significant effect on callus formation ranged from 27.58% to 51.41%.

When different hormone combinations were treated, such as IAA+IBA, IAA+2,4-D, IAA+BAP, IBA+2,4-D, and 2,4-D+BAP, it demonstrated varying effects on callus formation in root explants and these combinations enhanced callus induction compared to individual hormone. Luciani *et al.* (2006) evaluated callus formation in garlic plants and maximum callus induction was obtained on MS medium with 0.045 µM 2,4-D + BAP from basal plates (41%). Meanwhile, meristems, root-tips, and immature umbels showed 57%, 56%, and 20% of callus induction, respectively, when exposed to 0.45 µM 2,4-D on MS medium. In our study, a maximum 84.11% of callus from root explants of *R. tetraphylla* on MS medium with 2,4-D + BAP (2.5 mg/L each) was achieved. Application of specific PGRs and their combinations at different concentrations significantly influenced the callus formation in root explants of *R. tetraphylla*.

Dar *et al*. (2021) determined callus induction from root explants of *A. acuminata* Royle ex Lindl. at various combinations of PGRs (BAP, NAA, Kn, and 2,4-D) on MS medium. The maximum (100%) callus development from root explants was achieved on MS medium with BAP (0.5 mg/L) + NAA (1.0 mg/L). In the same way, Basiri *et al*. (2022) analysed *Eremurus spectabilis* M. Bieb of tuberous root explants and the maximum callus induction 76.67% were achieved on MS medium supplemented with BAP (10.0 mg/L). Similarly, *R. tetraphylla* root exhibited a callus formation of 51.41% when cultured on MS medium supplemented with BAP (2.5 mg/L).

4.4. Organogenesis

a. Rhizogenesis from Leaf Explants

Effect of different PGRs for the formation of direct root in leaf explants of *R. tetraphylla* using hormones such as IAA and a combination of 2,4-D, BAP and IBA at a concentration of 0.5 mg/L, 1.0 mg/L, and 1.5 mg/L were evaluated (Table 4 and Fig. 6). In IAA, leaf explants exhibited direct root formation ranged from 3.44% (0.5 mg/L) to 16.55% (1.5 mg/L). Whereas the combination of 2,4-D + BAP, three concentrations were tested such as 2,4-D (0.5 mg/L) + BAP (0.5 mg/L), 2,4-D (1.0 mg/L) + BAP (0.5 mg/L) and 2,4-D (1.5 mg/L) + BAP (0.5 mg/L), showed 13.44% to 26.55%. According to the increasing concentration of PGRs influenced direct root formation.

The various concentration of IAA + BAP showed 37.44%, 62.58%, 87.50% root induction on MS medium with IAA (0.5 mg/L) + BAP (0.5 mg/L), IAA (1.0 mg/L) + BAP (0.5 mg/L), and IAA (1.5 mg/L) + BAP (0.5 mg/L) respectively. The combination of IBA + BAP was also assessed, and root formation ranged from 13.16% to 35.50% on MS medium at three different concentrations of PGRs. It demonstrated that different concentrations of PGRs significantly influenced direct root formation in leaf explants of *R. tetraphylla*.

Pandey *et al*. (2010) analysed the leaf explant of *R. serpentina* (L.), root growth was observed on MS medium at different combinations of auxins and revealed that the best combination for inducing roots in *R. serpentina* leaf explant on MS basal media supplemented with para-amino benzoic acid (PABA) (1 mg/L) + NAA (4 mg/L). However, when the same combination of PABA + NAA and IBA + NAA was used in liquid MS media, poor regeneration

results were observed, with smaller numbers of roots. In our study, the maximum percentage (87%) of root formation in leaf explants of *R. tetraphylla* was obtained on MS medium with IAA + BAP.

b. Rhizogenesis from Nodal Explants

The impact of various PGRs on rhizogenesis from nodal explants of *R. tetraphylla* were analysed using IAA, 2,4-D + BAP, and IBA + BAP on MS medium (Table 4; Fig. 7). Increasing concentrations of auxin produced gradually increased percentage of root formation were observed in nodal explants. In IAA showed 2.5% to 37% whereas combination of 2,4-D + BAP had a significant impact on direct root formation, at 0.5 mg/L (2,4-D + BAP) showed 33% and 1.5 mg/L 2,4-D + 0.5 mg/L BAP further enhanced the effect, resulting in 62% direct root formation.

The combination of IBA + BAP observed direct root formation, at 0.5 mg/L IBA +0.5 mg/L BAP showed 32% of direct root formation and increased concentration produced 47% and 63% at 1.0 mg/L IBA + 0.5 mg/L BAP, and 1.5 mg/L IBA + 0.5 mg/L BAP, respectively. Rout (2006) analysed root formation from nodal explant of *Camellia sinensis var.* TV-20 with different concentrations of IAA, NAA and IBA and observed that IBA exhibited maximum root formation compared to IAA and NAA. Furthermore, in our study, a combination of IBA + BAP (2.5 mL) each demonstrated 63.16% root formation in nodal explants.

Interestingly, the combination of IAA + BAP showed positive effect of 0.5 mg/L (IAA + BAP) from nodal explants revealed 24% and a maximum of 83.16% of direct root formation at 1.5 mg/L IAA + 0.5 mg/L BAP. It demonstrated that different PGRs and their combinations had a significant impact on direct root formation in nodal explants of *R. tetraphylla*.

4.5. Caulogenesis and Multiple Shoot Formation

Effect of PGRs on direct shoot and multiple shoot formation from nodal explant of *R. tetraphylla* using BAP with 2,4-D, IAA, and KIN respectively (Table 5). Results revealed that increasing concentrations of BAP had a significant impact on both direct shooting and multiple shoot formation (Fig. 8 & 9). At a 0.5 mg/L BAP showed direct shooting formation ranged from 25% to 58. Similarly, for multiple shoot formation, the percentage increased from 21% (0.5 mg/L) to 55% (1.5 mg/L). The combination of 2,4-D + BAP also showed a positive effect on

direct shooting and multiple shoot formation. At 0.5 mg/L (2,4-D + BAP) exhibited 42% of direct shooting, which increased to 78% (1.5 mg/L). Similarly, the percentage of multiple shoot formation revealed 41% at 0.5 mg/L (2,4-D+BAP), 56% at 1.0 mg/L, and 73% at 1.5 mg/L.

The combination of IAA + BAP demonstrated positive results at 0.5 mg/L (IAA + BAP) exhibited 46% of direct shooting, which increased to 67% and 83% at concentrations of 1.0 mg/L and 1.5 mg/L, respectively. For multiple shoot formation, the percentages were 55% at 0.5 mg/L IAA+BAP, 72% at 1.0 mg/L, and 88% at 1.5 mg/L. Lastly, the combination of KIN + BAP also showed an optimistic effect on 0.5 mg/L KIN + BAP exhibited 38% of direct shooting, which increased to 54% and 75% at 1.0 mg/L and 1.5 mg/L, respectively. Similarly, multiple shoot formation showed 43% at 0.5 mg/L KIN+BAP, 61% at 1.0 mg/L, and 76% at 1.5 mg/L.

Verma *et al*. (2009) evaluated the regeneration response of cotyledonary node explants obtained from germinating seeds of peanut (*Arachis hypogaea* L.). When BAP (1 to 50 mg/L) was supplemented on MS medium, multiple shoots were observed to emerge. Among the various concentrations tested, maximum multiple shoot formation was observed at 15 mg/L in peanut varieties. The previous research resembles with our study in 15 mg/L of BAP on MS basal medium in peanut varieties, whereas in *R. tetraphylla* observed very minimum concentration of 1.5 mg/L on MS basal medium from the nodal explants.

Jin *et al*. (2014) analysed *in vitro* regeneration in nodal explant of *Pogostemon cablin* Benth. and explored the effects of PGRs on shoot proliferation and root formation. The maximum shoot formation (129.7–138.1 shoots per explant) was observed on MS medium with BAP (0.1–0.2 mg/L) and rooting of the regenerated shoots was achieved using half-strength MS medium with IBA (0.2 mg/L). Xhulaj and Doriana (2019) evaluated the multiple shoot regeneration of *Triticum aestivum* L. from mature embryos without the formation of callus using different PGRs such as 2,4-D, IBA, NAA, and BAP. The maximum direct shoot regeneration (2.5 shoots per explant) was observed on MS medium with BAP (2 mg/L) + 2,4-D (0.6 mg/L). In this study, *R. tetraphylla* showed the maximum direct shoot (78.44%) and multiple shoot induction (73.44%) was obtained on MS medium combined with BAP+2,4-D (1.5 mg/L each).

4.6. Somatic Embryogenesis

The impact of PGRs on somatic embryogenesis of *R. tetraphylla*, leaf and root explants were cultured on MS medium with different growth regulators. Preliminary experiments

identified 2,4-D and BAP (Fig. 10) as the most effective auxin and cytokinin at an optimal concentration of 2.5 mg/L. Based on this analysis, further experiments were focusing on leaf and root explants, and they were transferred to combination of MS medium containing different concentrations of 2,4-D and BAP (0.5 to 1.5 mg/L).

After a 4-week culture period, the leaf and root explants demonstrated the formation of globular stage embryos (Fig. 11). It indicated that the highest embryogenesis was observed on MS medium with BAP+2,4-D (1.5 mg/L). It suggested that these two plant hormones are conducive for the development of somatic embryos through direct somatic embryogenesis. Gerdakaneh and Mozaffari (2021) achieved plant regeneration through direct somatic embryogenesis in strawberry (Fragaria x ananassa Duch.) leaf blades on MS medium supplemented with Thidiazuron (TDZ) at concentrations of 1, 2, 3, and 4 mg/L, both alone and in combination with different concentrations (0, 0.25, 0.5, and 1 mg/L) of 2,4-D. The maximum somatic embryo was obtained on MS medium containing TDZ (3 mg/L) and 2,4-D, (0.25 mg/L) which resulted in the highest induction of embryogenesis.

Bhusare *et al*. (2020) analysed somatic embryogenesis in *Digitalis lanata* Ehrh., using different PGRs at different concentrations on a MS basal medium. Maximum somatic embryogenesis in leaf (100%) and root (85.7%) were obtained on MS medium with KIN + IBA (2.0 mg/L each). Chambhare and Nikam (2022) explored the effects of PGRs (BAP, kinetin, IAA, NAA, 2,4-D) on the induction of direct somatic embryogenesis in leaf explant of *Guizotia abyssinica* (L.f.) Cass. It revealed that MS medium with BAP (1.0 mg/L) along with IAA (0.5 mg/L) observed the maximum somatic embryogenesis. In this present study, both 2,4-D and BAP exhibited the favourable induction for somatic embryogenesis in *R. tetraphylla*.

4.7. Histology of Somatic Embryogenesis

Cell division occurs in the callus of both leaf and root explants are clearly defined by histological analysis. *R. tetraphylla* is a dicot plant and its cell division occurs through the process of eukaryotic cell division. Initially, rigid plant cells with distinct organelles such as the nucleus, nucleolar membrane and cytoplasm are formed (Fig. 12a). This sets the stage for the mitotic division during the interphase (Fig. 12b), a stage where cells are prepared for division. The subsequent phases include early and late prophase (Fig. 12c-d), characterized by the

replication of the cell nucleus. In metaphase, the nucleus disintegrates, and the cells chromosomes compact and align at the cells centre (Fig. 12e). During both early and late anaphase (Fig. 12f), the nucleus undergoes division. Finally, in the telophase (Fig. 12g) two distinct nucleus envelopes are formed. In cytokinesis, cell plate formed in the middle of the cell and divides into two daughter cells (Fig. 12h). This undifferentiated mass of cells contributes to the totipotency of *R. tetraphylla*, allowing it to potentially develop into various cell types and exhibit a wide range of differentiation capabilities. Callus cells exhibit pluripotency and totipotency under suitable *in vitro* conditions contributing to the understanding of cell differentiation. In subsequent *in vitro* stages in *R. tetraphylla*, different morphogenesis pathways emerge such as organogenesis (shoot and root development) and somatic embryogenesis (somatic embryo formation). These pathways eventually lead to the regeneration of complete plants in favourable *in vitro* conditions and a process known as *in vitro* plant regeneration (Kruglova *et al*., 2023).

Somatic embryogenesis in *R. tetraphylla* observed four weeks of culturing explants on a callus induction medium, somatic embryo (re-differentiated) development started at the outer edges of proliferated calli, while non-embryonic cells (parenchymatous cells) were found in the inner regions (Fig. 13a). Embryogenic cells at the outer layer were small, isodiametric with dense cytoplasm and a central nucleus while non-embryogenic cells were larger, vacuolated and had nuclei near the cell wall which have no specific structure formation was perceived (Sakr & Sayed, 2018).

Maturation stage of nodular structures of embryo development were observed in *R. tetraphylla*. Somatic embryo differentiation began with smaller meristematic cells in the primary tissue, characterized by dense cytoplasm and large, round, stained nuclei. Additionally, organized cell divisions led to the presence of a protodermis around the globular embryo (Fig. 13b). In the nodular calli, areas with high mitotic activity and isodiametric cells with prominent nuclei were observed. The initiation of pro-embryogenesis was linked to the presence of nodular calli, leading to the formation of induced pro-embryogenic masses (PEMs). Globular somatic embryos (gSEs) arising from PEMs showed radial development, with differentiation of primary meristematic tissues including the fundamental meristems and suspensor (Fig. 13c). Subsequent embryogenic stages saw a reduction in suspensor mass. During the development of embryogenic

calli (EC), the transition from globular to torpedo-shaped embryos occurred gradually, featuring a distinct polar structure (Fig. 13d-f). In longitudinal sections of embryos at the early differentiation stage, vascular tissue (vt) (Fig. 13g), root primordia (rp) (Fig. 13h-i) and shoot primordia (sp) (Fig. 13j-k) were clearly visible. Similarly, Panggabean *et al*. (2022) found that embryogenic callus retains its nodular structure due to active meristematic cell division. Sample preparation involved dehydration, FAA fixation, paraffin infusion and staining with safranin dye. *Elaeis guineensis* Jacq. somatic embryos progress through three phases, with globular-phase embryos exceeding 200 µm. They develop epidermal tissue from the protoderm, originating through a periclinal cleavage during the proembryonic-to-globular transition. This multiplication method supports the proliferation of the original cell mass, giving rise to new calli lineages, especially the embryogenic yellowish nodular lineage, from which somatic embryos develop.

Increased endogenous sugars are observed in somatic embryos of leaf and root explants of *R. tetraphylla*. The histological analysis of leaf and root (Fig. 14 a&b) showed higher starch accumulation were also mainly located in superficial cells, belonging to calli and neo-formed meristems. Clusters of dividing cells displayed starch deposits. These sugars protect cell membranes and proteins during dehydration and freezing by replacing water in the hydrate state. The interaction of endogenous sucrose with intracellular water can increase non-freezable water content (Bradaï *et al*. 2023).

4.8. Hardening

In vitro plantlets were transferred for hardening and evaluated visually based on their appearance. The regenerated plantlets of *R. tetraphylla* was hardened in a plastic cup by 1:2 ratio of sterile garden soil and sterilized vermiculite (Fig. 7h). Interestingly, Hussain (2021), analysed *R. tetraphylla* shoot tip explants in which *in vitro* plantlets were hardened under controlled conditions. *R. serpentina* (L.) Benth nodal explants were regenerated into *in vitro* plantlets and hardened using Sand, Soil, and FYM (1:1:1) in net house (Tripathi *et al.* 2022). Mahadik et al. (2020) determined hardening in *R. serpentina* through *in vitro* regenerated plantlets using soil, sand, and vermiculite; 1:1:1 under controlled conditions. Although the traits of *R. tetraphylla* were not quantitatively scored, the regenerated plants appeared phenotypically normal and true to type.

4.9. Qualitative Phytochemical Analysis of *Rauvolfia tetraphylla*

In the current study, sequential crude extracts of *R. tetraphylla* leaf and fruit were subjected to qualitative preliminary phytochemical analyses using hexane, chloroform, ethyl acetate, and methanol as solvents (Table 6 and 7). The analyses revealed the presence of various secondary metabolites such as alkaloids, carbohydrates, glycosides, oils and fats, phenolic compounds, tannins, quinones, cardiac glycosides, terpenoids, coumarins, phlobatannins, steroids, phytosteroids, anthraquinones, flavonoids, and proteins in all the extracts. In previous research similar to the above study were evaluated by Kavitha *et al*. (2012), Rohela *et al*. (2016), Behera *et al*. (2016), and Merlin *et al*. (2020) of *R. tetraphylla*, which also reported the presence of similar phytoconstituents in the plant extracts.

4.10. Quantitative Analysis

Based on the preliminary analysis, ethyl acetate and methanol extract of leaves and fruit from *R. tetraphylla* showed more activity compared to hexane and chloroform. So, for further studies ethyl acetate and methanol extracts were subjected to further analysis of alkaloid, flavonoid, phenolic content, and tannin.

4.10.1. Determination of Alkaloid Content

The estimation of alkaloids was determined by bromocresol green reagent using ethyl acetate and methanolic crude extracts of leaves and fruits of *R. tetraphylla*. Atropine was used as a standard compound and alkaloids were expressed as µg atropine equivalent (µg/ARP) per mg plant extracts using the standard curve equation: $y = 0.07x + 0.024$, $R^2 = 0.9929$ (Fig. 15a). In Table 8 showed the absorbance with concentration of Atropine. Table 12 showed the contents of alkaloids that were measured by bromocresol green reagent in terms of atropine equivalent. The alkaloids varied from 0.64 to 2.10 µg/mg in the extracts. The highest amount of alkaloid was present in the methanolic extract of leaf (2.10µg/mg) of *R. tetraphylla*. Alkaloids are a significant class of compounds present in *R. tetraphylla*, as reported by various researchers, including Gupta *et al*. (2012), Verma *et al*. (2012), Pandey *et al*. (2016) and Rohela *et al*. (2021).

4.10.2. Determination of Flavonoid Content

The estimation of flavonoid was determined by the Aluminium chloride colorimetric method using ethyl acetate and methanolic crude extracts of leaf and fruit of *R. tetraphylla*. Rutin

was used as a standard compound and flavonoid was expressed as µg rutin equivalent (µg/RUT) per mg plant extract by the standard curve equation: $y = 0.8845x + 0.0214$, $R^2 = 0.9993$ (Fig. 15b). Table 9 showed the absorbance with concentration of Rutin. Highest amount of flavonoids that were measured by aluminium chloride in terms of rutin equivalent (Table 12). The flavonoids varied from 0.71 to 1.92 µg/mg in the extracts. The maximum flavonoid content was found in the methanolic extract of leaf (1.92 µg/mg) of *R. tetraphylla*. Similarly, Kar and panda (2023) evaluated the flavonoid content of root from *R. tetraphylla* and maximum content was observed in methanolic extract ranging from 28.1 to 217.3 mg/g. Aluminium chloride can create stable complexes with the C4 keto groups and either the C-3 or C-5 hydroxyl groups present in flavonols and flavones. Subsequently, it can also form fewer stable complexes with hydroxyl groups located in the ortho position in the B-ring of flavonoids. Flavonoids are key compounds for good health in the human body (Yamin *et al*. 2020).

4.10.3. Determination of Total Phenolic Content

The amount of total phenolic content was determined by the Folin-Ciocalteu reagent using ethyl acetate and methanolic crude extracts of leaves and fruits of *R. tetraphylla*. Gallic acid was used as a standard compound and total phenols were expressed as µg gallic acid equivalent (µg/GAE) per mg plant extract using the standard curve equation: $y = 0.0057x + 0.0818$, $R^2 = 0.9928$ (Fig. 15c). Where y is absorbance at 760 nm and x is total phenolic content in the different extracts of *R. tetraphylla* expressed in µg/mg. Table 10 showed the absorbance with concentration of Gallic acid. Table 12 showed the contents of total phenols that were measured by the Folin Ciocalteu reagent in terms of gallic acid equivalent. The total phenol varied from 11.43 to 22.88 µg/mg in the extracts. The maximum phenolic content was found in the methanolic extract of fruit (22.88 µg/mg) of *R. tetraphylla*.

Mahesh *et al*. (2010) evaluated the similar research in methanol extracts of *R. tetraphylla* leaves, and it revealed that the total phenolic content ranged from 41.7 mg gallic acid equivalent/g dry weight (DW) of the sample. Similarly, Kar and Panda (2023) analysed the phenol content of root from *R. tetraphylla* in methanol and aqueous extract. Methanol extract showed highest tannin content (17.39 mg/g) compared to aqueous extract. Phenolic compounds exhibit redox potentials and can act as antioxidants by donating hydrogen atoms to free radicals and serves as a rapid screening tool for evaluating antioxidant activity (Yamin *et al*. 2020).

4.10.4. Determination of Tannin Content

The amount of tannin content was determined by the Folin-Ciocalteu reagent using ethyl acetate and methanolic crude extracts of leaves and fruit of *R. tetraphylla*. Gallic acid was used as a standard compound and tannin was expressed as µg gallic acid equivalent (µg/GAE) per mg plant extract using the standard curve equation: $y = 0.0042x + 0.0915$, $R^2 = 0.9948$ (Fig. 15d). Table 11 showed the absorbance with concentration of Gallic acid. Table 12 showed the tannin content that was measured by Folin Ciocalteu reagent in terms of gallic acid equivalent. The measured tannin content ranged from 17.02 to 33.92 µg/mg in the extracts. The maximum tannin content was found in the methanolic extract of leaf (33.92 µg/mg) of *R. tetraphylla*.

Similarly, Hossain *et al*. (2020) evaluated the tannin content in methanol extract of *Moringa oleifera* Lam., with the range from 6.46 to 3.91 g GAE/100g dry sample. In the same way, Kar, and panda (2023) evaluated the tannin content of root from *R. tetraphylla* showed maximum in methanolic extract (7.38 mg/g). Tannins are a group of polyphenolic compounds with molecular weights ranging between 120-3000 Da, and they exhibit solubility in water. These compounds have gained recognition for their diverse pharmacological effects, including their potential as anti-inflammatory, anticancer, antidiabetic, antioxidant, and antimicrobial agents and additionally it plays a role by providing natural colour (Gurning *et al*. 2022).

4.11. Gas Chromatography–Mass Spectrometry (GC-MS)

In mass spectrometry, organic molecules undergo bombardment with electrons leading to the formation of highly energetic charged ions. A mass spectrum, depicting the relative abundance of fragmented ions plotted against their mass-to-charge ratio, allows for accurate determination of the relative molecular mass and precise identification of the molecular formula based on fragmentation patterns.

GCMS analysis of methanol extract of *R. tetraphylla* showed the presence of several compound (Table 13; Fig.16) in which twelve compounds were reported. 1,9-Nonanediol (4.714%) (**C1**), 3-Furanol, tetrahydro-2,2,4,4-tetramethyl- (10.333%) (**C2**), 1D-1-O-Methyl-myo-inositol (39.216 %) (**C3**), (Z)-2-methylbutanal oxime (6. 646%) (**C4**), Arabino-heptitol, 2,3:5,6-dianhydro-1,7-dideoxy-2,6-di-C-methyl- (0.873%) (**C5**), 3-O-methyl-D-glucose (0.965%) (**C6**), DI-N-Octyl Phthalate (16.444%) (**C7**), 7-[3-Chloro-2-hydroxypropyl] guanine

(0.842%) (**C8**), 1-Naphthalenepropanol,.alp (1.002%) (**C9**), 1,3,3-trimethyl-2-hydroxymethyl-3,3-dimethyl-4-(3-methylbut-2-enyl)-cyclohexene (6.035%) (**C10**), β-Amyrone (3.390%) (**C11**) and (+)-Helminthogermacrene (9.539%) (**C12**). The most prominent peak area was indicated that 1D-1-O-Methyl-myo-inositol (39.216%).

1,9-Nonanediol (nano methylene glycol) is synthesized through the isomerization of allyl alcohol to aldehyde, followed by hydroformylation and reduction (Tsuji, 2002). **1D-1-O-Methyl-myo-inositol**, commonly known as myo-inositol, is a sugar alcohol with applications in addressing various human metabolic disorders linked to insulin resistance. These disorders include conditions such as polycystic ovary syndrome (Guarnieri *et al*. 2023), gestational diabetes mellitus (Pintaudi *et al*. 2016) and metabolic syndrome. Moreover, myo-inositol is utilized in the prevention or treatment of certain diabetic complications, such as neuropathy, nephropathy and cataract (Croze *et al*. 2013; Chhetri, 2019). Additionally, it plays a role in the treatment of breast cancer (Amabile *et al*. 2012).

2-methylbutanal oxime is an oxime produced from the amino acids isoleucine to the corresponding cyanohydrins (Jørgensen *et al*. 2011; Lai *et al*. 2020). It plays a crucial role in plant metabolism such as plant growth regulation, defence, pollinator attraction and communication (Sørensen *et al*. 2018). **Arabino-heptitol, 2,3:5,6-dianhydro-1,7-dideoxy-2,6-di-C-methyl-** was reported in hydro alcoholic leaves extract of *Aegle marmelos* L. using GC-MS analysis (Jay Prakash *et al*. 2021). **3-O-methyl-D-glucose** serves as a nonmetabolizable structural analog of glucose and finds application in tumour detection (Sehgal *et al*. 2019; Anemone *et al*. 2021). Additionally, this compound has been reported to exhibit positive effects in mitigating the neuropathological outcomes associated with ischemic damage, offering potential relief in cases of human stroke (Mbakazi *et al*. 2022).

Epichlorohydrin (ECH) is a key intermediate for industrial synthesis, utilized in the production of glycerin, dyes, surfactants, synthetic materials, and various polymers. It reacts predominantly with guanine in DNA at the N-7 position, forming 7-(3-chloro-2-hydroxypropyl) guanine, a crucial marker for assessing exposure in genotoxicological studies (Ordzhonikidze *et al*. 2021). The quantitative measurement of this DNA adduct in human leukocytes is employed to determine occupational ECH exposure among workers (Plna *et al*. 2000). **1-**

Naphthalenepropanol,.alp was reported in methanolic extract of *Morinda lucida* L. stem bark (Oloche *et al*. 2022). **1,3,3-trimethyl-2-hydroxymethyl-3,3-dimethyl-4-(3-methylbut-2-enyl)-cyclohexene** reported in ethanol/ methanol wood extracts of *Populus lasiocarpa* Oliv. (Peng *et al*. 2017) and methanol leaf extract of *Skimmia anquetilia* (N.P. Taylor and Airy Shaw) using GCMS analysis.

β-Amyrone is a pentacyclic triterpene is used to treat inflammation (de Almeida *et al*. 2015; Javaid *et al*. 2021), anti-α-glucosidase, anti-acetylcholinesterase, antimicrobial, anti-fungal activities (Ata *et al*. 2011) and antiviral activities (Bourjot *et al*. 2012). (+)-Helminthogermacrene is a sesquiterpene hydrocarbon group used for anti-inflammatory (Ramalakshmi & Muthuchelian, 2011) and repellent activity (Feng *et al*. 2022). The GC-MS profiling of methanol extract of *R. tetraphylla* has some phytoconstituents which may be responsible for the antioxidant, antimicrobial, anti-inflammatory, and wound healing activity.

4.12. Liquid Chromatography-Mass Spectrometry (LCMS)

The secondary metabolites that are present in methanol extracts of leaves of *R. tetraphylla* were analysed through LCMS technique. The peaks with mass range m/z 100 to 2000 were recorded by LCMS-ESI-MS fingerprints. Based on the molecular mass of the metabolites 10 peaks were exactly identified at m/z 183.0983 (Oxodecenoic acid), 273.0366 (Naringenin), 301.1407 (dihydrokaempferide), 349.1547 (serpentine), 355.2088 (yohimbine), 383.1972 (isoreserpinine), 411.1919 (darcyribeirine), 413.2159 (reserpiline), 429.2021 (carapanaubine), and 609.9797 (reserpine) (Table 14).

Oxodecenoic acid is a fatty acid. **Naringenin** is a flavanone, belongs to class flavonoid has been found in citrus family (Salehi *et al*. 2019) which have antibacterial, antioxidant, antifibrogenic, anticancer, anti-inflammatory, antiadipogenic, antiviral, diabetes, and cardioprotective effects (Joshi *et al*. 2018). It is used to treat inflammation-related disorders, such as sepsis, fibrosis, fulminant hepatitis, cancer (Zeng *et al*. 2018) and liver diseases (Hernández-Aquino & Muriel, 2018). **Dihydrokaempferide** is a flavonoid compound has been isolated in ethyl acetate extract of *Bauhinia championii* (Benth.) which possess apoptosis, antioxidant, anti-inflammatory activity (Zhang *et al*. 2018), anticancer and anti-aging agent (Chunhakant & Chaicharoenpong, 2019). It is used to treat acute pancreatitis (inflammatory diseases) (Liang *et*

al. 2020), acute liver failure (Zhang *et al*. 2021) and infantile pneumonia in Human fibroblast cells WI-38 (Wang *et al*. 2023).

Serpentine is an indole alkaloid (type II topoisomerase inhibitor) that exhibits antipsychotic properties and was identified in *R. serpentina* L. (Kumari *et al*. 2013). The peroxidase enzyme facilitates the conversion of ajmalicine to serpentine by catalysing the oxidation of bisindole alkaloid (Soni *et al*. 2016), which is used to treat hypertension (Lobay, 2015). **Yohimbine** is an indole alkaloid used to treat erectile disorder (Carey & Johnson, 1996), orgasmic dysfunction (Adeniyi *et al*. 2007), liver inflammation, fibrosis (Sharma *et al*. 2024), acute kidney injury (Shimokawa *et al*. 2020) and antidepressant properties (Tasleem *et al*. 2021).

Isoreserpinine is an alkaloid isolated from the roots of *R. densiflora* (Iqbal *et al*. 2013) and *R. tetraphylla* (Iqbal *et al*. 2013) used to treat antipsychotic activity (Otimenyin & Ior, 2021). **Darcyribeirine** is a pentacyclic indole alkaloid isolated from the *R. grandiflora* Mart. ex A.DC. root bark (Cancelieri *et al*. 2002). **Reserpiline** is an antipsychotic alkaloid and isolated from the leaves of *R. tetraphylla* (Maurya *et al*. 2013), root of *R. oreogiton* Mgf. (Timmins, 1974), *R. decurva* Hook (Atal, 1959), *R. densiflora* (Wall.) Benth. ex Hook.f. (Iqbal *et al*. 2013), *R. serpentina* (Kumari *et al*. 2013). **Carapanaubine** is an oxindole alkaloid were reported from the leaves of *R. vomitoria* Afzel. (Patel *et al*. 1964) and stembark of *Bleekeria vitiensis* (Markgr.) A.C.Sm., indicating substitute oxidative rearrangement products of the alkaloid isoreserpiline (Kanji & Sainsbury, 1974).

Reserpine is an indole alkaloid found in *Rauvolfia* species used to treat hypertension, tachycardia, and thyrotoxicosis (Lobay, 2015; Shamon *et al*. 2016; Siddiqui *et al*. 2020). It acts as an antihypertensive (Strawbridge *et al*. 2023), anti-arrhythmic (Ciofalo *et al*. 1966), antihyperlipidemic activity (Shah *et al*. 2020) and inhibit bacterial antibiotic resistance (Sridevi *et al*. 2017). Reserpine was identified in the extracts by LC–ESI – MS/MS analysis (Fig. 17), where detected by MS/MS spectrum, and compared with standard (Bindu *et al*. 2014). In this study, LCMS analysis of methanol extract from *R. tetraphylla* leaves contains various valuable secondary compounds which have various medicinal properties that can be useful for the treatment of various diseases. Secondary metabolites were found in the *R. tetraphylla* will be facilitating in the wound healing process.

4.13. Column Chromatography

Isolating bioactive compounds from the methanol extract of *R. tetraphylla* leaves using column chromatography. Silica gel used as the absorbent and fractions eluted by solvents of increasing polarity (hexane to methanol) (Fig. 18). Eighty fractions were collected and immediately analysed by TLC for the identification of single compound.

From fraction (F1) single compound was identified at R_f value 0.61 in TLC with solvent system of Hexane: Ethylacetate (4:1) solvent system (Fig. 19a). The spot was detected under short (256 nm) and long UV (356 nm), subsequently it was characterized with the help of UV spectrum, "FTIR, ^{1}H NMR spectrum, ^{13}C NMR Spectrum and GC Mass spectrum".

4.13.1. UV Spectrum

UV wavelengths of fraction (F1) observed at 270 nm showed organic compounds (Fig. 19b).

4.13.2. FTIR

Based on the UV spectrum results, the fraction (F1) was taken for FTIR analysis. Band at 3309.85 (OH stretch- strong, broad- alcohol), 2939.52 cm^{-1} and 2831.50 cm^{-1} (C-H stretch-alkane-medium), 2044.54 cm^{-1} (C=C=C stretch- medium- allene), 1450.47 cm^{-1} (C-H bend - alkane- medium), 1111.00 (C-O stretch- aliphatic ether- strong), 1026.13 cm^{-1} (C-F- fluoro compound- strong), 756.10 cm^{-1} (C-H bend- 1,2-disubstituted-strong), 686.66 cm^{-1} (C-H bend - benzene derivative), 509.21 cm^{-1} (C-I stretch - halo compound- strong) (Fig. 19c).

The 2831.50 cm^{-1} and 1450.47 cm^{-1} are the band indicates the of the alkane functional group which are present in the butyl group (-C4H9) of butyl cyclohexyl phthalate. The 1111.00 cm^{-1} band evidenced that the presence of an aliphatic ether functional group. Butyl cyclohexyl phthalate contains an ester functional group (-COO-), which might be responsible for this observed band. The 756.10 cm^{-1} band suggested the presence of 1,2-disubstituted alkane functional groups, which are present in the cyclohexyl ring of butyl cyclohexyl phthalate. The 686.66 cm^{-1} band is indicated the benzene derivatives, butyl cyclohexyl phthalate contains a cyclohexyl ring.

4.13.3. Nuclear Magnetic Resonance system (NMR)

^{1}H NMR spectrum

^{1}H NMR spectrum of signal δ at 3.558, 2.512, 1.61, 1.28. The two-methyl group attached to carbon showed a distinct peak at 3.55 δ value. The bunch of peaks in the region of 1-3 δ values correspond to –CH and –CH_2 of cyclohexane (Fig. 19d) (Masani *et al*. 2016).

4.13.4. ^{13}C NMR Spectrum

The ^{13}C-NMR exhibited numerous peaks near 39.34 to 40.59 δ, which corresponded to the carbon of cyclohexane and methyl groups (Fig. 19e) (Masani *et al*. 2016).

4.13.5. Mass Spectra

The fractions were analysed by NIST library of GC-MASS spectra and then directed towards isolating fractions F1 (Butyl cyclohexyl ester) resulting in the purification of compound which were subsequently characterized structurally (Fig. 19f). Further investigation is warranted to identify additional fractions and compounds.

Butyl cyclohexyl ester possesses antioxidants (Elmorsy *et al*., 2013), anticancer (Böckers *et al*. 2021) and hepatotoxicity (Radha *et al*. 2020).

4.14. ANTIMICROBIAL ACTIVITY

The antimicrobial activity was carried out in *R. tetraphylla* ethyl acetate and methanolic extract of leaves and fruits against Gram-positive (*S. aureus* and *E. faecalis*) and Gram-negative (*E. coli*) bacteria were analysed using the agar well diffusion method. All the extracts showed the zone of inhibition which has been calculated and shown in table 15 & 16; fig. 20 & 21. The maximum inhibition was observed in methanol extract of leaf and fruit against *E. coli* (100 µg/mL). All the extracts showed good antimicrobial activity.

Similarly, Suresh *et al*. (2008), evaluated ethanol extracts of *R. tetraphylla* leaves against various microorganisms, including *E. coli*, *Streptococcus lactis*, *Enterobacter aerogenes*, *Alcaligenes faecalis*, *P. aeruginosa*, and *Proteus vulgaris*. The ethanol extracts demonstrated notable antimicrobial activity, with the highest efficacy observed against *E. coli, E. aerogenes* and *A. faecalis*.

Rohela *et al*. (2016) analyseed the antimicrobial activity of *R. tetraphylla* leaf, stem, and root against various microorganisms, including *E. coli*, *P. aeruginosa*, *S. aureus*, *K. pneumonia*, *A. niger*, *Penicillium* spp, *C. albicans*, and *Fusarium oxysporum*. The tests revealed that the methanol-based leaf extracts exhibited the most significant bacterial growth inhibition zone, measuring 25.0 mm against *S. aureus*. The potential antimicrobial properties of different parts of *R. tetraphylla* and their effectiveness against specific bacterial and fungal strains. It opens possibilities for further exploration of *R. tetraphylla* potential applications in developing natural antimicrobial agents or remedies to combat microbial infections.

Antimicrobial activities of *R. serpentina* L., *Adhatoda vasica* L., *and Alstonia scholaris* (L.) R. Br. belongs to Apocynaceae family are tested in various solvents (water, ethyl acetate, chloroform, and methanol). The antibacterial activity of methanol extract was highest against two bacterial strains (*S. pyogenes* and *P. aeruginosa*). Methanol extraction of *R. serpentine* L. showed antimicrobial activity against bacteria tested (Ratnam, 2021).

4.14.1. Assessment of Minimum Inhibitory Concentration

A two-fold broth dilution approach was used to estimate the MIC against *E. coli*. The nutrient agar broth is utilised as a growth medium, ethyl acetate and methanol leaf and fruit extract of *R. tetraphylla* is diluted with DMSO. 200 µg/ mL, 100 µg/mL, 50 µg/mL, 25 µg/mL, 12.5 µg/mL, 6.25 µg/mL, 3.125 µg/mL, 1.56 µg/mL, and 0.78 µg/mL are the concentrations. The solution's turbidity is measured. The minimum growth of ethyl acetate and methanol extract of leaf is observed in the concentration 3.125 µg/mL and 1.56 µg/mL and the fruit of *R. tetraphylla* contain 25 µg/mL and 50 µg/mL respectively.

Similarly, Shariff *et al*. (2006), evaluated antimicrobial activity of different extracts from the leaves and calli of *R. tetraphylla* against several bacteria, including *B. subtilis*, *E. coli*, *P. solanacearum*, *X. axonopodis*, and *X. vesicatoria*. The extraction process involved using absolute alcohol, benzene, chloroform, methanol, and petroleum ether. The results showed that the extracts exhibited significant antimicrobial properties, with the minimum inhibitory concentration (MIC) ranging from 0.25 to 6 mg/ml. It suggested that *R. tetraphylla* extracts have the potential to inhibit the growth of the tested bacteria at relatively low concentrations.

Interestingly, PA, Hosamani (2023) analysed antimicrobial activity of leaf extract of *R. tetraphylla* against *B. subtilis, S. aureus, P. aeruginosa, C. albicans, A. niger* and *Penicillum chrysogenum*. All the extracts (chloroform, acetone, ethanol, and water) showed good MIC values by serial dilution method.

Aqueous extracts of Apocynaceae and Solanaceae family were analysed for antimicrobial activity against *S. aureus* and *E. faecalis* using the broth microdilution method, and they had shown some inhibition of bacterial growth at concentrations of 100 g/mL (Suffredini *et al*., 2004). Two indole alkaloids were isolated from *Rauvolfia caffra* Sond from stem barks such as rauvolfianoids A (1) and B (2). It was analysed antimicrobial activity against three bacterial strains (*E.* coli [ATCC 35218], *Shigella* sp, and *Salmonella* sp). Compound 1 exhibited moderate antimicrobial activity against *Salmonella* sp with 25 mg/mL MIC values compared to compound 2 (Bitombo *et al*. 2021).

4.15. ANTIOXIDANT ASSAY

4.15.1. DPPH Assay

Balancing free radicals through adequate levels of antioxidants is crucial for cell and tissues of human health and to prevent the damaging tissues and inflammation, chronic diseases, aging, etc. In this present study, antioxidant activity was analysed by ethyl acetate and methanol extracts from *R. tetraphylla* of leaf and fruit by DPPH method (Table 18). The colour changed from purple to yellow indicate the presence of antioxidant activity. Ascorbic acid is used as a standard (IC_{50} = 46.28 µg/mL) (Table 17). The maximum activity was observed in methanol extract of fruit (IC_{50} = 60.37 µg/mL) followed by methanol extract of leaf (IC_{50} = 62.61µg/mL) (Fig. 22 & 23).

Radical scavenging percentage of all extracts were higher when compared to standard. Alkaloids and flavonoids were present in *R. tetraphylla* extracts could be responsible for antioxidant activity (Behera *et al*. 2016), Similarly, leaf and fruit of *R. tetraphylla* were evaluated by various extracts in which methanol extracts showed more activity compared to n-hexane and dichloromethane (Vinay *et al*., 2016). Maheshu *et al*., (2010) examined methanol extract of

leaves of *R. tetraphylla* exhibited antioxidant activity against DPPH, ABTS and reducing power assays. Various antioxidant assays were determined in methanol extract of *R. tetraphylla* which showed dose dependent antioxidant activity (Prasad *et al*., 2013; Nair *et al*., 2012; Archana and Jeyamanikandan 2015; Oza and Solanki, 2016). Silver nanoparticles from leaf extract of *R. tetraphylla* were determined by DPPH method which showed maximum IC_{50} value of 82.13 µg/mL. (Vinay *et al*., 2019). In our study, all extracts of *R. tetraphylla* showed radical scavenging activity in dose dependent manner, which is key factor for wound healing property.

4.15.2. Ferric Reducing Antioxidant Power (FRAP) Assay

Assessment of radical scavenging activity of *R. tetraphylla* leaves and fruits extracts using FRAP assay across a range of concentrations (20 to 100 µg/mL), the FRAP values revealed the reduction of Fe^{3+} to Fe^{2+} ions within the ferricyanide complex employing donor electrons from the *R. tetraphylla* antioxidants leading to the formation of a deep blue. Notably, a clear dose-response relationship was evident in the FRAP assay, with absorbance levels increasing in tandem with the escalating concentration of each individual extract. Among these extracts, the methanolic extract from the leaves emerged as the most potent antioxidant across all concentration levels in the reduction assay. In terms of the overall trend observed, the activity towards reduction followed this order RLM < RL EA < RFM < RF EA (Table 19 & Fig. 24). This sequence delineates the ascending order of antioxidant potential within the respective extracts of *R. tetraphylla* exhibiting the antioxidant activity.

Al-Laith *et al*. (2019) assessed antioxidant activity of dried materials in wild medicinal plants using the FRAP assay. *Emex spinosus* (L.) Campd. leaves from significantly exhibited antioxidant activity than *Aizoon canariense* L. and *Asphodelus tenuifolius* Cav. Seeds of *A. tenuifolius* had lower antioxidant activity compared to its leaves and all plants demonstrated lower activity than ascorbic acid. Similarly, Liaqat *et al*., (2021) analysed antioxidant assay of wheat germ of acetone, hexane, ethanol, HWE (hot water extract); SWE (subcritical water extract); UWE (ultrasonic water extract) in which maximum FRAP value was observed in hexane extract. The importance of assessing antioxidant activity in natural products and emphasizes the variations in concentration dependent. It contributes to the potential health benefits associated with these plant extracts and provides valuable information for wound healing activity from *R. tetraphylla*.

4.15.3. Evaluation of Total Antioxidant Activity

TAA of *R. tetaphylla* leaf and fruit extracts was analysed using the phosphomolybdenum method, with ethyl acetate and methanol extracts. The results (Fig. 25 & 26) revealed that methanol extract of the leaf exhibited highest antioxidant activity with an IC_{50} value of 63.05 µg/mL, followed by the methanol extract of the fruit with an IC_{50} value of 65.37 µg/mL (Table 20 & 21). Similarly, in a separate study by Maswada & Maswada (2013), the total antioxidant activity of hydro-ethanolic extracts from *Asparagus stipularis* Forssk., *Cyperus capitatus* Vand., and *Stipagrostis lanata* (Forssk.) De Winter was investigated. It demonstrated that these plant extracts displayed promising antioxidant properties. In another study by Kamath *et al*. (2015), examined various consumed food items, including vegetables, fruits, seeds, berries, cereals, and herbs, in Moodbidri, Karnataka, India for phenolic content and total antioxidant activity by phosphomolybdenum method.

Notably, *Murraya koenigii* L. showed significantly high phenolic content (18.40 mg GAE/g), which correlated with its elevated antioxidant activity (48.94 mg AAE/g). It is essential to note the importance of plants and their extracts as potential sources of natural antioxidants, which have been proven beneficial for health and wellness. Therefore, evaluation of reducing power could play eminent factor for the assessment of wound healing property.

4.16. Evaluation of *in vitro* Anti-Inflammatory Activity

Anti-inflammatory activity of *R. tetraphylla* leaves and fruits of various extracts were evaluated against denaturation of egg albumin method. This *in vitro* technique assessed natural product anti-inflammatory activity quickly by inhibiting albumin protein denaturation (Chandra *et al*., 2012). The maximum inhibition percentage was perceived in both leaf and fruit methanol extracts at 100 µg/mL. The inhibition of egg albumin denaturation for methanol extracts increased gradually. The IC_{50} value of methanol extract of leaf and fruit was 72.44 µg/mL and 78.04 µg/mL (Table 23; Fig. 28). In addition, the IC_{50} value of standard diclofenac sodium was 73.02 µg/mL, and it showed a concentration-dependent response (r^2 = 0.9806) (Table 22; Fig. 27). The leaf extract has a bit of higher anti-inflammatory than the standard drug. Similarly, Yadav & Mohite (2020) analysed anti-inflammatory activity of aqueous extract *Malvastrum coromandelianum* (L.) Garcke on protein denaturation with different concentration. The

maximum inhibition percentage was observed at 100 µg/mL with a significant inhibition rate of 74.17%, while standard diclofenac sodium exhibited with inhibition rate (76.50%) at 100 µg/mL.

Heendeniya *et al*. (2018) analysed anti-inflammatory activity of aqueous extracts of *Syzygium caryophyllatum* (L.) Alston, which showed a dose-dependent response, with IC_{50} value of 6.229 x 10^3 µg/mL. Dharmadeva *et al*. (2018) investigated anti-inflammatory potential of *Ficus racemose* L. bark through both cold and hot water extraction methods. The inhibition of egg albumin denaturation increased progressively with concentration, and higher inhibition observed in the cold-water extracts and hot water extracts at 1000 µg/mL with IC_{50} values were 3691.97 µg/mL and 4207.1 µg/mL, respectively. Mirke *et al*. (2020) evaluated the anti-inflammatory activity of a combination of *Eucalyptus* oil and aqueous extract from *Glycine max* (L.) Merr., which also exhibited a concentration-dependent response, with the highest inhibition rate of 98.06% observed at a concentration of 1000 µg/mL. These studies collectively emphasize the ability of natural products in controlling inflammation during various concentrations and mechanisms, providing valuable insights into their wound healing applications. Our findings also revealed that the potent anti-inflammatory activity of *R. tetraphylla* could attribute the reduction of inflammation at wound site. Hence, it could be considered a promising candidate for anti-inflammatory activity.

4.17. CYTOTOXICITY ACTIVITY

The cytotoxicity of ethyl acetate and methanol extracts derived from *R. tetraphylla* leaves and fruits examined through visual observation and MTT assay against African Green Monkey Kidney (Vero) cells and 3T3 mouse embryonic fibroblast cells. MTT is a light-sensitive yellow tetrazole solution utilized for evaluating cell viability percentages post-treatment with cytotoxic agents. Viable cells facilitate the transformation of yellow solution into a purple formazan through the catalytic action of NADPH-dependent cellular oxidoreductase enzymes. MTT method was employed to quantitatively assess cell viability. Vero cells and 3T3 cells were seeded in 96-well plates and exposed to various concentrations (0 to 100 µg/mL) of extracts. After incubation, absorbance measurements at 570 nm were taken to calculate cell viability. To assess the cytotoxicity of the *R. tetraphylla* extracts in Vero and 3T3 cells and determine the CC_{50} value.

4.17.1. Cytotoxicity Activity of *R. tetraphylla* Extracts against Vero Cells

The *in vitro* cytotoxicity activity of different extracts of *R. tetraphylla* was measured using MTT assay against Vero cell lines at various concentrations (5, 10, 15, 25, 50 and 100 µg/mL). The results emphasized concentration-dependent cytotoxic effects of *R. tetraphylla* extracts (Fig. 29), emphasizing the importance of considering dosage when assessing their impact on cell health. The assessment of cytotoxicity of *R. tetraphylla* extracts were expressed as CC_{50} values against Vero cells. When surpassing the CC_{50} value, the concentration led to noticeable damage in over 50% of the cells. The *R. tetraphylla* ethyl acetate extract from the leaf, methanol extract from the leaf and methanol extract from the fruit can be considered safe, as their CC_{50} values exceed 100 µg/mL. Additionally, the ethyl acetate extract from the fruit is also safe, as its CC_{50} value is 21 µg/mL. It indicates that all these extracts are less likely to induce significant cytotoxic effects on Vero cells at the specified concentrations suggesting their potential safety for wound healing applications. Visual observation entailed a 24-hours incubation of Vero cells with varying concentrations (0, 25, 50 100 µg/mL) of the test samples. The *R. tetraphylla* leaf and fruit extracts can be considered as a safe as the value of CC_{50} is > 20 µg/mL (Zirihi *et al*. 2005; Mongalo *et al*. 2017; Afagnigni *et al*. 2020).

Chiamenti *et al*., (2019) evaluated the cytotoxicity of the *Cassia surattensis* Burm.f. methanolic seed extract using the MTT assay on Vero cells. This assay involved testing the extract at ten different concentrations, ranging from 400 µg/mL to 0 µg/mL. It indicated that the cytotoxic concentration at which 50% of Vero cells were affected (CC_{50}) for the *C. surattensis* seed extract was determined to be 332.87 µg/mL. According to Njeru *et al*., (2021) assessed the cytotoxicity of *Aspilia pluriseta* Schweinf. solvent extract fractions using Vero cells. The methanolic crude extract fell within acceptable toxicity limits (CC_{50} = 24.51 µg/mL). Fractionation identified cytotoxic fraction of petroleum ether (CC_{50} 78.6 µg/mL), dichloromethane (CC_{50} 191.7 µg/mL) and ethyl acetate (CC_{50} 500 µg/mL) remained non-toxic. This information informs the safety and ability of *A. pluriseta* extract fractions. Mansour *et al*. (2022) employed an MTT assay to determine the cytotoxic concentration at which 50% of cells are affected for various samples on VERO cells. Specifically, the CC_{50} values for ethanolic extracts of *Jasminum humile* L., *J. grandiflorum* L. and *Olea europaea* L., which ranged from 63.39 to 108.60 mg/mL.

In *J. humile*, were investigated its petroleum ether, methylene chloride, ethyl acetate, and n-butanol fractions. These fractions exhibited a range of CC_{50} values, spanning from 26.51 to 108.13 mg/mL, indicating varying levels of cytotoxicity. Additionally, compounds were isolated and tested individual compounds from these extracts revealing cytotoxicity values that ranged from 44.73 to 210.17 mg/mL. The diverse range of CC_{50} values underscores the importance of evaluating specific fractions and isolated compounds for their bioactivity. The CC_{50} value serves as a crucial parameter for understanding the exact potential impact on cell viability, which is essential for considering its safety and potential applications.

4.17.2. Cytotoxicity Activity of *Rauvolfia tetraphylla* Extracts against 3T3 Cells

The cytotoxicity screening of ethyl acetate and methanol extracts of leaves and fruit of *R. tetraphylla* assessed using MTT assay against mouse fibroblast 3T3 cell lines at different concentrations (0, 25, 50 100 µg/mL) to determine CC_{50} value. The results showed that cytotoxicity of all the four extracts was found to be dose dependent (Fig. 30). All the extracts of *R. tetraphylla* exhibited CC_{50} values greater than 100 µg/mL, indicating a lack of significant lethality and suggesting better proliferation activity towards 3T3 cell lines within the tested concentration range. Our result was similar to the present work done by Zingue *et al*. (2018) they had shown moderate cytotoxicity of hydroethanolic extract of *Acacia seyal* Del. against murine fibroblast cells (NIH/3T3) where the CC_{50} is 36 µg/mL. Malematja *et al*. (2018) analysed the effect of *Senna italica* Mill. acetone leaf extract by 3T3-L1 which showed non-toxic with CC_{50} values of the extract were >1000 µg/mL. The safety of *R. tetraphylla* extracts for normal cell proliferation further supports their potential applications in therapeutic wound healing properties.

4.18. SCRATCH ASSAY

Cell migration is a key aspect of wound healing that is assessed using African Green Monkey Kidney cells (Vero) cell line and mouse embryonic fibroblast (3T3) cell line against ethyl acetate and methanol crude extracts of *R. tetraphylla*. Initially, the cells were cultured on six-well plates and allowed to form a monolayer. Subsequently, wounds were carefully introduced (0.9 mm) into all wells using a sterile micro-tip, creating a uniform starting point for the analysis. Then, a test sample at 100 µg/mL concentration is applied to the wounds and the

entire setup is placed in a CO_2 incubator for incubation. After a 24-hour incubation period, the wounds are scrutinized using an inverted microscope to observe any changes. Specifically, the distance between the wounds is documented. Photographs are also captured to provide a visual record of the wound area (Fig. 31 & 32).

The crucial observation is that the distance between the wounds appears to have decreased compared to the initial wound size, indicating a closure of the wound. It suggested that the cells have migrated within the test sample group. Moreover, comparing these results to the control group, it evidenced that the cell migration in the sample group is more pronounced demonstrating the wound-healing properties of the test sample. Wound closure of the ethyl acetate and methanol extract of leaves was observed 78.94% & 84.21% against the Vero cell line, 83.8% & 84.8% against the 3T3 cell line. Wound closure of ethyl acetate and methanol extract of fruit showed 80% & 83.15% against Vero cell line, 79.7% & 82.8% against 3T3 cell line. The control group showed 11.54% and 16.16% against Vero and 3T3 cell lines, respectively. As a result, the healing process of the cell line increased up to 72.67% than that of control. The maximum healing was increased in methanol extract of leaves against Vero cell line.

Faujdar (2021) used a scratch assay to evaluate the wound healing potential in Vero cell lines of a hydro-alcoholic extract from *Ocimum sanctum* L. leaves demonstrated strong wound healing capabilities. Nandhidha & Punnagai, (2022) investigated the wound healing potential of sodium glucose co-transporter2 inhibitors (Canagliflozin, Dapagliflozin, Empagliflozin) on Vero cell lines and found that Dapagliflozin showed significant wound healing activity, surpassing the standard drug Phenytoin with over 60% wound closure. Roy *et al*. (2023) examined the effects of *Glycyrrhiza glabra* L. ethanolic extract on wound healing in Vero cell lines. Both the experimental and control groups were subjected to a 0.6 mm wound, observed at 0 and 24 hours. After 24 hours, the extract was found to enhance wound healing by approximately 24% compared to the control group showing its potential for promoting cell migration and tissue repair. Muthukumar *et al*. (2023) utilized an herb ointment containing *Tridax procumbens* (L.) plant extract and gelatin-stabilized silver nanoparticles (G-AgNPs). This ointment, formulated using a biosurfactant, demonstrated excellent wound healing potential. In a wound scratch assay against Vero cell lines, it significantly enhanced cell migration (90% in 3 days) than control (62%). Vaid *et al*. (2020) investigated the wound healing potential of recombinant human

gelsolin (rhuGSN) on 3T3-L1 fibroblast cells with rhuGSN (12.5, 25, 50, and 100 µg/mL) resulted in accelerated wound closure by 24 h, with the 12.5 µg/mL concentration showing superior efficacy. These results highlight the promising therapeutic application of this nano-topical herb ointment for wound healing. This study corroborated previous research by demonstrating the different kind of medicinal plant species have regeneration of cells on the wound site.

4.19. CHICK CHORIOALLANTOIC MEMBRANE (CAM) ASSAY

CAM assay using *in-ovo* method was performed by ethyl acetate and methanol extracts from leaf and fruit of *R. tetraphylla* to evaluate the angiogenic potential. Analysis of the data presented in Tabel 24 & Fig. 33 revealed that the ethyl acetate extracts displayed limited angiogenic effects, while the methanol extracts exhibited the highest angiogenic potency compared to all other tested materials. However, it is important to note that all the extracts demonstrated significant angiogenesis. As a result, it can be concluded that all the tested extracts, including ethyl acetate and methanol extracts from both the leaf and fruit of *R. tetraphylla*, exert substantial impact on angiogenesis effects. Therefore, their overall angiogenic properties can be considered neutral in the context of wound healing applications. Vascular morphology has been evaluated by qualitative method. Blood vessels were also present on the materials covering at least half of the disk. Moreover, in about half of the experiments the collagen/elastin membrane was found to be completely enclosed by the chorioallantoic membrane.

In contrast to the initially limited angiogenic effects observed in the ethyl acetate extracts, further evaluation revealed that the methanol extracts displayed substantial angiogenic potency. This observation indicates that these extracts have a notable influence on angiogenesis, which is a crucial process in wound healing. The significant angiogenesis effects demonstrated by all the tested extracts suggested their potential of wound healing properties. Our research depicts natural components which responsible for the angiogenesis compared with previous studies, it's evident that other natural substances, such as the essential oil of *Eugenia dysenterica* DC. leaves, have demonstrated the ability to promote angiogenesis in the Chick Chorioallantoic Membrane assay, even at specific concentrations of 292 µg/mL (Mazutti da Silva *et al*. 2018).

Similarly, *Raphanus sativus* seed extract-containing hydrogels (Zahid *et al*. 2021) and green ZnO nanorods (Hassan *et al*. 2021) have showed significant wound-healing and

angiogenic effects in their respective studies, indicating their potential for application in wound healing. Furthermore, research on *Ephedra ciliata* Fisch. & C.A.Mey. quercetin-rich methanolic extract showed its safety at doses up to 2000 mg/kg, as well as its wound healing and anti-inflammatory activity, potentially through the downregulation of TNF-α (Yaseen *et al*. 2020).

It highlights the potential for creating dermatological treatments and wound healing solutions by harnessing the angiogenic properties of natural extracts. The extracts from *R. tetraphylla* initially exhibited varying levels of angiogenic activity; however, further analysis revealed a pronounced effect on angiogenesis, highlighting their potential use in wound healing applications.

The results of this study mark a notable advancement in vascular formation observed in incubated chick embryos. Angiogenesis is crucial factor for healing of wound by supplying oxygen, nutrients to the injured tissues, facilitating faster recovery. Our results align with other previous research highlighting the angiogenic potential of natural extracts, emphasizing their role in tissue repair and wound healing.

4.20. HEAT STRESS ASSAY

Heat stress lethality causing to an organism were exposed to extreme heat, which cannot persistence such heat condition leading to fatal and due to the inability to regulate internal body temperature. Intense heat affects physiological functions at the cellular, tissue, and all systemic levels, ultimately resulting in the organ failure or death if not managed promptly.

Some medicinal plants protect the heat stress by using ethyl acetate and methanolic extracts of leaf and fruit of *R. tetraphylla* were used to enhance resistance against stress in *Ceanorhabditis elegans*. All the extracts showed the survival rate, and maximum was observed in methanol extracts of leaf (22) followed by fruit (21) (Table 25 & Fig. 34). Pandey et al. (2013) evaluated the heat stress for adult *C. elegans* against 37℃ for 4 h, whereas pretreated with aqueous extract from *O. sanctum* L. adult worms' survival rate increased by 16%. Lin et al. (2021) reported the heat stress activity from *C. elegans* were enhanced by *Momordica saponin* extract. Wang et al. (2018) evaluated the stress resistance (temperature) using *C. elegans* in blueberry extract. Chuaijit et al. (2024) determined that heat stress caused lethality in aged, synchronized worms of *C. elegans* exposed in 20℃ at 48 h heat stress. The worms pretreated

with ethanol extracts of *Garcinia atroviridis* were survived up to 12.75 %. Similarly, our study observed that heat stress assay highlighted the active and motile worms in ethyl acetate and methanol extracts of leaf and fruit of *R. tetraphylla* and the results representing improved heat stress resistance and vitality of the *C. elegans*. These findings suggested to pave the way for future investigation and potential angiogenetic drug development.

4.21. EVALUATION OF *IN VIVO* WOUND HEALING

Wound healing was observed in ethyl acetate and methanol extracts of leaves and fruits from *R. tetraphylla* (Fig. 35). Incisional wounds were created by cutting the caudal fins with a scalpel (Roubal & Bullock, 1988). On the 0^{th} day, the fin was incised, initiating a process where haemostasis and blood coagulation became active in initial days following the wound infliction (Sveen *et al*. 2019).

Subsequently, by the 3^{rd} day, a slight regeneration of the wounded fin became apparent. On 7^{th}, 10^{th}, 14^{th} day regeneration is enlarged. and 21^{st} day, the caudal fin regenerated to the normal homocercal lobed position. The structural elements likely contribute to the preliminary wound surface smoothing, facilitating the early migration of keratocyte cells (Sveen *et al.* 2018). Rapid rearrangements of these cells during migration are made possible by cells extensively from the neighbouring epidermis. The primary source of the keratocytes is proposed to be the inter-scale pockets, underscoring the significance of scales and scale pockets in the rate re-epithelialization (Richardson *et al*. 2016). The process of skin regeneration is primarily characterized by re-epithelialization, followed by the regeneration of scales. Within 21 days of the initial injury, the skin fully regenerated including scales and pigmentation (Richardson *et al*. 2013). The fishes were treated with 100 µg/mL of ethyl acetate and methanol extracts of *R. tetraphylla* which showed maximum fin regenerated on the 21^{st} day than control. Histochemical analysis further confirmed the regeneration of tissues (Fig. 36). Control group showed least neutrophils than sample group treated with the ethyl acetate and methanol extracts.

Similarly, Shaibi *et al*. (2022) studied wound healing effects of ethanol extract of *Turbinaria ornate* (Turner) J. Agardh, that the treated group showed a higher neutrophil count compared to the control group, consistent with our observations. The presence of bioactive components in *R. tetraphylla* suggests its potential as a therapeutic agent for wound healing. *R.*

tetraphylla contained various phytoconstituents such as alkaloids, flavonoids, tannins, terpenoids, saponins, polyphenols, and glycosides (Mahalakshmi *et al*. 2019). These natural compounds are recognized for their potential in promoting wound healing (Kan *et al*. 2023).

Comprehended the molecular-level effects on wound healing, the transcriptional response of genes plays a key role in tumour necrosis factor-alpha (TNF-α), an inflammatory cytokine in the inflammation phase; transforming growth factor-beta (TGF-β) is a multifunctional growth factor regulating various aspects of wound healing and interleukin-10 (IL-10), a cytokine produced by different cell types of post-injury. Additionally, matrix metalloproteinases (MMPs), particularly MMP13 and MMP-9, showed significant roles in angiogenesis, keratinocyte migration, and wound contraction (Rajapaksha *et al*. 2020). Our study promised a positive effect on wound healing and based on the histological observation of *R. tetraphylla* showed a multifaceted role as a therapeutic agent which stimulates fast healing of wounded sites.

4.22. Isolation of TDC gene

Tryptophan decarboxylase (TDC) gene present in *R. tetraphylla* which promotes the biosynthesis of monoterpenoid indole alkaloids (MIAs) (Liu *et al*., 2012). It was identified in many medicinal plants, including *Rauvolfia verticillate* (Lour.) Baill. var. TDC gene meticulously isolated using DNeasy plant mini kit (Varma *et al*., 2007) method in *R. tetraphylla.* TDC from *R. verticillate* is used as a reference sequence for primer design. PCR was used to isolate the TDC sequence from *R. tetraphylla* (Fig. 37). Sequenced PCR product obtained and confirmed the TDC gene using Sanger sequencing method and deposited in NCBI portal (Accession No: OR105870). This gene was aligned with 95.39% of similarities of *R. verticillate.* This information is important for the secondary metabolic pathway to produce indole alkaloids in *Rauvolfia tetraphylla*.

TDC is an enzyme, catalysed for the formation of tryptamine (López-Meyer and Nessler, 1997; O'Connor and Maresh, 2006). It was first obtained in *C. roseus* to produce vincristine, an indole alkaloid (De Luca *et al*., 1989). In *Capsicum annuum* L., *Ophiorrhiza pumila* Champ. ex Benth., *Oryza sativa* L., and *R. verticillate*, TDC gene was observed by homology cloning (Yamazaki *et al*., 2003; Kang *et al*. 2007; Park *et al*. 2009).

In *R. verticillate* TDC gene was isolated which is responsible for enzyme activity (Liu *et al*. 2012). CanTDC1 and CanTDC2 are two TDC gene were obtained in *C. annuum*. CanTDC1 exhibited highly induced expression in response to elicitors, while CanTDC2 showed constitutive expression at a minimum level (Park *et al*. 2009). Seven genes were isolated in *O. sativa* in which two genes (OsTDCAK31 and OsTDCAK53) showed effective response in *E. coli*. TDC encoding gene identified after the discovery of catalytic decarboxylation in medicinal plants (Kang *et al*. 2007).

TDC gene (CaTDC1 and CaTDC2) from *Camptotheca acuminata* Decne produce camptothecin compound by enzyme decarboxylation of L-tryptophan (López-Meyer and Nessler, 1997). Moreover, gene expression studies (Góngora-Castillo *et al*. 2012) and data from sequencing the genome (Zhao *et al*. 2017; Kang *et al*. 2021) have proposed existence of additional TDCs in *C. acuminata*. CaTDC3 from *C. acuminata* further confirmed the catalysis for L-tryptophan (Qiao *et al*. 2022). Therefore, it was speculated that TDC gene from *R. tetraphylla* involved in indole alkaloid synthesis, and it provides further investigations by gene manipulation.

4.22.1. Prediction of Protein

3D structure of TDC monomer model predicted using SWISS MODEL with reference to *Cantharanthus roseus*, hence TDC monomer was an unknown 3D structure.

In *C. roseus*, the protein is annotated as TDC due to its known substrate specificity (De Luca *et al*. 1989), making its reference model for comparison with Citrus pTDC (Facchiano *et al*. 2019). Comparative modelling has been successful due to its reliance on two crucial assumptions. The first assumption is that structural similarity implies functional resemblance. The second assumption is that the folding of homologous proteins is better conserved than their amino acid sequences. Leveraging these principles, comparative modelling has proven to be an effective method for predicting the 3D structures of proteins by utilizing information from related homologous proteins (Facchiano, 2017).

In RCSB PDB database have lack of TDC secondary metabolite proteins from *R. tetraphylla* and it was curated from SWISS MODEL. Hence, optimized template (PDB ID 6EEW) was used for built the 3D model which contain 500 amino acids. The quality and

suitability of this template for modelling the target protein, assessed by two critical metrics – Global Model Quality Estimate (0.97) and Sequence-Overlap Quality (0.88). This high sequence similarity (88.96%) indicated significant correlation between target and template, enhanced reliability of the model. This template-based approach holds great potential for gaining insights into the structural and functional characteristics of target protein.

Saves server tool were used to examine the Ramachandran plot for homology model (Fig. 38), elaborated stereochemical quality of protein structure including distribution of phi (ϕ) and psi (ψ) angles (Sheik *et al*. 2002; Laskowski *et al*. 2013). In this present study over 90% of residues of protein were occupied favourable region in the Ramachandran plot. It indicated energetically favourable and most stable conformations, while the allowed region represents conformations that are sterically permissible. This high percentage of residues falling within these regions signifies that the homology models have adopted favourable and permissible conformations.

Validation of durability of the protein model by Deep View Swiss PDB tool (Guex *et al*. 2009). This observation is crucial as steric hindrances, caused by clashes between atoms, could lead to unstable protein structures. In this presence study, steric hindrances were not observed between the residue model. Hence, it suggested that the 3D protein structures were free from hindrances. It recommended strong evidence supporting the reliability and stability of the homology models.

4.22.2. Multiple Sequence Alignment of *RtTDC*

Analogously *R. tetraphylla*, TDC encompassed 1,500 bp (499 aa) with *RvTDC* and TDC sequence is a conserved region for the *R. verticillata* (Rv), *R. tetraphylla* (Rt), and *C. roseus* (Cr), represented in Fig. 39. Conserved regions in the alignment are areas where the amino acid residues are highly similar or identical across the different sequences, suggested that these regions have important functional or structural roles that are conserved throughout evolution.

One of the main functions of Tryptophan Decarboxylase is to facilitate the decarboxylation of L-tryptophan, an essential amino acid, to produce tryptamine. Tryptamine serves as a precursor for various indole alkaloids, which have important roles in the physiology and defence mechanisms of plants. The conserved region identified in the multiple sequence alignment likely encompasses key residues involved in the catalytic mechanism of

decarboxylation. Moreover, the conserved region may also include residues critical for the interaction with substrates. It plays a crucial role in substrate binding and positioning, allowing the enzyme to efficiently catalyse the decarboxylation reaction. The presence of conserved regions among TDC sequences from different plant species (*Rv, Rt,* and *Cr*) suggested that Tryptophan Decarboxylase has been evolutionarily conserved over time. This conservation indicated the significance of this enzyme in the biosynthetic pathways of alkaloids, which have essential functions in various biological processes in plants

RtTDC exhibited high analogous to various aminoacid residues of plant TDCs (López-Meyer and Nessler, 1997; Liu *et al*. 2012), and predictable that Lys319 plays a key role in *RtTDC* enzymatic activity. *C. roseus* (*CrTDC*) (De Luca *et al*. 1989), *O. pumila* (*OpTDC*) (Yamazaki *et al*. 2003), *R. verticillata* (*RvTDC*) (Liu *et al*. 2012) and *Gelsemium sempervirens* (*GsTDC*) (Franke *et al*. 2019) are some medicinal plants contained TDC gene. It suggested that *RtTDC* have related enzymatic activity with these characterized TDCs. Understanding the functional significance of the conserved region in the Tryptophan Decarboxylase enzyme can have practical implications, such as facilitating protein engineering or drug discovery efforts.

4.22.3. Phylogenetic Tree with Related Sequences

Phylogenetic tree showed three clades (Fig. 40), in which one of the branches showed common ancestor for *RtTDC*, TDC CATRO, RAUVE and ORYSJ. Among them *RtTDC* exhibited close relationship with RAUVE. The result from the neighbour-joining (1000 bootstrap) phylogenetic analysis of 12 demonstrative species within flowering plants suggested that *R. tetraphylla* is closely related to *R. verticillata*. *C. roseus* (Mehrotra *et al*. 2013), *R. verticillata* (Liu *et al*. 2012), *O. sativa* (Kang *et al*. 2007) evaluated Tryptophan decarboxylase can act as an enzyme to produce alkaloids. In addition, Phylogenetic analysis maintained this suggestion as TDC sequences in the second branch contain terpenoid indole alkaloids.

4.22.4. Physicochemical Characterization of TDC

Expasy's Prot-param tool were used to predict physicochemical character of Tryptophan Decarboxylase (Table 26). It contained 499 amino acids, 55,729.29 Daltons of molecular weight, 5.37 theoretical isoelectric point (pI), 70,860 M^{-1} cm^{-1} extinction coefficient, 47.92 instability

index, 94.19 aliphatic index, and 0.029 Grand Average of Hydropathicity (GRAVY) were analysed. The Prot-param analysis also revealed the distribution of charged residues within the protein. It contained 61 negatively charged residues, comprising aspartic acid (Asp) and glutamic acid (Glu), and 48 positively charged residues, including arginine (Arg) and lysine (Lys). Kyte and Doolittle hydrophobicity plot of *RtTDC* protein (Fig. 41) observed high hydrophobicity with the GRAVY value. These parameters play significant roles in determining the protein's structure, function, and interactions with other molecules.

There are 20 standard amino acids residues observed in *RtTDC* (Table 27), leucine (L) is the most abundant, with a total count of 57 residues, consisted 11.4% of the protein. Following closely, alanine (A) and serine (S) each account for 8.0% and 8.2% of the protein, respectively, with 40 and 41 residues present. Other amino acids that contributed notably to the protein's composition include valine (V) at 7.6% (38 residues), glutamic acid (E) at 7.0% (35 residues), and threonine (T) at 6.4% (32 residues). A set of amino acids with moderate representation includes glycine (G) at 5.0% (25 residues), aspartic acid (D) at 5.2% (26 residues), and proline (P) at 5.0% (25 residues). Additionally, isoleucine (I), lysine (K), and methionine (M) each account for 5.0% (25, 25, and 17 residues, respectively), while phenylalanine (F) and arginine (R) contribute 4.6% (23 residues each). Asparagine (N) and tyrosine (Y) represent 3.2% (16 residues) and 2.8% (14 residues) of the protein composition, respectively. The remaining amino acids – cysteine (C), glutamine (Q), histidine (H), and tryptophan (W) - showed relatively lower abundance, each contributing approximately 1.8% (9 residues) to the overall amino acid content.

C. roseus TDC and *Drosophila melanogaster* DDC1 showed structural similarities using hydropathy profile, except for the regions near the amino terminus. The amino acid sequence comparison between *C. roseus* TDC and *D. melanogaster* DOPA decarboxylase (DDC) revealed 39% similarity (De Luca *et al*. 1989; Goddijn *et al*. 1994).

Campotheca TDC1compared with *Catharanthus* TDC showed 69% similarity index. Remarkably, a stretch of 40 amino acid residues surrounding the pyridoxal phosphate binding site was found to be completely identical in both enzymes (López-Meyer and Nessler, 1997). Furthermore, De Masi *et al*. (2017) examined an extensive search in *Citrus* genome databases and identified putative TDC (pTDC) sequences by comparing them to the known *C. roseus* TDC sequence. Based on these results, it suggested that *RtTDC* have similar properties. This

comprehensive analysis of the protein's Tryptophan Decarboxylase emphasizes molecular features and its potential implications in various biochemical processes.

4.22.5. Secondary Structure Prediction of TDC

HNN software is used to predict secondary feature of *RtTDC* protein and presented in Fig. 42 (a-b), indicating that these amino acids have high helix-forming propensities, making alpha helix the dominant secondary structure in these proteins. This observation is also supported by the analysis of the HNN result.

The secondary structure analysis of the protein revealed alpha helix (Hh) (253 residues), approximately 50.70% of the protein. In contrast, there are no residues found in the 310 helix (Gg), Pi helix, or beta bridge (Bb) and beta turn (Tt) or bend region (Ss) categories. However, extended strand (Ee) in the protein contained 61 residues (12.22%).

Random coil (Cc) contained 185 residues (37.07%), it lacked a well-defined regular structure and are often associated with flexible regions in the protein. These regions played an essential role in facilitating protein-protein interactions, substrate binding, or enzymatic activities. The secondary structure analysis provided a conformational feature of the protein, aiding in understanding its potential functions and structural characteristic feature. The prevalence of alpha helices and extended strands suggested that regions of stable and organized structures within the protein. Furthermore, the presence of a significant portion of random coils indicates flexible and dynamic regions that may be functionally relevant. The generated models exhibited structural properties that are consistent with TDCs. Hence, we utilized them for docking with Tryptophan (Trp) to gather more insights and validate the binding site properties and the specific amino acids that are involved in the binding process.

In this present study, *RtTDC* sequence were isolated and characterized a full-length DNA. The first study of this gene in this species, revealed significant similarity to TDC proteins in other species. Notably, Pyridoxal phosphate (PLP) functions as a coenzyme and forms a Schiff-base linkage (internal aldimine) with a specific lysine residue in the decarboxylase enzyme during certain amino acid decarboxylation reactions (Toney, 2005). *RvTDC* (Liu *et al*. 2012) showed Lys319 residue directly participated in binding to pyridoxal phosphate-binding proteins and conserved in other decarboxylases, including 3,4-dihydroxyphenylalanine (DOPA)

decarboxylases from *C. acuminata* (Lopez-Meyer and Nessler, 1997). Furthermore, the presence of similarities around the PLP binding site in other decarboxylases, such as pig kidney DDC (Bossa *et al*. 1977), *D. melanogaster* DDC (Clark *et al*. 1978), and feline glutamate decarboxylase (Kobayashi *et al*. 1987) and periwinkle TDC (De Luca *et al*. 1989), effectively suggested that lysine-319 of Tryptophan decarboxylase is key enzyme for binding to PLP. Based on these verdicts, it can be inferred that the observed amino acid differences between *RtTDC* proteins are not likely to significantly affect their secondary structures.

4.22.6. Ligand Binding to *RtTDC*

Docking analysis were carried out by 3D structure of *RtTDC* protein as receptor and L-tryptophan as ligand. AutoDock 4.2.6 was used to dock the ligands with the target protein. The results revealed that highest binding energy (-4.69) with RMSD value as shown in Table 28. Each entry represented a substructure with its corresponding ranks and values. The goal is likely to identify the most favourable substructures based on these properties.

The binding affinity between protein and ligand were visualized by pharmacophore model (Fig. 43). Pharmacophore-based drug design is used to identify the key features required for a compound to bind to a specific receptor and induce the desired biological effect. In docking studies, the pharmacophore is used to guide the ligand towards the active site of the receptor by identifying the key chemical interactions that are necessary for binding.

The results of the molecular docking suggested that *RtTDC* may detect L-tryptophan derivatives, due to the relatively large spatial volume of enzyme pocket. Therefore, *RtTDC* has the capability to catalyse the L-tryptophan analogs due to their potential recognition by the enzyme's relatively spacious catalytic pocket. Tryptophan Decarboxylases of plant act as a catalyst to remove carbon-di-oxide from L-tryptophan and 5-hydroxy-L-tryptophan (Torrens-Spence *et al*. 2014; Günther *et al*. 2019).). Amines from plants significant in various pathways, especially alkaloid biosynthesis (Torrens-Spence *et al*. 2020).

Aromatic amines are fundamental molecules found in all living organisms, and their synthesis is facilitated by aromatic amino acid decarboxylases (AADCs). Plant AADCs, including Tryptophan Decarboxylases, exhibit diverse substrate specificities, contributing to the synthesis of biogenic amines essential for various metabolic pathways in plants (Kang *et al*.

2021). This enzymatic process is crucial for unravelling the complexities of plant metabolism and potential applications in drug discovery and biotechnology.

Protein-ligand interactions are crucial for numerous biological processes. Hydrogen bond interactions are based on molecular complementarity and enable the transmission of signals through ligands. Hydrogen bond between *RtTDC* and L-tryptophan interaction were depicted in Fig. 44. Confirmation of the binding properties of *R.tetraphylla* TDC active site with the substrate L-tryptophan were evaluated by docking simulations. This information provides valuable insights into the binding mechanism of TDC with its substrate and aids in understanding the enzyme-substrate interaction.

In a previous TDC comparison, the analysis of amino acid sequence alignments from both plant and animal kingdoms revealed a remarkable level of sequence conservation, with high similarity in sequence and structural motifs (Facchini *et al*. 2000; De Luca *et al*. 1989). Fig. 45 showed *RtTDC* binding pocket residues interacting with Trp from molecular docking simulations. Similarly, Facchiano et al. (2019) identified Lys319 as a key residue in *C. roseus* TDC binding to L-tryptophan.

4.22.7. TDC Enzymatic Assay

Tryptophan decarboxylase enzyme play a crucial role in terpenoid indole alkaloid biosynthetic pathway (Fig. 46). TDC catalytic activity of *R. tetraphylla* were analysed, as shown in the provided figure 47. The HPLC retention time of the catalytic reaction product matched with tryptamine, confirming that *RtTDC* decarboxylates L-tryptophan to produce tryptamine, a key step in alkaloid biosynthesis in *R. tetraphylla*. The efficient decarboxylation of diverse substrates by CaTDC3 highlights its potential as a versatile tool in synthetic biology to produce pharmaceutical compounds (Qiao *et al*. 2022).

Tryptophan exhibited efficacy as a topical agent for wound healing which inhibiting stress-induced reductions in myofibroblast density, collagen deposition, and wound contraction, while enhancing cell migration and activate protein kinase in phosphorylation of dermal fibroblasts under high epinephrine levels (Barouti *et al*. 2015). Moreover, tryptophan may accelerate cutaneous wound healing in stressed mice by reducing inflammatory response and indoleamine 2,3-dioxygenase expression (Bandeira *et al*. 2015). The tryptophan indole pathway

converts tryptophan into indole and its derivatives, showing potential implications in wound healing and tissue repair due to their anti-inflammatory, antimicrobial, and immunomodulatory properties. Indole compounds may reduce inflammation, prevent infections, and promote immune balance, supporting tissue regeneration (Jin *et al*. 2014; Elías-Arnanz *et al*. 2010; Bansal *et al*. 2010). Yet, further research is necessary to understand their mechanisms and therapeutic applications in wound management. The TDC gene is isolated from *R. tetraphylla* due to its potential involvement in tryptophan metabolism and the production of tryptamine. However, further studies would be necessary to elucidate the potential therapeutic implications of this gene in wound healing.

4.23. MOLECULAR DOCKING ANALYSIS

Concerning side effects of conventional treatments, plant-derived medicines emerge as promising alternatives. The potential of *R. tetraphylla* in wound healing mechanisms, active bioactive constituents of *R. tetraphylla* were examined. The objective was to anticipate the most probable binding interactions between these plant-derived ligands and specific proteins associated with wound healing through docking analysis. This computational approach holds immense significance in drug development, enabling the screening of potential candidates before embarking on costly and time-consuming *in vitro* and *in vivo* experiments. Through this docking study, the compounds identified by GCMS and LCMS analysis could potentially interact with key proteins involved in wound healing processes.

4.23.1. Docking

In silico docking were analysed using wound healing protein (6Y8M, 6B8Y, 1GEN) with selected compounds (1,9-Nonanediol, 1D-1-O-Methyl-myo-inositol, (Z)-2-methylbutanal oxime, 3-O-methyl-D-glucose, 7-[3-Chloro-2-hydroxypropyl]guanine, 1-Naphthalenepropanol,.alp, Butyl cyclohexyl phthalate, Serpentine, Yohimbine, Isoreserpinine, Darcyribeirine, Reserpiline, and Carapanaubine).

In the context of the protein structure with PDB ID 6Y8M, various ligands were docked, and their binding affinities were evaluated (Table 29). Among these ligands, compounds such as 1,9-Nonanediol (-4.59 kcal/mol), 1D-1-O-Methyl-myo-inositol (-4.29 kcal/mol), and (Z)-2-methylbutanal oxime (-4.12 kcal/mol) exhibited moderate binding affinities, interacting with

amino acid residues including LEU134, PHE133, GLU25, THR79 and VAL132. Conversely, compounds like 7-[3-Chloro-2-hydroxypropyl]guanine (-5.82 kcal/mol), Butyl cyclohexyl phthalate (-7.67 kcal/mol), and Isoreserpinine (-8.25 kcal/mol) displayed stronger binding affinities, forming interactions with amino acids like PHE133, LEU134, LEU80 and GLU25. Notably, Reserpiline (-7.78 kcal/mol) and Carapanaubine (-7.77 kcal/mol) exhibited relatively lower binding affinities, yet still interacting with critical residues such as PHE133, GLN81, LEU82, SER84, TYR24 and GLU25. It offered the potential ligand-protein interactions within the given protein structure, which could aid in further understanding their pharmacological significance and potential therapeutic applications.

In the protein structure with PDB ID 6B8Y, various ligands were docked and assessed for their binding energies, ligand efficiencies, and inhibitor constants (Table 30). 1,9-Nonanediol (-5.36 kcal/mol), 1D-1-O-Methyl-myo-inositol (-5.69 kcal/mol) and (Z)-2-methylbutanal oxime (-5.30 kcal/mol) showed moderate binding affinity interacted with amino acids such as ALA403, ASP400, ARG332, and LEU334. In addition, compounds like 7-[3-Chloro-2-hydroxypropyl]guanine (-6.62 kcal/mol), Butyl cyclohexyl phthalate (-7.70 kcal/mol) and Carapanaubine (-8.63 kcal/mol) displayed strong binding affinities. 1-Naphthalenepropanol (-7.71 kcal/mol), Serpentine (-7.2 kcal/mol), Yohimbine (-7.0 kcal/mol), Isoreserpinine (-7.63 kcal/mol), Darcyribeirine (-6.56 kcal/mol), and Reserpiline (-7.1 kcal/mol) also formed significant interactions with specific amino acids.

In the protein structure with PDB ID 1GEN (Table 31), and various ligands examined, which revealed their binding energies, ligand efficiencies, and inhibitor constants. 1,9-Nonanediol (-4.79 kcal/mol), 1D-1-O-Methyl-myo-inositol (-4.52 kcal/mol), and (Z)-2-methylbutanal oxime (-4.58 kcal/mol) exhibited moderate interactions. Exemplified, compounds like 7-[3-Chloro-2-hydroxypropyl]guanine (-7.16 kcal/mol), 1-Naphthalenepropanol (-7.69 kcal/mol), and Carapanaubine (-8.22 kcal/mol) displayed strong binding affinities. Serpentine (-6.83 kcal/mol), Yohimbine (-6.23 kcal/mol), Isoreserpinine (-5.98 kcal/mol), Darcyribeirine (-5.88 kcal/mol) and Reserpiline (-5.67 kcal/mol) also formed significant interactions with specific amino acids. Compared to other secondary metabolites alkaloids showed more binding affinity. It provides the potential ligand-protein interactions within the protein structure, which could aid in further understanding their pharmacological significance and potential therapeutic applications.

Poupon & Nay identified many alkaloids such as serpentinin, ajmaline, sandwicine, sandwicencine, tetraphylline, tetraphyllicin and mauiensine from *Rauvolfia* genus (Poupon & Nay, 2011). Alkaloids belonging to the family of Ajmalines common to genus *Rauvolfia* are exploited in pharmacology due to their anti-arrhythmic, anti-depressive, antioxidant and anti-tumoral activities. *From R. nukuhivensis*, Martin *et al*. (2012) isolated derivatives of indolo [2,3-a] quinolizinium (nukuhivensium and N12-methyl-nukuhivensium) and demonstrated their anti-arrhythmic activity, by their action on the hERG potassium channel. *Stryphnodendron adstringens* (*barbatimão*) is a tannin-rich Brazilian native plant and its wound-healing properties have been described in the literature since the colonial period (Drigo *et al*., 2024). *Barbatimão* is mainly used in topical preparations made from the bark of the stem in macerations, infusions, and decoctions. Martin *et al*. (2015) investigated the biological effects induced by RNE stimulation in human keratinocytes. Our study showed positive effect on wound healing and based on the observation of biological activities from *R. tetraphylla* showed multifaceted role as a therapeutic agent which stimulates wound healing.

Table 1. Effect of surface sterilization of *Rauvolfia tetraphylla* L. seeds with Sodium hypochlorite (1%) and mercuric chloride (0.1%).

S. No.	$NaHCl_3$/Min	$HgCl_2$/Min	Percentage of sterile plantlets
1	10	1	84.11 ± 0.59
2	15	2	91.55 ± 0.36
3	20	3	98.44 ± 0.37

Table 2. Germination percentage of *Rauvolfia tetraphylla* L. seeds

S. No	No. of Seed tested	No. of seed germination	Percentage of germination	Mean ± SD
1	control	0	0	0
2	25	22	88	83.33±4.74
3	20	15	75	
4	30	25	83.33	

Table 3. Effect of different plant growth hormones on callus formation (%) from leaf, node, internode, and root explants of *Rauvolfia tetraphylla* L.

Hormones	**Concentrations (mg/L)**	**Leaf explants**	**Node explants**	**Internode explants**	**Root explants**
IAA	0.5	22.40 ± 0.39^{e}	11.37 ± 0.42^{e}	05.51 ± 0.34^{e}	02.40 ± 0.39^{e}
	1.0	28.62 ± 0.41^{d}	14.48 ± 0.34^{d}	11.37 ± 0.42^{d}	04.48 ± 0.34^{d}
	1.5	35.51 ± 0.34^{c}	16.55 ± 0.36^{c}	16.55 ± 0.36^{c}	08.62 ± 0.41^{c}
	2.0	42.40 ± 0.39^{b}	21.37 ± 0.42^{b}	22.40 ± 0.39^{b}	13.44 ± 0.37^{b}
	2.5	**51.37** ± 0.42^{a}	**23.44** ± 0.37^{a}	**28.08** ± 0.27^{a}	**16.55** ± 0.36^{a}
IBA	0.5	19.86 ± 0.40^{e}	08.44 ± 0.37^{e}	03.94 ± 0.40^{e}	01.45 ± 0.36^{e}
	1.0	25.75 ± 0.50^{d}	13.45 ± 0.36^{d}	10.50 ± 0.33^{d}	03.51 ± 0.34^{d}
	1.5	30.58 ± 0.38^{c}	20.16 ± 0.55^{c}	17.59 ± 0.39^{c}	07.58 ± 0.38^{c}
	2.0	37.41 ± 0.38^{b}	23.44 ± 0.37^{b}	23.44 ± 0.37^{b}	11.38 ± 0.41^{b}

	2.5	**41.93** ± 0.25[a]	**26.58** ± 0.38[a]	**30.16** ± 0.22[a]	**15.58** ± 0.39[a]
2,4-D	0.5	34.48 ± 0.34[e]	22.40 ± 0.39[e]	43.44 ± 0.37[e]	13.44 ± 0.37[e]
	1.0	38.62 ± 0.41[d]	26.55 ± 0.36[d]	48.62 ± 0.41[d]	15.51 ± 0.34[d]
	1.5	44.00 ± 0.66[c]	31.37 ± 0.42[c]	54.48 ± 0.34[c]	17.59 ± 0.39[c]
	2.0	55.73 ± 0.61[b]	38.62 ± 0.41[b]	59.33 ± 0.44[b]	20.50 ± 0.33[b]
	2.5	**67.22** ± 0.52[a]	**46.55** ± 0.36[a]	**65.14** ± 0.56[a]	**22.41** ± 0.38[a]
BAP	0.5	25.51 ± 0.34[e]	26.55 ± 0.36[e]	38.46 ± 0.30[e]	27.58 ± 0.38[e]
	1.0	36.83 ± 0.55[d]	33.44 ± 0.37[d]	44.48 ± 0.34[d]	33.45 ± 0.36[d]
	1.5	43.58 ± 0.38[c]	37.59 ± 0.39[c]	50.50 ± 0.33[c]	38.62 ± 0.41[c]
	2.0	50.20 ± 0.53[b]	47.58 ± 0.38[b]	56.55 ± 0.36[b]	44.48 ± 0.34[b]
	2.5	**58.58** ± 0.38[a]	**55.51** ± 0.34[a]	**62.40** ± 0.39[a]	**51.41** ± 0.38[a]
IAA+IBA	0.5+0.5	35.08 ± 0.44[e]	27.59 ± 0.39[e]	16.55 ± 0.36[e]	15.51 ± 0.34[e]
	1.0+1.0	43.44 ± 0.37[d]	33.45 ± 0.36[d]	22.40 ± 0.39[d]	20.41 ± 0.38[d]
	1.5+1.5	51.55 ± 0.36[c]	38.62 ± 0.41[c]	28.62 ± 0.41[c]	27.59 ± 0.39[c]
	2.0+2.0	59.58 ± 0.38[b]	44.48 ± 0.34[b]	32.50 ± 0.33[b]	33.44 ± 0.37[b]
	2.5+2.5	**71.55** ± 0.36[a]	**51.41** ± 0.38[a]	**37.59** ± 0.39[a]	**38.62** ± 0.41[a]
IAA+2,4-D	0.5+0.5	44.46 ± 0.35[e]	35.51 ± 0.34[e]	33.44 ± 0.37[e]	07.22 ± 0.52[e]
	1.0+1.0	50.08 ± 0.61[d]	42.40 ± 0.39[d]	43.44 ± 0.37[d]	11.00 ± 0.66[d]
	1.5+1.5	61.37 ± 0.42[c]	46.55 ± 0.36[c]	48.62 ± 0.41[c]	17.59 ± 0.39[c]
	2.0+2.0	66.53 ± 0.35[b]	53.44 ± 0.37[b]	56.55 ± 0.36[b]	23.44 ± 0.37[b]
	2.5+2.5	**72.40** ± 0.39[a]	**62.41** ± 0.38[a]	**66.51** ± 0.34[a]	**30.50** ± 0.33[a]
IAA+BAP	0.5+0.5	38.62 ± 0.41[e]	28.62 ± 0.41[e]	40.70 ± 0.46[e]	04.48 ± 0.34[e]
	1.0+1.0	45.51 ± 0.34[d]	33.45 ± 0.36[d]	44.48 ± 0.34[d]	08.62 ± 0.41[d]
	1.5+1.5	52.40 ± 0.39[c]	41.38 ± 0.41[c]	50.70 ± 0.46[c]	15.51 ± 0.34[c]
	2.0+2.0	57.59 ± 0.39[b]	46.58 ± 0.38[b]	55.51 ± 0.34[b]	21.03 ± 0.69[b]
	2.5+2.5	**66.55** ± 0.36[a]	**53.41** ± 0.38[a]	**61.37** ± 0.42[a]	**26.55** ± 0.36[a]
IBA+2,4-	0.5+0.5	33.76 ± 0.82[e]	30.58 ± 0.38[e]	47.59 ± 0.39[e]	05.51 ± 0.34[e]

D	1.0+1.0	41.63 ± 1.11^{d}	35.51 ± 0.34^{d}	54.48 ± 0.34^{d}	11.38 ± 0.41^{d}
	1.5+1.5	49.88 ± 1.25^{c}	42.50 ± 0.33^{c}	58.62 ± 0.41^{c}	16.55 ± 0.36^{c}
	2.0+2.0	58.77 ± 0.81^{b}	48.61 ± 0.41^{b}	63.44 ± 0.37^{b}	22.40 ± 0.39^{b}
	2.5+2.5	**66.99** ± 0.88^{a}	**56.55** ± 0.36^{a}	**68.41** ± 0.38^{a}	**27.88** ±0.88^{a}
2,4-D+BAP	0.5+0.5	46.55 ± 0.36^{e}	45.51 ± 0.34^{e}	33.81 ± 0.54^{e}	44.48 ± 0.34^{e}
	1.0+1.0	55.51 ± 0.34^{d}	53.44 ± 0.37^{d}	40.41 ± 0.38^{d}	50.41 ± 0.38^{d}
	1.5+1.5	67.59 ± 0.39^{c}	61.37 ± 0.42^{c}	49.50 ± 0.33^{c}	61.37 ± 0.42^{c}
	2.0+2.0	76.18 ± 0.54^{b}	72.40 ± 0.39^{b}	61.37 ± 0.42^{b}	72.40 ± 0.39^{b}
	2.5+2.5	**88.62** ± 0.41^{a}	**83.45** ± 0.36^{a}	**79.66** ± 0.55^{a}	**84.11** ± 0.59^{a}

Values represent mean ± standard deviation of three replicates per treatment. Means in a column with same letter are significantly ($p \leq 0.05$) difference according to Duncan's Multiple Range Test

Table 4. Influence of different PGRs on direct root formation from leaf and nodal explants of *Rauvolfia tetraphylla* L.

Hormones	Concentrations (mg/L)	Leaf explants	Nodal explants
IAA	0.5	03.44 ± 0.37^{c}	02.50 ± 0.33^{c}
	1	09.50 ± 0.33^{b}	12.83 ± 0.77^{b}
	1.5	**16.55** ± 0.36^{a}	**37.58** ± 0.38^{a}
2,4-D+BAP	0.5+0.5	13.44 ± 0.37^{c}	33.77 ± 0.81^{c}
	1.0+0.5	20.00 ± 0.66^{b}	50.00 ± 0.66^{b}
	1.5+0.5	**26.55** ± 0.36^{a}	**62.77** ± 0.51^{a}
IAA+BAP	0.5+0.5	37.44 ± 0.37^{c}	24.00 ± 0.66^{c}
	1.0+0.5	62.58 ± 0.38^{b}	52.50 ± 0.33^{b}
	1.5+0.5	**87.50** ± 0.33^{a}	**83.16** ± 0.55^{a}
IBA+BAP	0.5+0.5	13.16 ± 0.55^{c}	32.43 ± 0.95^{c}
	1.0+0.5	25.66 ± 0.44^{b}	47.50 ± 0.33^{b}
	1.5+0.5	**35.50** ± 0.33^{a}	**63.16** ± 0.55^{a}

Values represent mean ± standard deviation of three replicates per treatment. Means in a column with same letter are significantly ($p \leq 0.05$) difference according to Duncan's Multiple Range Test

Table 5. Influence of PGRs on direct and multiple shoot induction from nodal explants of *Rauvolfia tetraphylla* L.

Hormones	Concentrations (mg/L)	Direct shoots (%)	Multiple shoots (%)
BAP	0.5	25.50 ± 0.33^{c}	21.55 ± 0.36^{c}
	1	41.55 ± 0.36^{b}	38.44 ± 0.37^{b}
	1.5	**58.44** ± 0.37^{a}	**55.00** ± 0.66^{a}
2,4-D+BAP	0.5+0.5	42.40 ± 0.49^{c}	41.00 ± 0.66^{c}
	1.0+1.0	58.41 ± 0.38^{b}	56.55 ± 0.36^{b}
	1.5+1.5	**78.44** ± 0.37^{a}	**73.44** ± 0.37^{a}
IAA+BAP	0.5+0.5	46.55 ± 0.36^{c}	55.00 ± 0.66^{c}
	1.0+1.0	67.21 ± 0.52^{b}	72.22 ± 0.52^{b}
	1.5+1.5	**83.44** ± 0.37^{a}	**88.44** ± 0.37^{a}
KIN+BAP	0.5+0.5	38.44 ± 0.37^{c}	43.44 ± 0.37^{c}
	1.0+1.0	54.01 ± 0.68^{b}	61.00 ± 0.66^{b}
	1.5+1.5	**75.00** ± 0.66^{a}	**76.55** ± 0.36^{a}

Values represent mean ± standard deviation of three replicates per treatment. Means in a column with same letter are significantly ($p \leq 0.05$) difference according to Duncan's Multiple Range Test

Table 6. Preliminary qualitative analysis on the phytochemicals of various crude extracts of leaves of *Rauvolfia tetraphylla* L.

S.No.	Tests	Hexane crude extract	Chloroform crude extract	Ethyl acetate crude extracts	Methanol crude extracts
1 A	**Alkaloids** Mayer's test	+	–	+	+
B	Wagner's test	+	–	+	+
C	Drangendorff's test	+	–	+	+
2 A	**Carbohydrates** Molisch's test	+	+	+	+
B	Fehling test	+	+	+	+
C	Barfoed test	+	+	+	+
D	Bendict's test	+	+	+	+
E	Legal's test	+	+	+	+
3	**Saponin test**	–	–	–	–

4	**Oils and fats test** Spot test	–	–	–	–
5 A	**Phenolic and tannin test** Ferric chloride Test	–	–	–	+
B	Gelatin test	–	–	–	+
C	Lead acetate test	+	–	–	++
D	Alkaline reagent test	–	–	–	+
E	Magnesium and hydrochloric acid test	–	–	–	+
6	**Quinones test**	+	–	++	+
7	**Glycosides test**	–	+	+	++
8	**Cardiac glycosides**	++	+	–	–
9	**Terpenoids**	++	+	+	+
10	**Coumarins test**	–	+	–	++
11	**Phlobatannins test**	–	+	–	–
12	**Steroids**	+	+	–	+
13	**Phytosteroids**	–	–	++	–
14	**Anthraquinones** (Borntrager's test)	–	–	–	–
15	**Flavonoids** (Shinoda test)	–	–	+	++
16	**Protein** (Xanthoproteic test)	+	–	++	+

"+" – Present; "-" Absent

Table 7. Preliminary qualitative analysis on the phytochemicals of various crude extracts of fruits of *Rauvolfia tetraphylla* L.

S. No.	Tests	Hexane crude extract	Chloroform crude extract	Ethyl acetate crude extracts	Methanol crude extracts
1 A	**Alkaloids** Mayer's test	+	–	+	+
B	Wagner's test	+	–	+	+
C	Drangendorff's test	+	–	+	+
2 A	**Carbohydrates** Molisch's test	+	+	+	+

B	Fehling test	+	+	+	+
C	Barfoed test	+	+	+	+
D	Bendict's test	+	+	+	+
E	Legal's test	+	+	+	+
3	**Saponin test**	–	–	–	–
4	**Oils and fats test** Spot Test	–	–	–	–
5 A	**Phenolic and tannin test** Ferric chloride Test	–	–	–	++
B	Gelatin test	–	–	–	++
C	Lead acetate test	+	+	–	++
D	Alkaline reagent test	–	–	–	++
E	Magnesium and hydrochloric acid test	–	–	–	++
6	**Quinones test**	++	+	++	+
7	**Glycosides test**	++	+	++	++
8	**Cardiac glycosides**	+	+	++	+
9	**Terpenoids**	++	++	++	–
10	**Coumarins test**	–	+	–	++
11	**Phlobatannins test**	–	+	–	–
12	**Steroids**	++	++	–	–
13	**Phytosteroids**	–	–	++	–
14	**Anthraquinones** (Borntrager's test)	–	–	+	+
15	**Flavonoids** (Shinoda test)	–	++	+	++
16	**Protein** (Xanthoproteic test)	+	–	++	+

"+" – Present; "-" Absent

Table 8. Absorbance of Standard Atropine for Alkaloids

S. No.	Concentration (µg/mL)	Absorbance of Atropine
1	0.4	0.052
2	0.6	0.068
3	0.8	0.077
4	1	0.094
5	1.2	0.109

Table 9. Absorbance of Standard Rutin Compound for Flavonoids

S. No.	Concentration (µg/mL)	Absorbance of Rutin
1	0.05	0.07
2	0.15	0.15
3	0.25	0.24
4	0.35	0.33
5	0.45	0.415
6	0.55	0.52
7	0.65	0.597
8	0.75	0.68

Table 10. Absorbance of Standard Gallic acid for Total Phenol Content

S. No.	Concentration (µg/mL)	Absorbance of Gallic acid
1	10	0.131
2	20	0.206
3	40	0.318
4	60	0.413
5	80	0.508
6	100	0.667

Table 11. Absorbance of Standard Gallic Acid for Tannin

S. No.	Concentration (µg/mL)	Absorbance of Gallic acid
1	20	0.164
2	40	0.273
3	60	0.343
4	80	0.42
5	100	0.507

Table 12. Quantitative Analysis of *Rauvolfia tetraphylla* in Various Extracts of Leaf and Fruit

S. No	Sample	Concentrations (µg/mL)	Alkaloids	Flavonoids	Phenols	Tannin
1	RLEA	1000	0.64	1.40	13.75	9.64
2	RLM	1000	3.52	1.92	14.63	29.16
3	RFEA	1000	1.07	0.71	11.43	14.64
4	RFM	1000	1.64	1.02	22.88	26.54

Table 13. GC-MS Profiles of the Compounds Identified from *Rauvolfia tetraphylla* L.

S. No	Retention time	Name of the compounds	Height	Area	Area (%)	Normality (%)	Molecular formula	Nature of compounds
1	**17.315**	1,9-Nonanediol	91,777,720	9,109,052.0	4.714	12.02	$C_9H_{20}O_2$	Aliphatic alcohol
2	**17.540**	3-Furanol, tetrahydro-2,2,4,4-tetramethyl-	125,240,072	19,966,596.0	10.333	10.333	$C_8H_{16}O_2$	cycloalkene
3	**17.680**	1D-1-O-Methyl-myo-inositol	126,342,728	75,778,064.0	39.216	100.00	$C_7H_{14}O_6$	sugar alcohol
4	**19.366**	(Z)-2-methylbutanal	43,191,7	12,842,7	6.64	16.95		aldoxime

		oxime	24	35.0	6		$C_5H_{11}NO$	
5	**19.806**	Arabino-heptitol, 2,3:5,6-dianhydro-1,7-dideoxy-2,6-di-C-methyl-	17,242,060	1,687,162.0	0.873	2.23	$C_9H_{16}O_3$	Sugar alcohol
6	**19.866**	3-O-methyl-D-glucose	13,506,950	1,865,415.9	0.965	2.46	$C_7H_{14}O_6$	Simple sugar
7	**22.757**	Butyl cyclohexyl phthalate	44,478,712	1,197,175.1	8.346	9.11	$C_{18}H_{24}O_4$	Phthalate Esters
8	**27.079**	7-[3-Chloro-2-hydroxypropyl]guanine	17,365,868	1,626,987.8	0.842	2.15	$C_8H_{10}ClN_5O_2$	nucleoside analogue
9	**29.320**	1-Naphthalenepropanol,.alp	12,684,078	1,935,868.5	1.002	2.55	$C_{20}H_{34}O$	Alcohol
10	**29.795**	1,3,3-trimethyl-2-hydroxymethyl-3,3-dimethyl-4-(3-methylbut-2-enyl)-cyclohexene	62,874,824	11,661,319.0	6.035	15.39	$C_{15}H_{26}O$	sesquiterpene alcohol
11	30.010	β-Amyrone	66,394,260	6,551,254.5	3.390	8.65	$C_{30}H_4O$	Triterpene
12	30.580	(+)-Helminthogermacrene	158,874,400	18,432,592.0	9.539	24.32	$C_{15}H_{26}$	Sesquiterpene

Table 14. LC-MS Profiles of the Compounds Identified from *Rauvolfia tetraphylla* L.

S. No.	Compound Name	Molecular formula	Molecular weight	m/z	Mode (+/-)
1	Oxodecenoic acid	$C_{10}H_{16}O_3$	184.23	183.0983	-
2	Naringenin	$C_{15}H_{12}O_5$	272.25	273.0366	+
3	Dihydrokaempferide	$C_{16}H_{14}O_6$	302.28	301.1407	-
4	Serpentine	$C_{21}H_{21}N_2O_3^+$	349.4	349.1547	-
5	Yohimbine	$C_{21}H_{26}N_2O_3$	354.44	355.2088	+
6	Isoreserpinine	$C_{22}H_{26}N_2O_4$	382.45	383.1972	+
7	Darcyribeirine	$C_{23}H_{26}N_2O_5$	410.46	411.1919	+
8	Reserpiline	$C_{23}H_{28}N_2O_5$	412.48	413.2159	+
9	Carapanaubine	$C_{23}H_{28}N_2O_6$	428.48	429.2021	+
10	Reserpine	$C_{33}H_{40}N_2O_9$	608.68	609.9797	+

Table 15. Antibacterial Activity of Leaf Extracts of *Rauvolfia tetraphylla* in Crude Extracts

Sample	Negative control	Positive control	Ethyl acetate extracts of Leaves				Methanol extracts of Leaves			
			Zone of inhibition (mm)							
Concentrations	**DMSO**	**Ampicillin**	**25 µg/mL**	**50 µg/mL**	**75 µg/mL**	**100 µg/mL**	**25 µg/mL**	**50 µg/mL**	**75 µg/mL**	**100 µg/mL**
Staphylococcus aureus	0	13	2	6	9	11	3	7	10	14
Escherichia coli	0	15	5	7	9	12	10	12	16	**19**
Enterococous faecalis	0	14	9	10	10.5	11	11	13	14	15

Table 16. Antibacterial Activity of Fruit Extracts of *Rauvolfia tetraphylla* in Crude Extracts

Sample	Negative control	Positive control	Ethyl acetate extracts of Fruits (mm)				Methanol extracts of Fruits (mm)			
			Zone of inhibition (mm)							
Concentrations	**DMSO**	**Ampicillin**	**25 µg/mL**	**50 µg/mL**	**75 µg/mL**	**100 µg/mL**	**25 µg/mL**	**50 µg/mL**	**75 µg/mL**	**100 µg/mL**
Staphylococcus aureus	0	13	3	7	8	11	2	4	6	10
Escherichia coli	0	15	4	6	9	12	10	12	14	19
Enterococous faecalis	0	14	8	9	10.5	11	10	11	12	15

Table 17. DPPH Radical Scavenging Activity of Standard Ascorbic Acid

S. No.	Conc. (µg/mL)	Ascorbic acid
1	20	28.91 ± 3.95^{c}
2	40	$42.64 \pm 4.07^{b, c}$
3	60	$69.13 \pm 5.60^{a, b}$
4	80	75.14 ± 2.71^{a}
5	100	81.14 ± 0.86^{a}
	IC_{50} Value	46.28

Values represent mean ± standard deviation of three replicates per treatment. Means in a column with same letter are significantly ($p \leq 0.05$) difference according to Duncan's Multiple Range Test

Table 18. DPPH Assay of Various Extracts of Leaves and Fruits of *Rauvolfia tetraphylla* L.

Conc. (µg/mL)	RL EA	RLM	RFEA	RFM
20	21.03 ± 2.38^{d}	27.41 ± 0.305^{d}	32.97 ± 0.43^{d}	35.30 ± 1.70^{e}
40	30.67 ± 1.71^{c}	42.54 ± 1.26^{c}	47.00 ± 0.60^{c}	45.69 ± 2.60^{d}
60	$34.78 \pm 0.57^{b, c}$	50.26 ± 0.18^{b}	49.43 ± 0.008^{b}	50.40 ± 0.65^{c}
80	40.29 ± 2.96^{b}	58.19 ± 0.56^{a}	$50.84 \pm 0.25^{b, c}$	54.70 ± 0.88^{b}
100	51.28 ± 1.45^{a}	65.55 ± 0.92^{a}	62.90 ± 0.10^{a}	63.28 ± 0.44^{a}
IC_{50} Value	101.02	62.61	64.27	**60.37**

Group a has the best treatment and group d & e has the poorest performing treatments. Values represent mean ± standard deviation of three replicates per treatment. Means in a column with same letter are significantly ($p \leq 0.05$) difference according to Duncan's Multiple Range Test

Table 19. Ferric Reducing Antioxidant Power (FRAP) Assay

Conc. (µg/mL)	RL EA (µM Fe+2/g)	RL M (µM Fe+2/g)	RF EA (µM Fe+2/g)	RF M (µM Fe+2/g)
20	0.7472^{e}	0.9914^{e}	0.2888^{e}	0.3106^{e}
40	1.0902^{d}	1.1882^{d}	0.7106^{d}	0.8953^{d}
60	1.3224^{c}	1.3531^{c}	0.8306^{c}	1.1377^{c}
80	1.5630^{b}	1.4428^{b}	1.1142^{b}	1.3955^{b}
100	1.6251^{a}	**1.6675^{a}**	1.4510^{a}	1.5359^{a}

Group a has the best treatment and group e has the poorest performing treatments. Values represent mean ± standard deviation of three replicates per treatment. Means in a column with same letter are significantly ($p \leq 0.05$) difference according to Duncan's Multiple Range Test

Table 20. Total Antioxidant Activity of Standard Ascorbic Acid

S. No.	Conc.(µg/mL)	Ascorbic acid
1	20	29.10 ± 0.005^{d}
2	40	34.02 ± 0.004^{d}
3	60	45.15 ± 0.002^{c}
4	80	58.20 ± 0.035^{b}
5	100	74.318 ± 0.001^{a}

Group a has the best treatment and group d has the poorest performing treatments. Values represent mean ± standard deviation of three replicates per treatment. Means in a column with same letter are significantly ($p \leq 0.05$) difference according to Duncan's Multiple Range Test

Table 21. Total Antioxidant Activity of Various Crude Extracts of Leaf and Fruit of *Rauvolfia tetraphylla* L.

Conc. (µg/mL)	RL EA	RLM	RFEA	RFM
20	28.45 ± 0.005^{e}	26.61 ± 0.004^{e}	31.04 ± 0.005^{d}	24.86 ± 0.005^{e}
40	38.96 ± 0.004^{d}	39.63 ± 0.005^{d}	35.86 ± 0.005^{c}	36.85 ± 0.004^{d}
60	45.53 ± 0.002^{c}	54.24 ± 0.003^{c}	44.404 ± 0.005^{b}	48.52 ± 0.004^{c}
80	50.61 ± 0.002^{b}	59.27 ± 0.004^{b}	47.41 ± 0.006^{b}	56.75 ± 0.002^{b}
100	53.99 ± 0.001^{a}	63.14 ± 0.003^{a}	52.707 ± 0.003^{a}	68.58 ± 0.003^{a}
IC_{50} Value	80.69	**63.05**	88.104	**65.37**

Group a has the best treatment and group e has the poorest performing treatments. Values represent mean ± standard deviation of three replicates per treatment. Means in a column with same letter are significantly ($p \leq 0.05$) difference according to Duncan's Multiple Range Test

Table 22. Anti-inflammatory Activity of Diclofenac Sodium Standard

S. No.	Conc. (µg/mL)	Percentage inhibition
1	20	24.88 ± 0.002^{d}
2	40	36.19 ± 0.004^{c}
3	60	$47.05 \pm 0.006^{b,c}$
4	80	$55.65 \pm 0.002^{a,b}$
5	100	60.18 ± 0.002^{a}
6	120	68.32 ± 0.005^{a}
	IC_{50}	73.02

Group a has the best treatment and group d has the poorest performing treatments. Values represent mean ± standard deviation of three replicates per treatment. Means in a column with same letter are significantly ($p \leq 0.05$) difference according to Duncan's Multiple Range Test

Table 23. Anti-inflammatory Activity of Various Crude Extracts of Leaves and Fruits of *Rauvolfia tetraphylla*. L.

Conc. (µg/mL)	RL EA	RLM	RFEA	RFM
20	$11.\ 80 \pm 0.06^{c}$	13.39 ± 0.04^{c}	10.91 ± 0.025^{c}	10.80 ± 0.002^{d}
40	$23.29 \pm 0.05^{b,c}$	29.90 ± 0.002^{b}	$26.20 \pm 0.016^{b,c}$	33.10 ± 0.004^{c}
60	$44.72 \pm 0.02^{a,b}$	45.79 ± 0.002^{b}	$40.17 \pm 0.0007^{a,b}$	49.47 ± 0.002^{b}
80	55.59 ± 0.006^{a}	59.50 ± 0.01^{a}	50.21 ± 0.001^{a}	$55.74 \pm 0.002^{a,b}$
100	64.90 ± 0.006^{a}	68.84 ± 0.002^{a}	55.89 ± 0.002^{a}	62.36 ± 0.002^{a}
120	69.87 ± 0.01^{a}	73.52 ± 0.002^{a}	58.51 ± 0.002^{a}	63.76 ± 0.002^{a}
IC_{50} Value	78.16	**72.44**	90.09	78.04

Group a has the best treatment and group c & d has the poorest performing treatments. Values represent mean ± standard deviation of three replicates per treatment. Means in a column with same letter are significantly ($p \leq 0.05$) difference according to Duncan's Multiple Range Test

Table 24. CAM Assay of Various Extracts from Leaf and Fruit of *Rauvolfia tetraphylla* L.

Sample	Extract Concentration	Replicate	Budding of blood vessels
RL EA	100	R1	++
		R2	++
		R3	++
	50	R1	+
		R2	+
		R3	+
	10	R1	+

		R2	+
		R3	+
RL M	100	R1	++++
		R2	++++
		R3	++++
	50	R1	+++
		R2	+++
		R3	+++
	10	R1	++
		R2	++
		R3	++
RF EA	100	R1	++
		R2	++
		R3	++
	50	R1	+
		R2	+
		R3	+
	10	R1	+
		R2	+
		R3	+
RF M	100	R1	+++
		R2	+++
		R3	+++
	50	R1	++
		R2	++
		R3	++
	10	R1	++
		R2	++
		R3	++

Table 25. Heat Stress Assay of Various Extracts of *Rauvolfia tetraphylla* L.

Treatment	Survival Rate (Days)	Percentage of effect (%)
Control	18	100
RLEA	19	107
RLM	22	**125**
RFEA	18	101
RFM	21	116

Table 26. Physiochemical Characters

Protein	Tryptophan decarboxylase
Sequence Length	499
Molecular weight	55729.29
Theoretical Pi	5.37
Total number of negatively charged residues (Asp + Glu)	61
Total number of positively charged residues (Arg + Lys)	48
Extinction Coefficient	70860
Instability Index	47.92
Aliphatic Index	94.19
Grand average of hydropathicity (GRAVY)	0.029

Table 27. Amino Acid Composition of *RtTDC*

S.No	Composition of amino acids	Percentage (%)
1	Ala (A) 40	8.0
2	Arg (R) 23	4.6
3	Asn (N) 16	3.2
4	Asp (D) 26	5.2
5	Cys (C) 9	1.8
6	Gln (Q) 9	1.8
7	Glu (E) 35	7.0
8	Gly (G) 25	5.0
9	His (H) 10	2.0
10	Ile (I) 25	5.0
11	**Leu (L) 57**	**11.4**
12	Lys (K) 25	5.0
13	Met (M) 17	3.4
14	Phe (F) 23	4.6
15	Pro (P) 25	5.0
16	Ser (S) 41	8.2
17	Thr (T) 32	6.4
18	Trp (W) 9	1.8
19	Tyr (Y) 14	2.8
20	Val (V) 38	7.6

Table 28. Binding Energy and RMSD (Å) Value of Docking

Rank	Sub- Rank	Run	Binding Energy	Cluster RMSD	Reference RMSD	Grep Pattern
1	1	14	-4.69	0.00	28.56	RANKING
2	1	27	-4.58	0.00	61.50	RANKING
3	1	4	-4.49	0.00	40.28	RANKING
3	2	19	-4.25	0.35	40.19	RANKING
3	3	47	-3.58	1.78	40.42	RANKING
4	1	16	-4.49	0.00	54.44	RANKING
5	1	39	-4.48	0.00	60.37	RANKING
5	2	8	-4.39	1.39	59.42	RANKING
6	1	45	-4.47	0.00	49.99	RANKING
7	1	2	-4.40	0.00	49.03	RANKING
8	1	18	-4.15	0.00	48.81	RANKING
9	1	40	-4.11	0.00	61.04	RANKING
10	1	23	-4.09	0.00	36.98	RANKING

Table 29. Binding Affinities of *Rauvolfia tetraphylla* Compounds with IL-1β Wound Healing Protein

Compound	Protein	Binding energy	Ligand efficiency	Inhibitor Constant (µM)	Amino acids	Structure and its interactions
1,9-Nonanediol	6Y8M	-4.59	-0.42	431.72	LEU134, PHE133, VAL132, LEU26, GLU25, LEU 80, THR 79	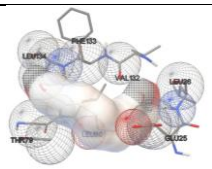
1D-1-O-Methyl-myo-inositol	6Y8M	-4.29	-0.33	722.04	LEU80, THR79, LYS77, LEU134, PHE133, PRO131, VAL132, GLU25	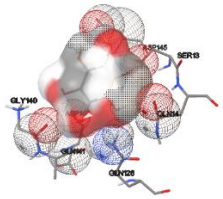
(Z)-2-methylbutanal oxime	6Y8M	-4.12	-0.59	960.53	GLU25, LEU80, THR79, LEU134, PHE133, VAL132	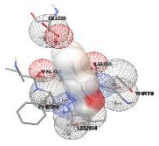

3-O-methyl-D-glucose	6Y8M	-3.12	-0.24	5.17	GLU25, TYR24, LEU26, VAL132, PHE133, THR79, LEU80, GLN81	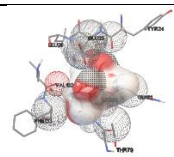
7-[3-Chloro-2-hydroxypropyl]guanine	6Y8M	-5.82	-0.36	53.83	PHE133, GLU25, LEU134, LYS77, PRO78, THR79, LEU80	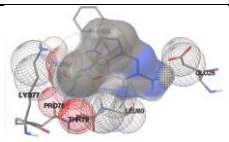
1-Naphthalenepropanol,.alp	6Y8M	-6.80	-0.32	10.45	LEU62, MET20, GLU38, VAL41, VAL40, GLN39, LYS63	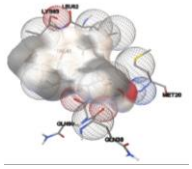
Butyl cyclohexyl ester	6Y8M	-7.67	-0.35	2.38	LYS77, LEU134, PHE133, PRO131, VAL132, LEU26, GLU25, LEU80, THR79, LYS74	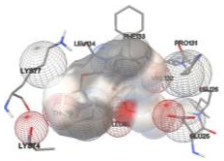
Serpentine	6Y8M	-6.33	-0.24	22.96	LEU82, GLN81, LEU80, THR79, GLU25, VAL132, LEU134, PHE133, TYR24	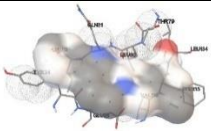
Yohimbine	6Y8M	-6.48	-0.25	17.46	SER84, LEU69, GLN81, THR79, LEU80, PHE133, VAL132, LEU82, TYR24, GLU24, LEU26	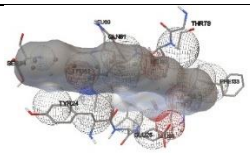
Isoreserpinine	6Y8M	-8.25	-0.29	890.25	LEU82, SER84, LEU80, LEU26, GLU25, TYR24, LEU69, GLN81, PRO131, VAL132, PHE133	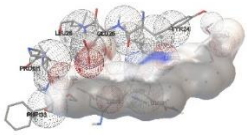
Darcyribeirine	6Y8M	-7.46	-0.25	3.41	GLU25, TYR24, SER84, LEU82, LEU80, GLN81, PHE135, LEU134, PRO78	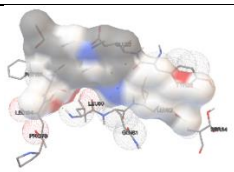
Reserpiline	6Y8M	-7.78	-0.26	1.99	SER84, LEU89, GLN81, LEU80, PHE133, VAL132, PRO131, GLU25, LEU25, TYR24, LEU82	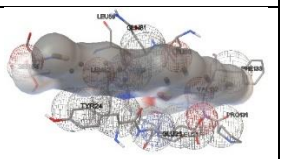

Carapanaubine	6Y8M	-7.77	-0.25	2.02	PHE133, LEU134, PRO78, THR79, LEU80, GLU25, GLN81, GLU83, LEU82, SER84, TYR24	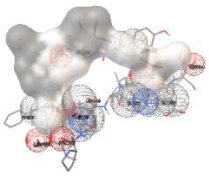

Table 30. Binding Affinities of *Rauvolfia tetraphylla* Compounds with TGF-β Wound Healing Protein

Compound	Protein	Binding energy	Ligand efficiency	Inhibitor Constant (µM)	Amino acids	Structure and its interactions
1,9-Nonanediol	6B8Y	-5.36	-0.49	117.98	VAL383, GLY374, ARG332, PHE396, ALA399, ASP400, ALA403, MET379, LEU334	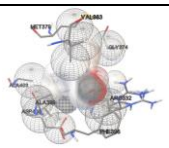
1D-1-O-Methyl-myo-inositol	6B8Y	-5.69	-0.44	67.75	ALA403, LEU334, MET379, THR375, ASP333, ARG332, ALA399, ASP400	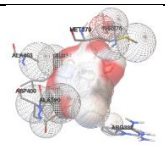
(Z)-2-methylbutanal oxime	6B8Y	-5.30	-0.79	130.59	ALA403, ASP400, ARG332, ASP333, THR375, TYR378, LEU334	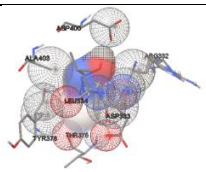
3-O-methyl-D-glucose	6B8Y	-4.34	-0.33	659.96	ASP400, ALA380, ALA399, MET379, LEU334, TYR378, VAL383, ARG332, GLY374, VAL373, PHE396	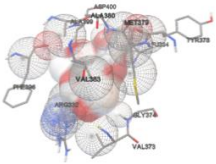
7-[3-Chloro-2-hydroxypropyl]guanine	6B8Y	-6.62	-0.41	13.97	GLU245, ARG244, GLY353, ASP351, LEU354, ARG215, PHE216, LYS232, SER241	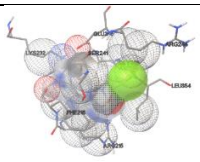

1-Naphthalenepropanol,.alp	6B8Y	-7.71	-0.37	2.23	ARG255, LEU254, MET253, VAL252, TYR249, PHE262, GLN250	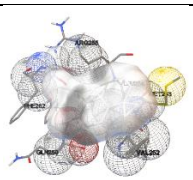
Butyl cyclohexyl ester	6B8Y	-7.70	-0.35	2.26	ARG255, HIS256, LEU254, MET253, GLN250, TYR249, PHE262, LEU260, ILE259	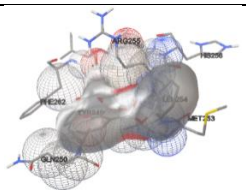
Serpentine	6B8Y	-7.2	-0.28	5.27	ILE201, ILE263, ALA264, PHE262, ASP266, ARG255, GLN250, VAL252	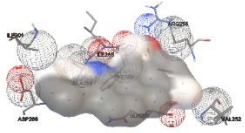
Yohimbine	6B8Y	-7.0	-0.27	7.4	VAL252, MET253, ARG255, PHE262, ALLA264, ILE263, THR200, ASP266, ILE201, LEU254, THR251	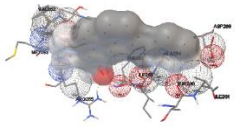
Isoreserpinine	6B8Y	-7.63	-0.27	2.54	LEU486, THR484, ALA485, ILE401, MET318, GLU394, LYS397, HIS317, ALA314	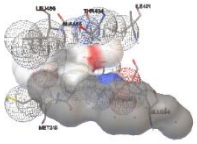
Darcyribeirine	6B8Y	-6.56	-0.22	2.54	THR200, MET199, HIS198, TRP224, ASP281, LYS342, LYS343, ASN344, GLU284, HIS283, GLU228, TYR282	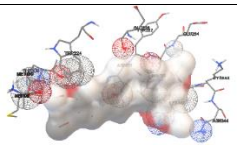
Reserpiline	6B8Y	-7.1	-0.24	6.29	ASP266, ALA265, ALA264, ILE263, THR200, MET199, GLN250, GLU247, PHE243	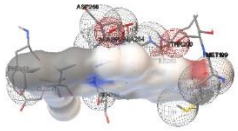
Carapanaubine	6B8Y	-8.63	-0.28	469.26	LEU486, LYS489, ALA314, GLU319, MET318, ILE320, VAL321, HIS256	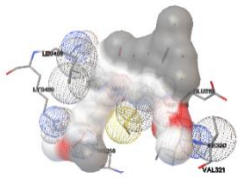

Table 31. Binding Affinities of *Rauvolfia tetraphylla* Compounds with MMP Wound Healing Protein

Compound	Protein	Binding energy	Ligand efficiency	Inhibitor Constant (µM)	Amino acids	Structure and its interactions
1,9-Nonanediol	1GEN	-4.79	-0.44	309.32	ARG482, GLU525, TYR524, ASN573, PHE672, VAL621, GLN480, GLY483,	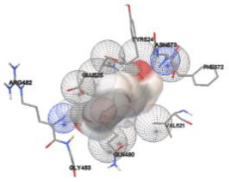
1D-1-O-Methyl-myo-inositol	1GEN	-4.52	-0.35	483.38	ASN578, ASP622, GLN480, GLN624, GLU525	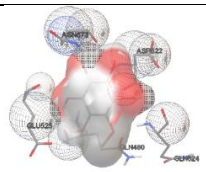
(Z)-2-methylbutanal oxime	1GEN	-4.58	-0.65	437.7	LEU658, CYS469, LYS654, ILE653, ALA635, ASP472, ILE473, GLN471	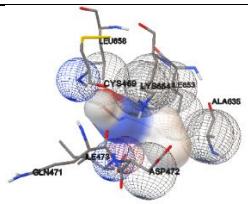
3-O-methyl-D-glucose	1GEN	-3.93	-0.3	1.32	PHE572, ASP622, VAL621, GLN624, GLN480, ALA479, GLU525, TYR524, ASN573	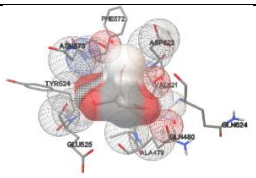
7-[3-Chloro-2-hydroxypropyl]guanine	1GEN	-7.16	-0.45	5.61	TYR524, ASN573, GLU525, ALA571, PHE572, VAL620, ASP622, VAL621, GLN480	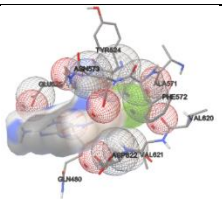

1-Naphthalenepropanol,.alp	1GEN	-7.69	-0.37	2.3	GLU525, TYR524, ASN573, PHE572, ASP622, VAL621, GLN480, GLN624, GLY483	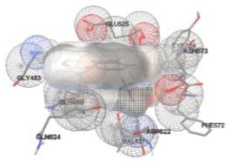
Butyl cyclohexyl ester	1GEN	-6.29	-0.28	26.0	GLN624, LEU623, GLN480, GLY483, ALA479, GLU525, PRO527, TYR524, ASN573, PHE572, SER575, ASP622, VAL621, ARG482	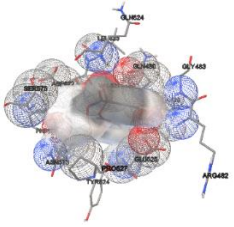
Serpentine	1GEN	-6.83	-0.26	9.89	ASP622, GLN480, GLN624, GLY483, PRO527, GLU525, GLU530, ARG482	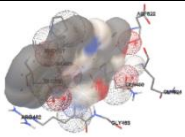
Yohimbine	1GEN	-6.23	-0.24	27.15	SER558, PRO562, GLY560, TYP589, MET598, LYS596, LYS597, PRO600, TYR591, GLY601, PHE602	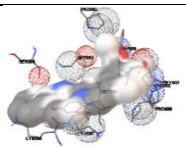
Isoreserpinine	1GEN	-5.98	-0.21	41.35	THR465, VAL464, GLN471, ASP472, PHE492, LYS489, VAL474, ASP490, ARG491	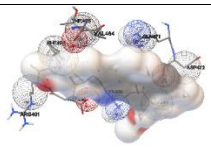
Darcyribeirine	1GEN	-5.88	-0.2	49.2	GLN624, GLN480, GLY483, GLU525, GLU530, ARG482, ASN573, LYS578, VAL621, SER575	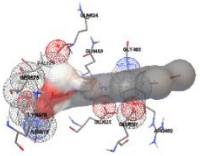
Reserpiline	1GEN	-5.67	-0.19	70.21	ASP615, PRO614, LYS633, TYR636, PHE650, ALA607, ALA612	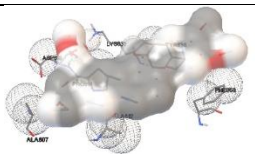
Carapanaubine	1GEN	-8.22	-0.27	949.07	LYS646, ASN611, VAL648, TYR636, ILE613, ALA607, ASP605, PRO614, LYS633	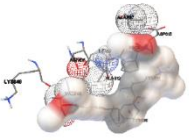

Figure 1. *In vitro* Seed Culture of *Rauvolfia tetraphylla* L.

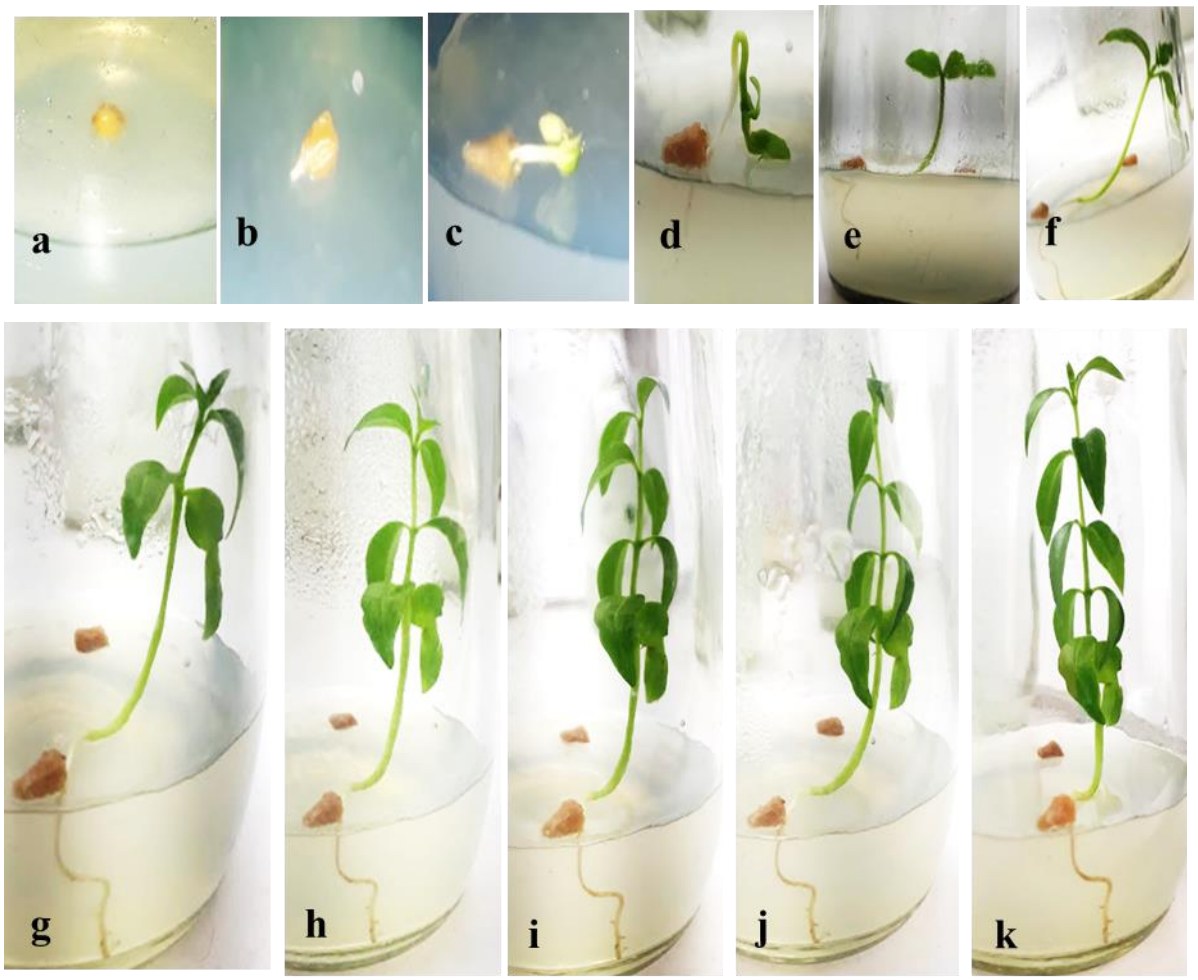

(a) On the day; (b) 7th day; (c) 17th day; (d) 27th day; (e) 34th day; (f) 55th day; (g) 77th day; (h) 105th day; (i) 124th day; (j) 152th day; (k) 184th day

Figure 2. Effect of different PGRs on callus development from leaf of *Rauvolfia tetraphylla* L.

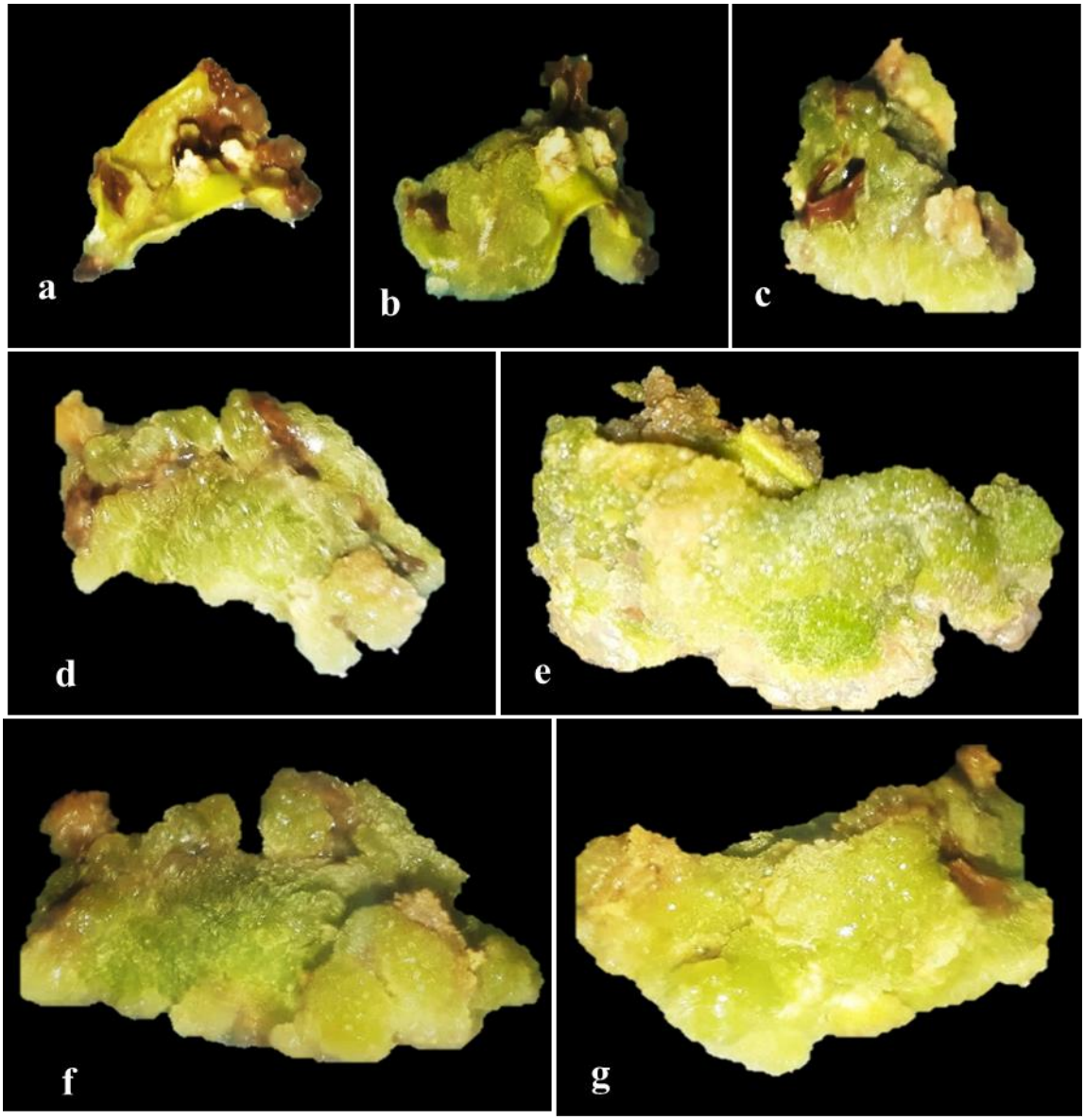

Callus formation (**a**) 15th day (**b**) 27th day (**c**) 45th day (**d**) 60th day (**e**) 75th day of inoculation on MS + 2,4D+BAP (**f**) MS medium with IAA+ 24D after 12 weeks of inoculation (**g**) MS medium with IAA+IBA after 12 weeks of inoculation

Figure 3. Effect of different PGRs on callus development from node of *Rauvolfia tetraphylla* L.

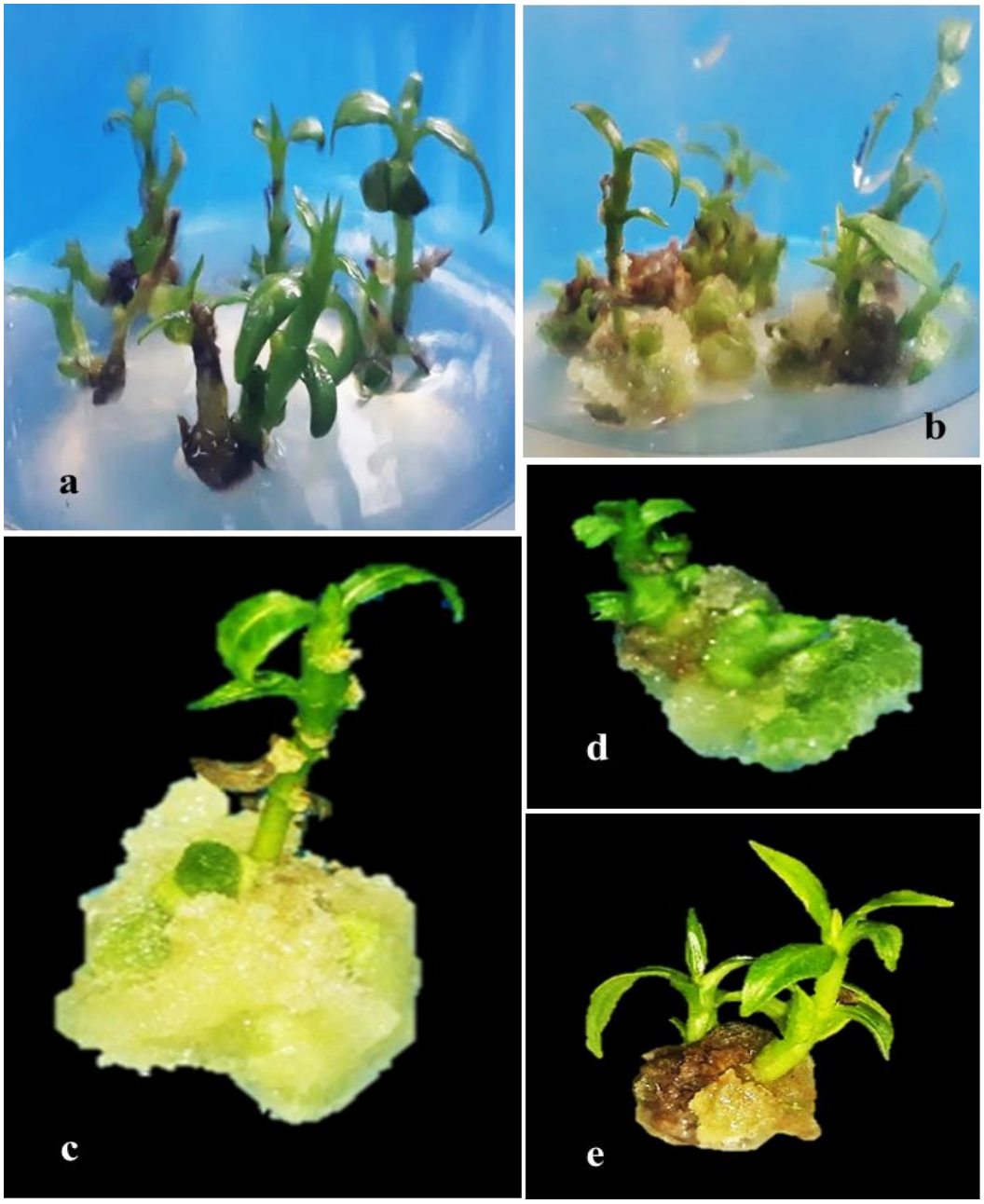

Callus formation

(**a**) on 7th day of inoculation (**b**) 4th week of subculture

(**c**) MS medium with 2.5 mg/L of 2,4-D+BAP after 8 week of culture

(**d**) MS medium with 2.5 mg/L of IAA+ 2,4-D after 8 week of culture

(**e**) MS medium supplemented with 2.5 mg/L of IBA+2,4-D after 8 weak of culture

Figure 4. Effect of different PGRs on callus formation from internode of *Rauvolfia tetraphylla* L.

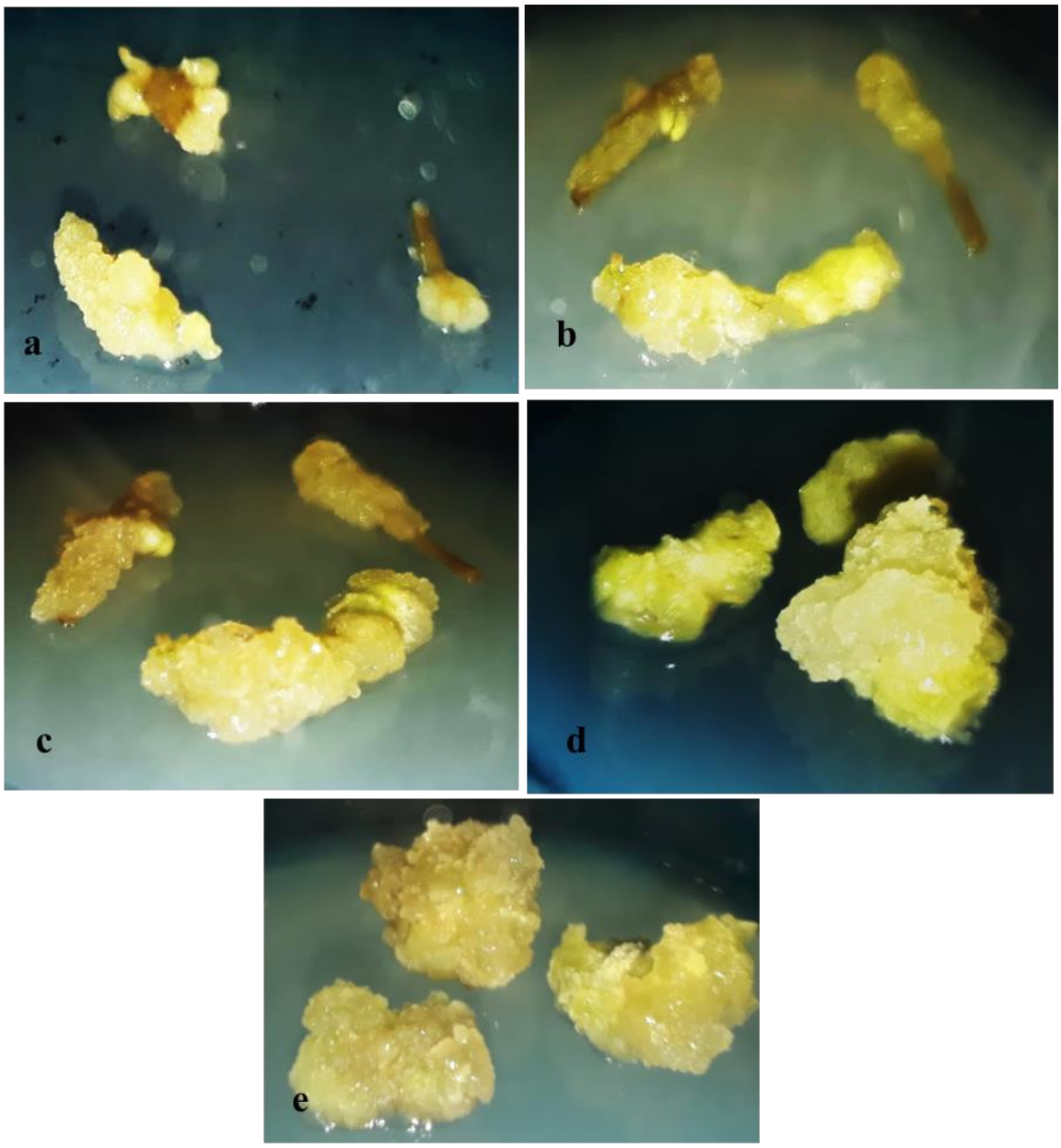

Callus formation of internodal explant of *R. tetraphylla*

(a) 15 days of inoculation

(b) 4 weeks of culture (c) 6 weeks after culture

(d) 8 weeks after inoculation on MS medium with 2.5 mg/L of 2,4-D + BAP

(e) 8 weeks after inoculation on MS medium with 2.5 mg/L of IBA +2 ,4-D

Figure 5. Effect of different PGRs on callus development from root of *Rauvolfia tetraphylla* L.

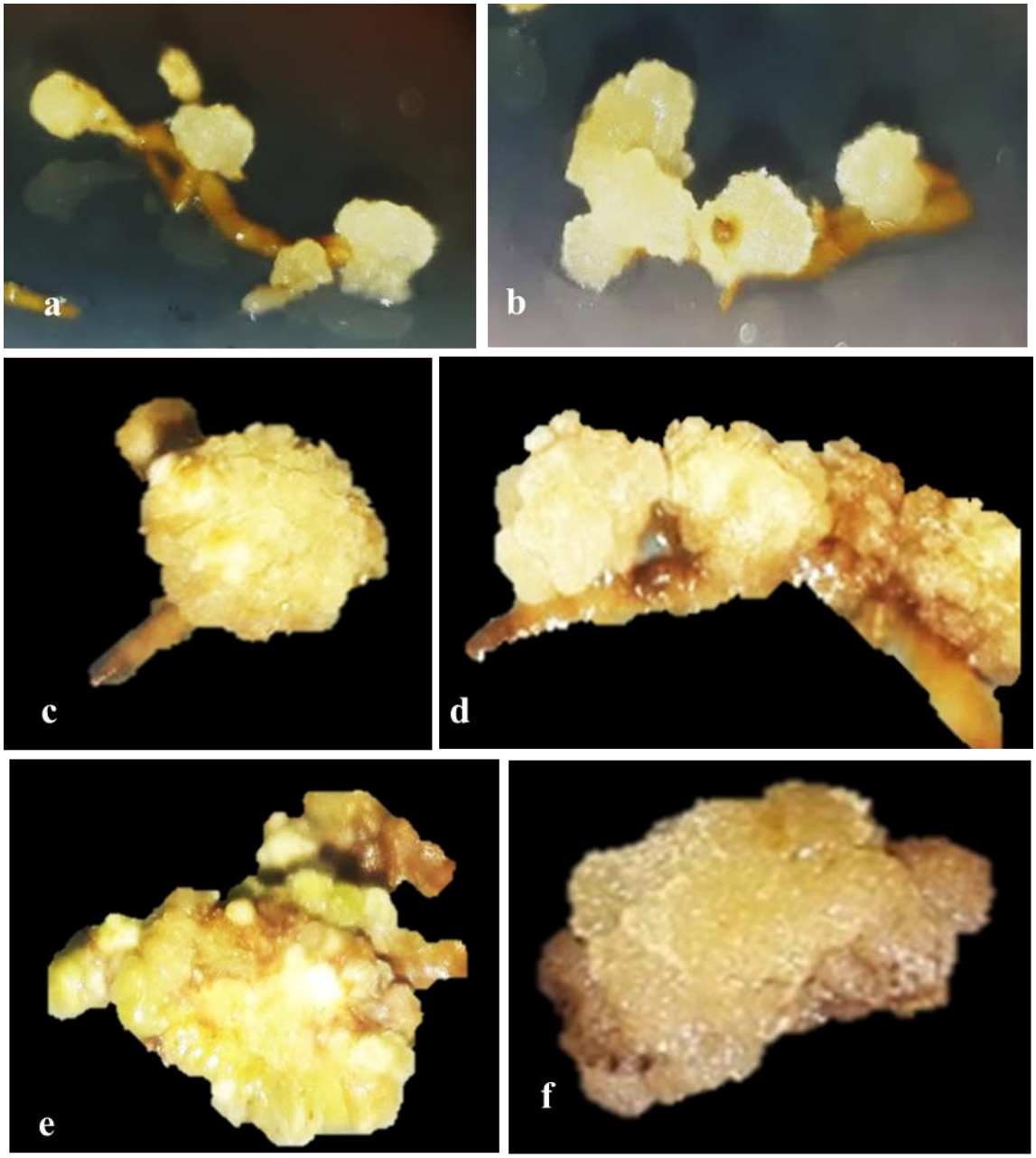

Callus formation of root explant

(**a**) 15 days of inoculation

(**b**) 3 weeks of inoculation

(**c**) 4 weeks after inoculation

(**d**) 6 weeks after inoculation

(**e**) 8 weeks after inoculation MS medium with 2.5 mg/L of 2,4-D+BAP

(f) 8 weeks after inoculation on MS medium with 2.5 mg/L of BAP

Figure 6. Effect of different PGRs on direct rhizogenesis from leaf explants of *Rauvolfia tetraphylla* L.

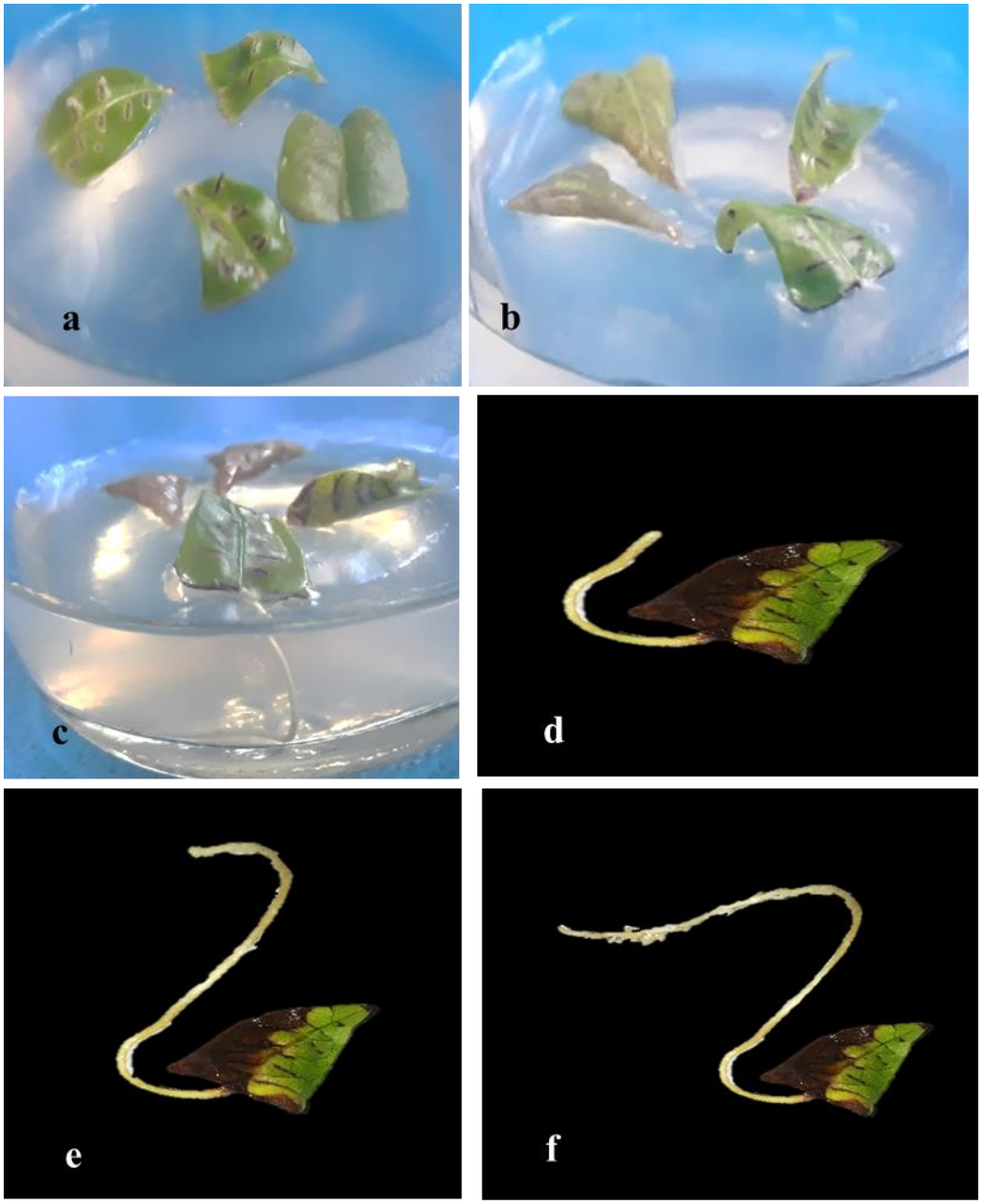

(a) On 7th day of inoculation on leaf explant

(b) 15th day after inoculation

(c) 3 weeks after culture

(d) 4 weeks of inoculation

(e) 5 weeks of inoculation

(f) 6 weeks of after culture

Figure 7. Effect of different PGRs on direct rhizogenesis from nodal explants of *Rauvolfia tetraphylla* L.

(**a**) on the day of inoculation of nodal explant

(**b**) direct root formation in nodal explant after 3 weeks of inoculation

(**c**) 6 weeks of inoculation

(**d**) 8 weeks of inoculation

(**e**) rooting of *in vitro* regenerated shoots on MS medium supplemented with 1.5 mg/L of IBA & 0.5 mg/L of BAP"

(**f**) Hardening of regenerated plantlet in sterile soil mixture (Vermiculite + soil – 2:1)

Figure 8. Effect of different PGRs on direct caulogenesis from nodal explants of *Rauvolfia tetraphylla* L.

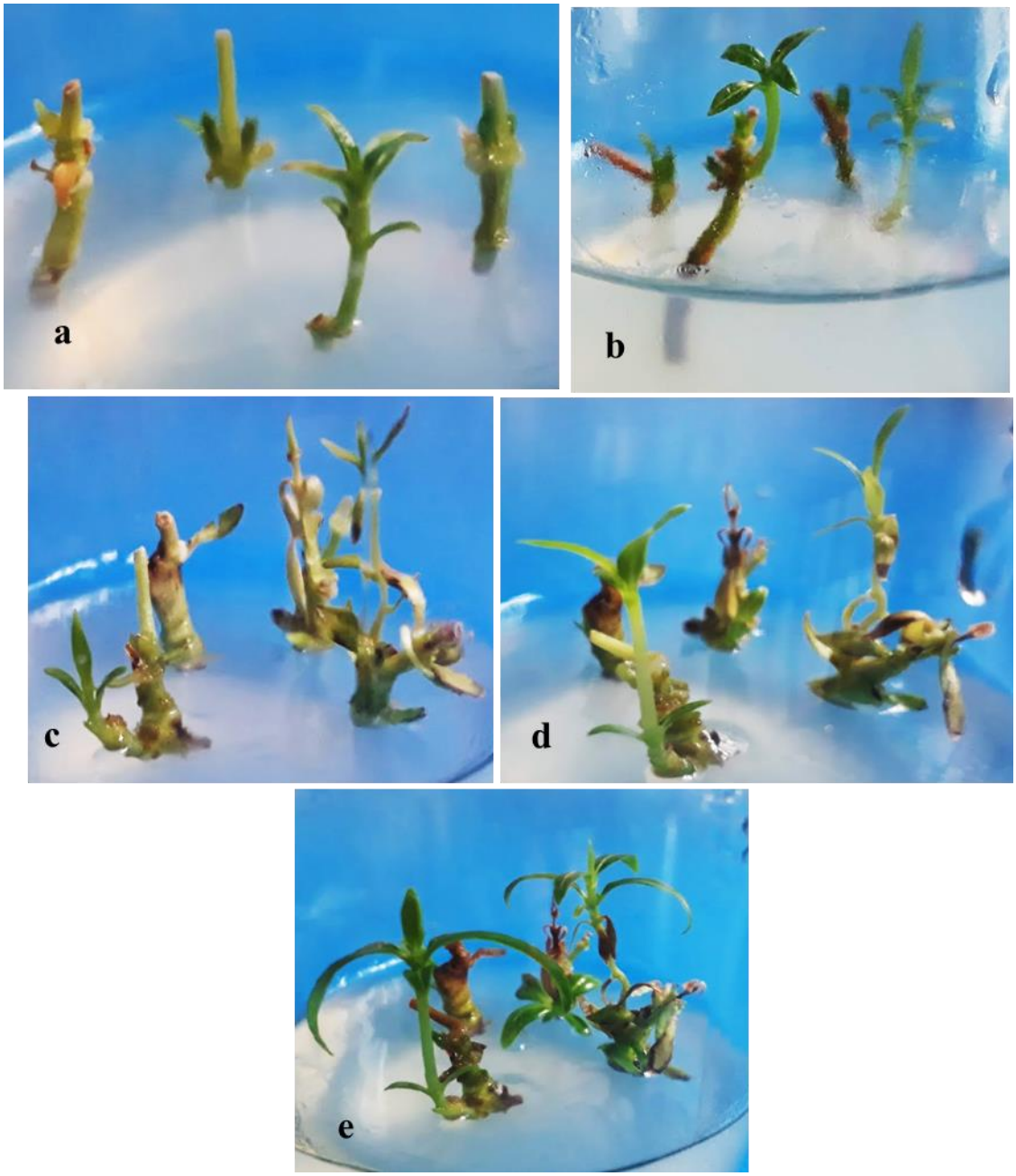

Root formation of nodal explant

(**a**) on the of inoculation

(**b**) 3 weeks of inoculation

(**c**) 4 weeks after inoculation

(**d**) 5 weeks after inoculation

(**e**) 6 weeks after inoculation

Figure 9. Effect of different PGRs on multiple shoot formation from nodal explants of *Rauvolfia tetraphylla* L.

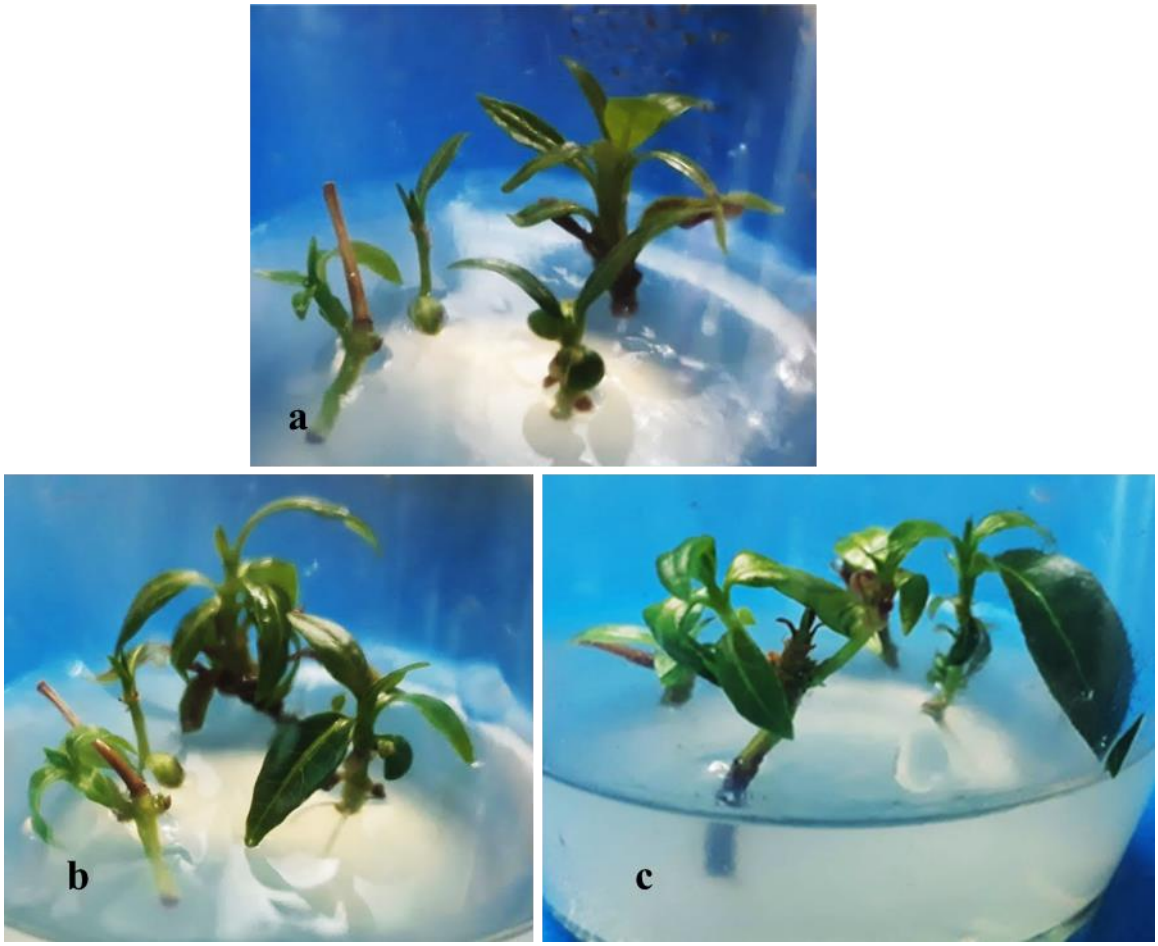

(a) Multiple shoot formation from nodal explant cultured on MS medium after 7th day of inoculation

(b) Multiple shoot formation from cotyledonary nodal explant cultured on "MS medium supplemented with 2,4-D + BAP after 4 weeks of inoculation

(c) Shoot elongation on *in vitro* generated shoot after 6 weeks of culture

Figure 10. Heat map of different PGRs on callogenesis from leaf, node, internode and root of *Rauvolfia tetraphylla* L.

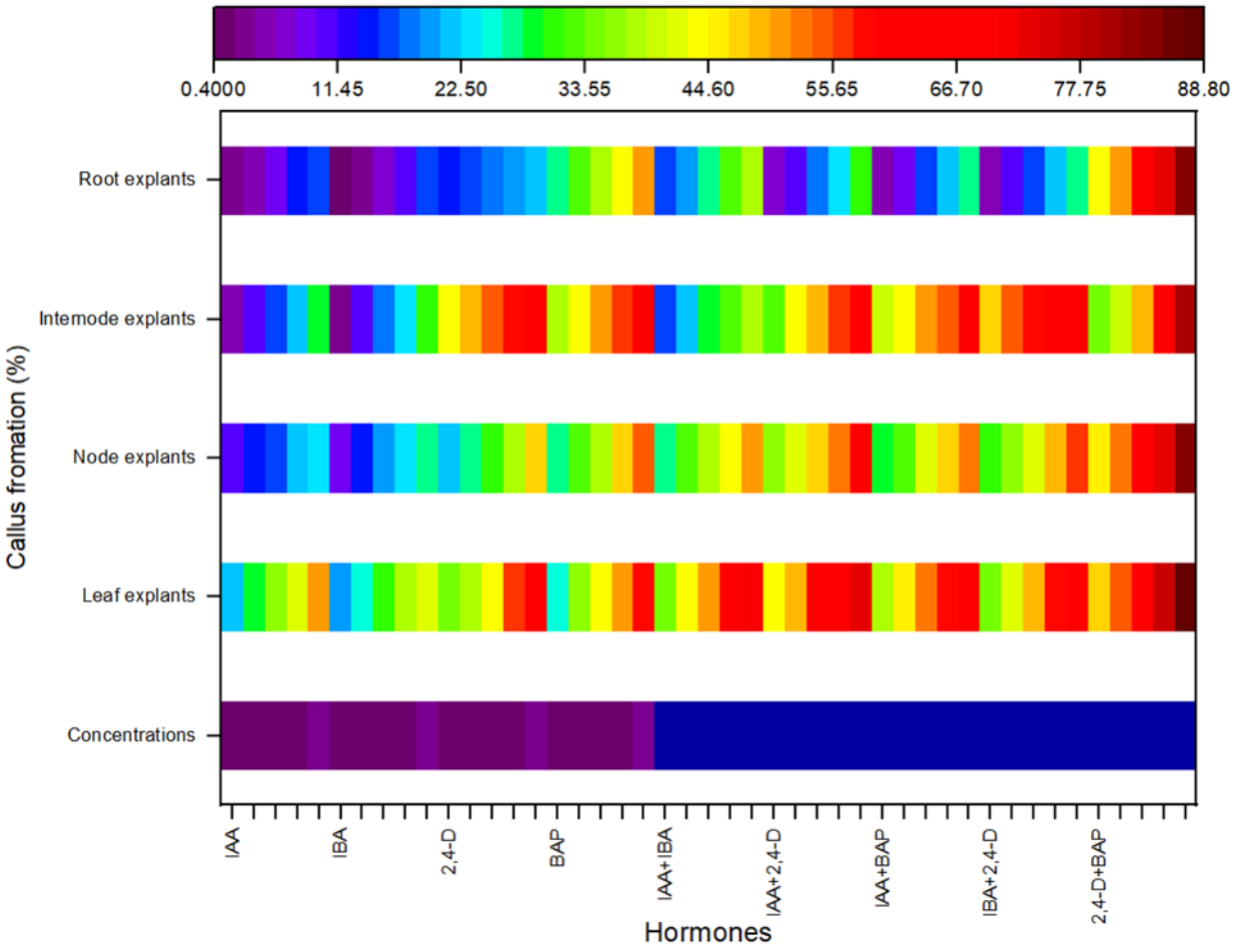

Figure 11. Somatic embryogenesis from leaf and root of *Rauvolfia tetraphylla* L.

Morphology of somatic embryogenesis in leaves of *R.tetraphylla*. Somatic embryo cluster with well-formed globular embryos after 4 weeks in maturation conditions of leaf explant on the edge of the distal region

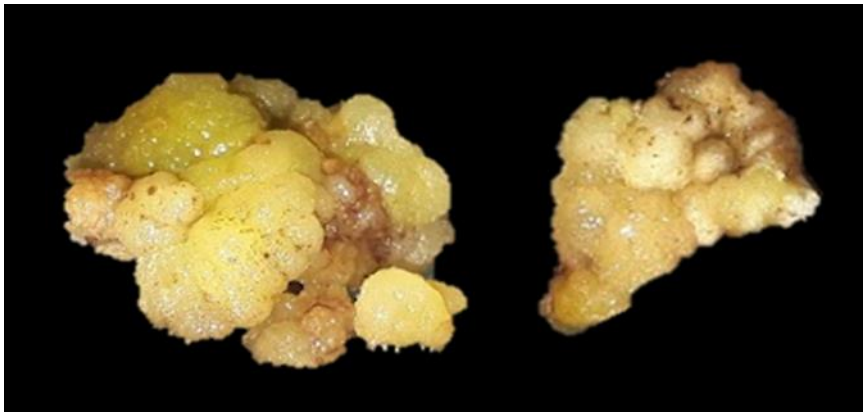

Morphology of somatic embryogenesis in root of *R.tetraphylla*. somatic embryo from root explant after 4 weeks of culture

Figure 12. Histology of mitotic cell division

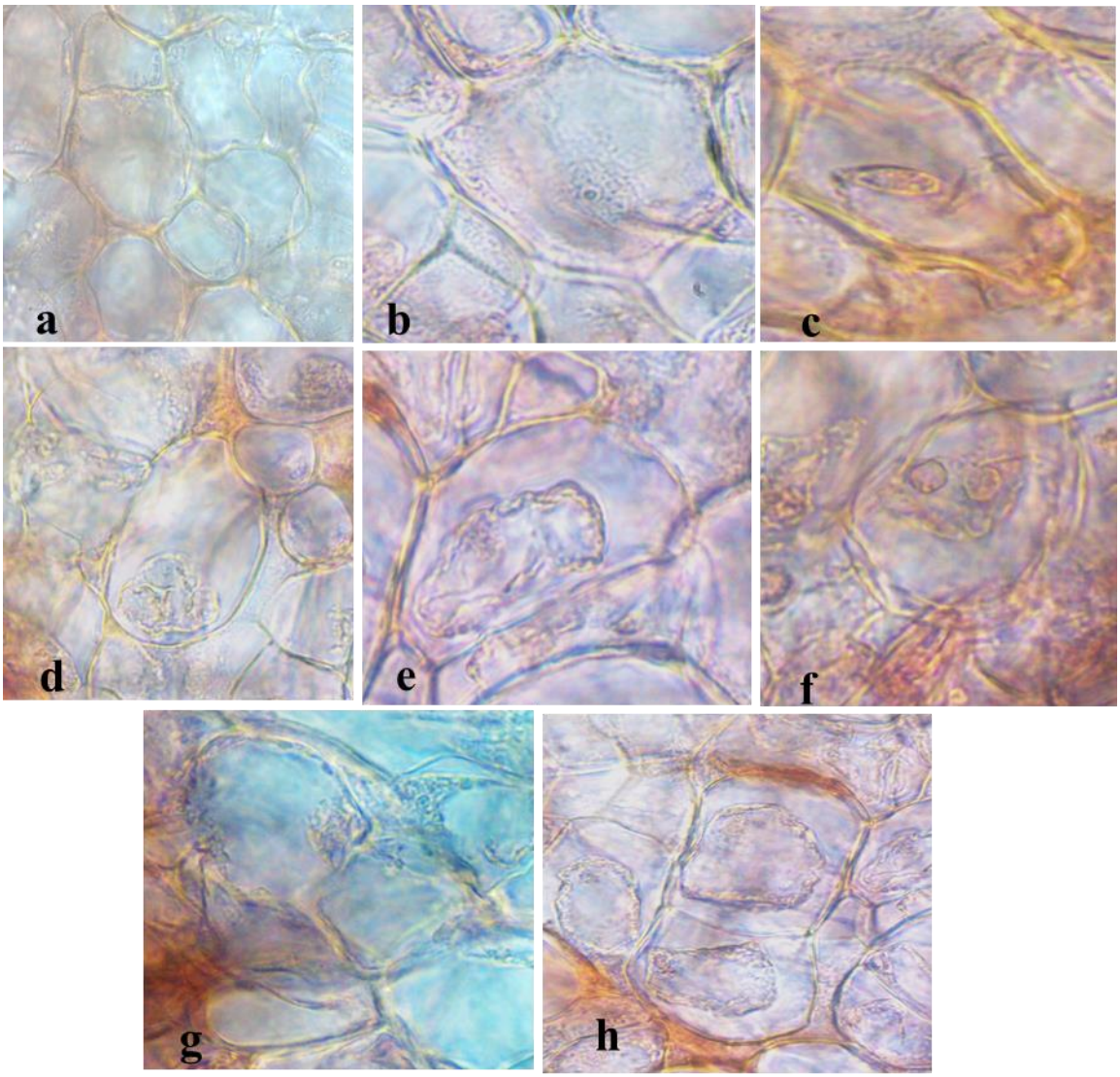

(a) Cell wall; (b) Interphase; (c) Early Prophase; (d) Late Prophase; (e)Metaphase; (f) Anaphase; (g) Telophase; (h) Cytokinesis

Figure 13. Histology of somatic embryogenesis of *Rauvolfia tetraphylla* L.

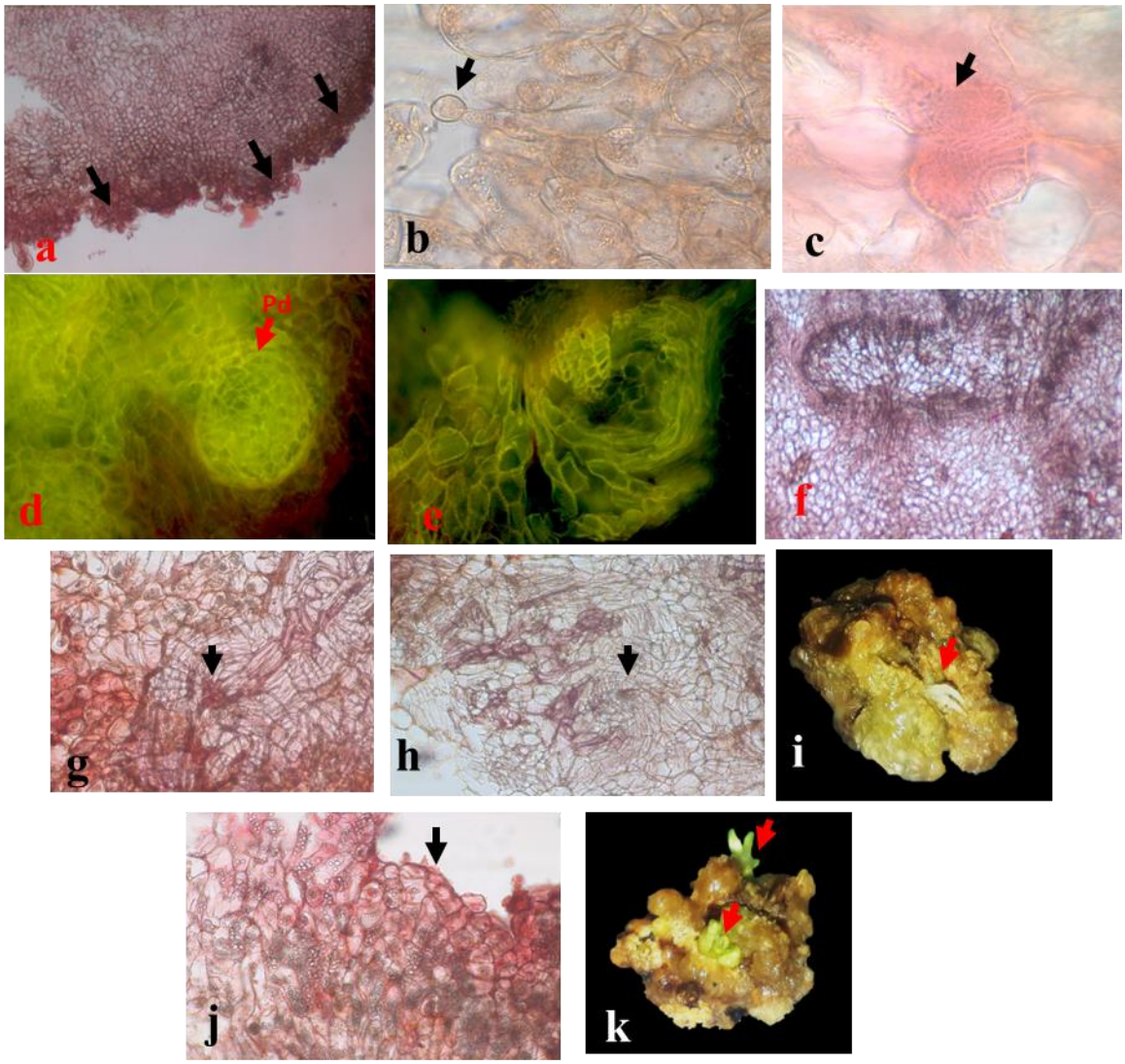

(**a**) culture on 10 days showing Primary callus containing meristematic clusters on the periphery (arrows) (callus distal region) (**b**) culture of 20 days showing proembryo with suspensor (**c**) culture on 30 days Proembryo showing multicellular suspensor (**d**) culture on 40 days showing a well-developed globular somatic embryo in the region of embryogenic callus and protoderm (**e**) culture on 50 days showing a heart-shaped somatic embryo (**f**) culture on 60 days showing somatic embryo in torpedo state (**g**) culture on 75 days showing provascular band (**h**) root primordia (**i**) morphology of root organogenesis (**j**) shoot primordia (**k**) morphology of shoot organogenesis.

Figure 14a. Endogenous sugar in observed in callus of leaf of *Rauvolfia tetraphylla* L.

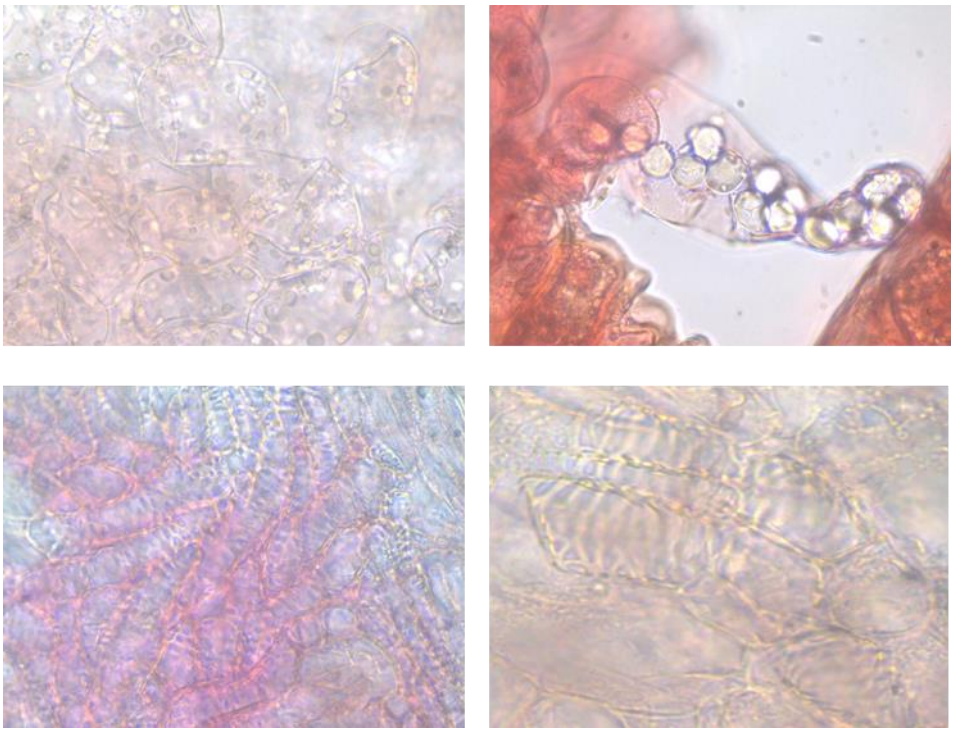

Figure 14b. Endogenous sugar in observed in callus of root of *Rauvolfia tetraphylla* L.

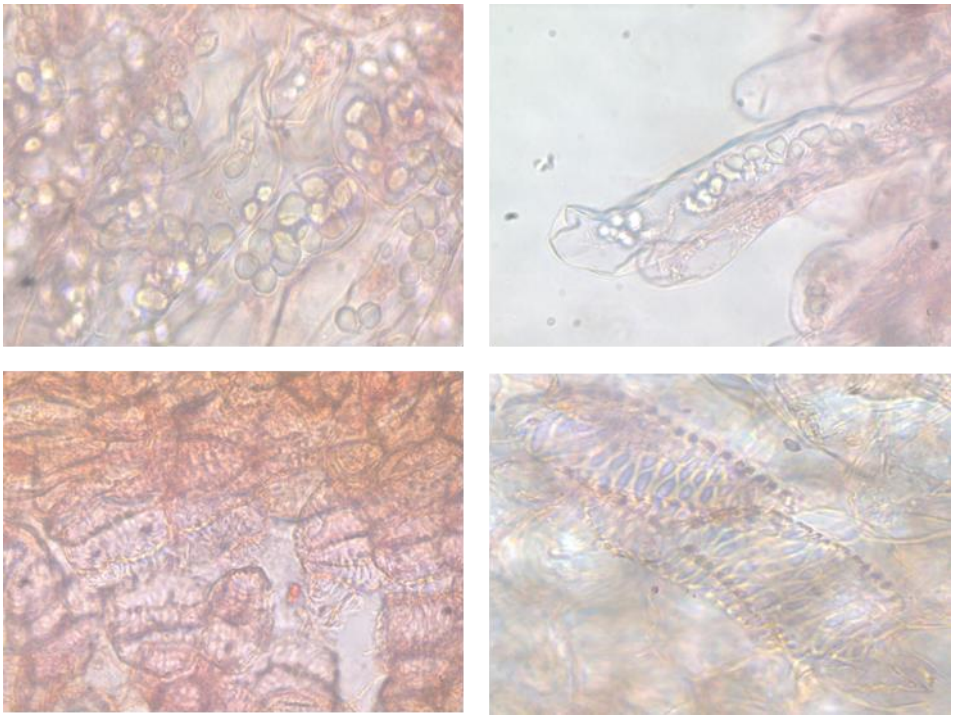

Fig. 15 Quantitative analysis of *Rauvolfia tetraphylla* L. from leaf and fruit

a. Atropine standard Curve for alkaloids

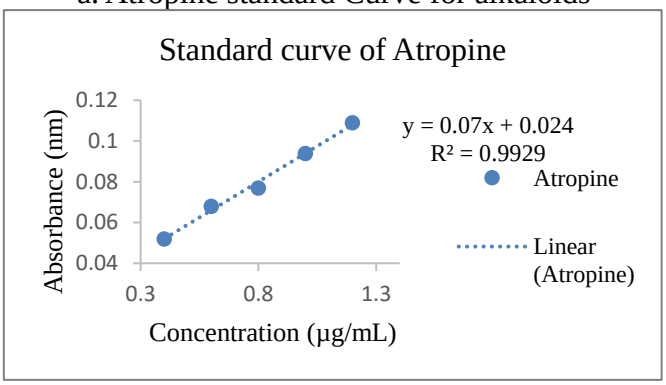

b. Rutin Standard Curve for flavonoids

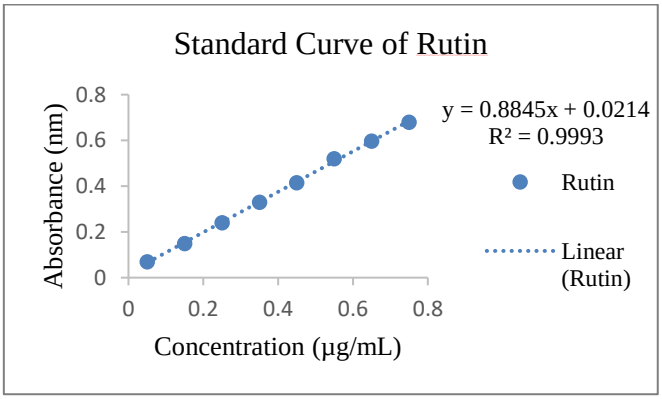

c. Gallic acid standard curve for total phenol content

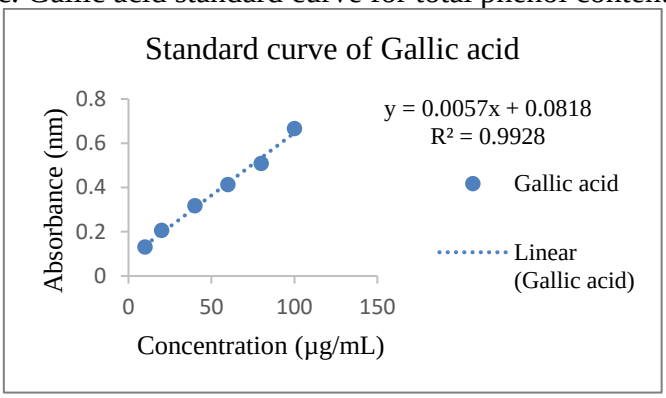

d. Gallic standard curve for tannin

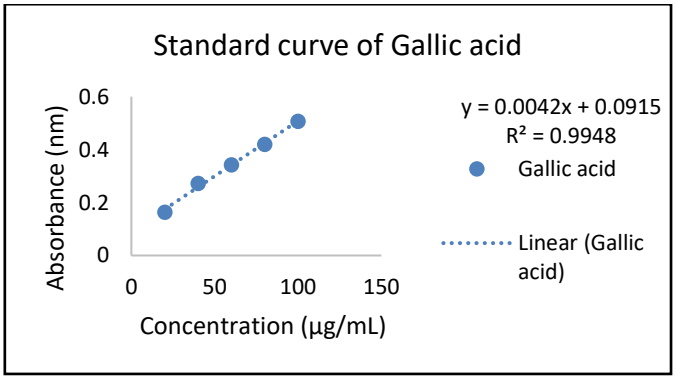

Fig. 16 GC-MS spectra of identified compounds from *Rauvolfia tetraphylla* L. methanolic fractions

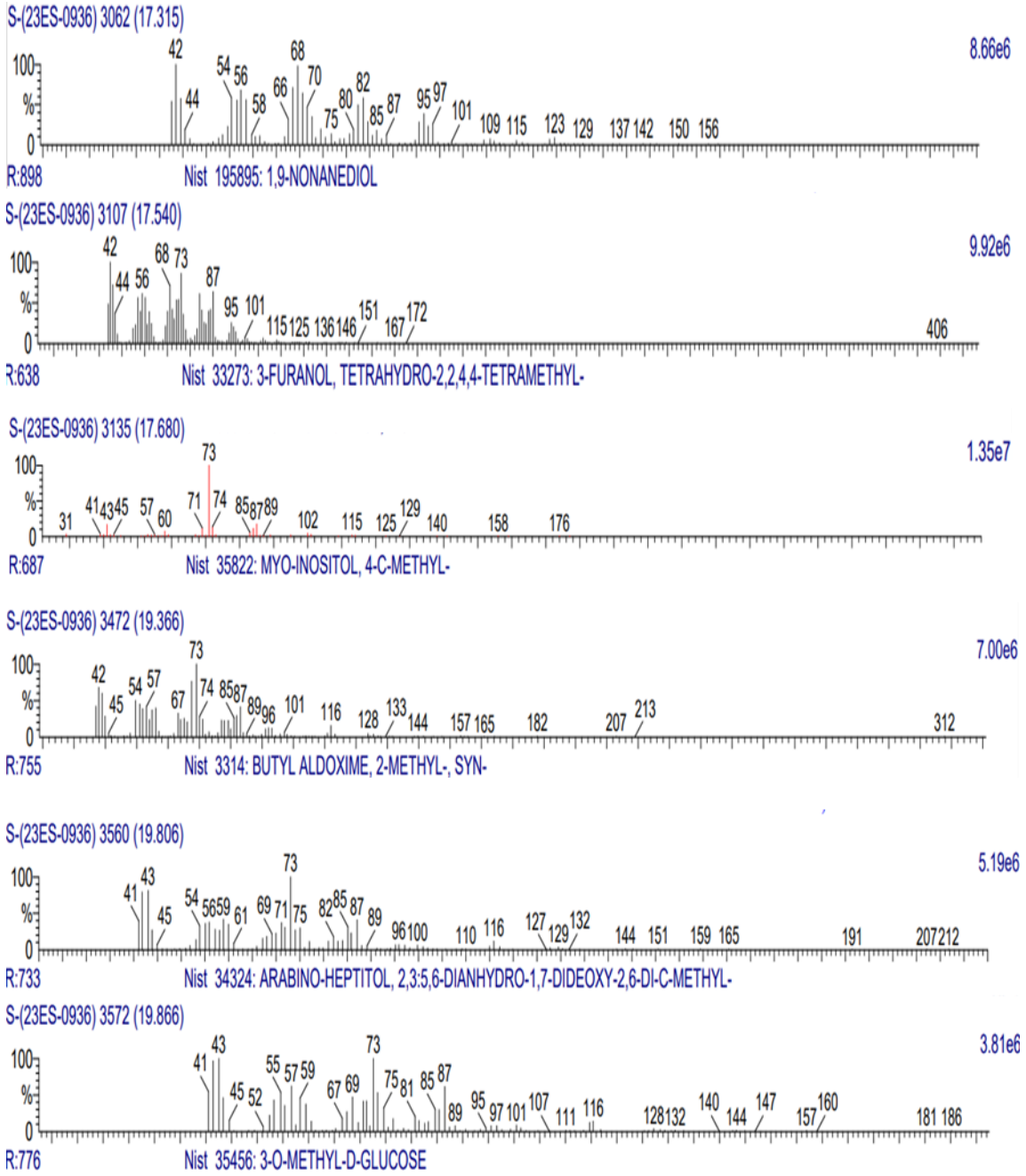

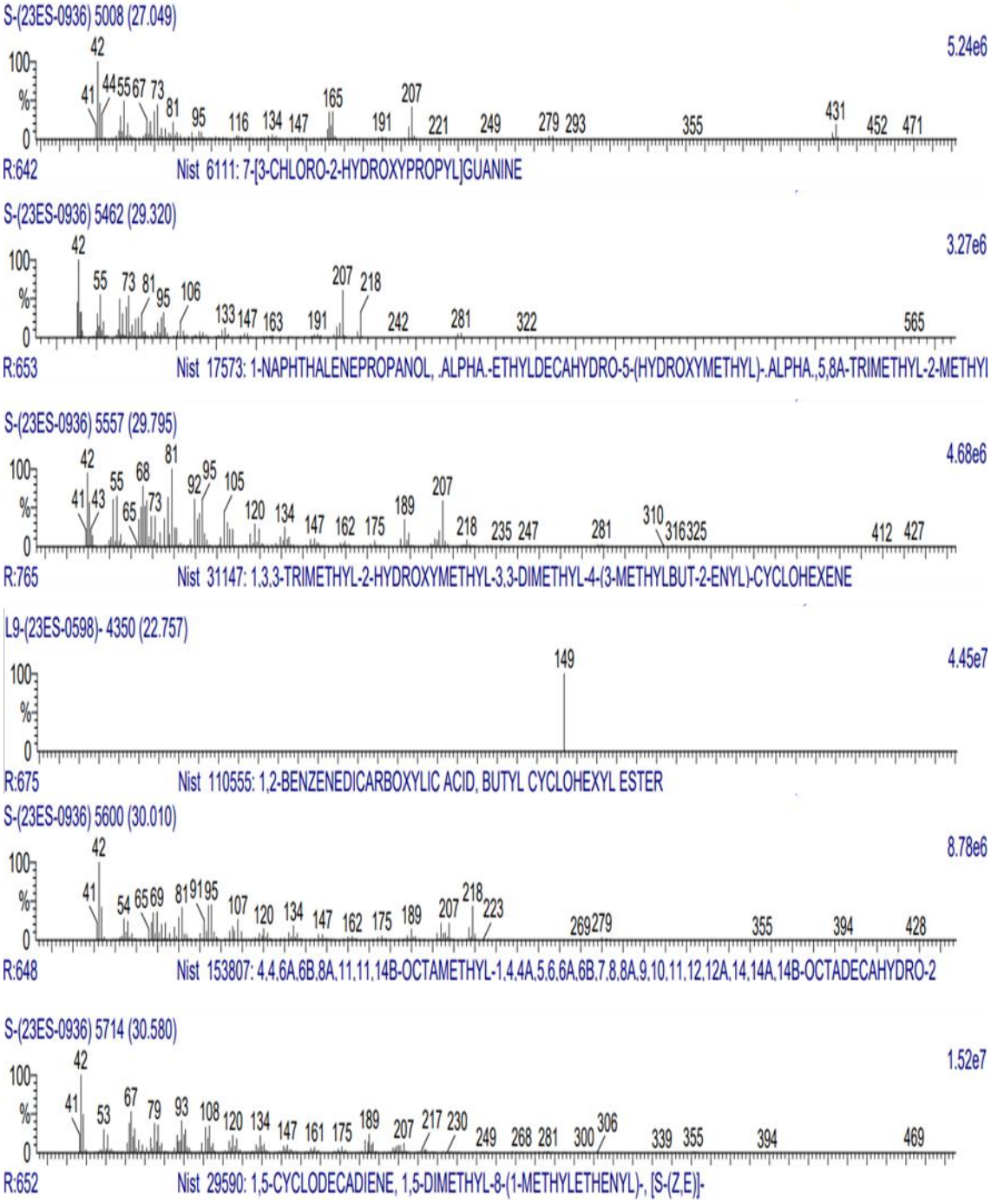
S-(23ES-0936) 5008 (27.049)
5.24e6
R:642
Nist 6111: 7-[3-CHLORO-2-HYDROXYPROPYL]GUANINE
S-(23ES-0936) 5462 (29.320)
3.27e6
R:653
Nist 17573: 1-NAPHTHALENEPROPANOL, .ALPHA.-ETHYLDECAHYDRO-5-(HYDROXYMETHYL)-.ALPHA.,5,8A-TRIMETHYL-2-METHYI
S-(23ES-0936) 5557 (29.795)
4.68e6
R:765
Nist 31147: 1,3,3-TRIMETHYL-2-HYDROXYMETHYL-3,3-DIMETHYL-4-(3-METHYLBUT-2-ENYL)-CYCLOHEXENE
L9-(23ES-0598)- 4350 (22.757)
4.45e7
R:675
Nist 110555: 1,2-BENZENEDICARBOXYLIC ACID, BUTYL CYCLOHEXYL ESTER
S-(23ES-0936) 5600 (30.010)
8.78e6
R:648
Nist 153807: 4,4,6A,6B,8A,11,11,14B-OCTAMETHYL-1,4,4A,5,6,6A,6B,7,8,8A,9,10,11,12,12A,14,14A,14B-OCTADECAHYDRO-2
S-(23ES-0936) 5714 (30.580)
1.52e7
R:652
Nist 29590: 1,5-CYCLODECADIENE, 1,5-DIMETHYL-8-(1-METHYLETHENYL)-, [S-(Z,E)]-

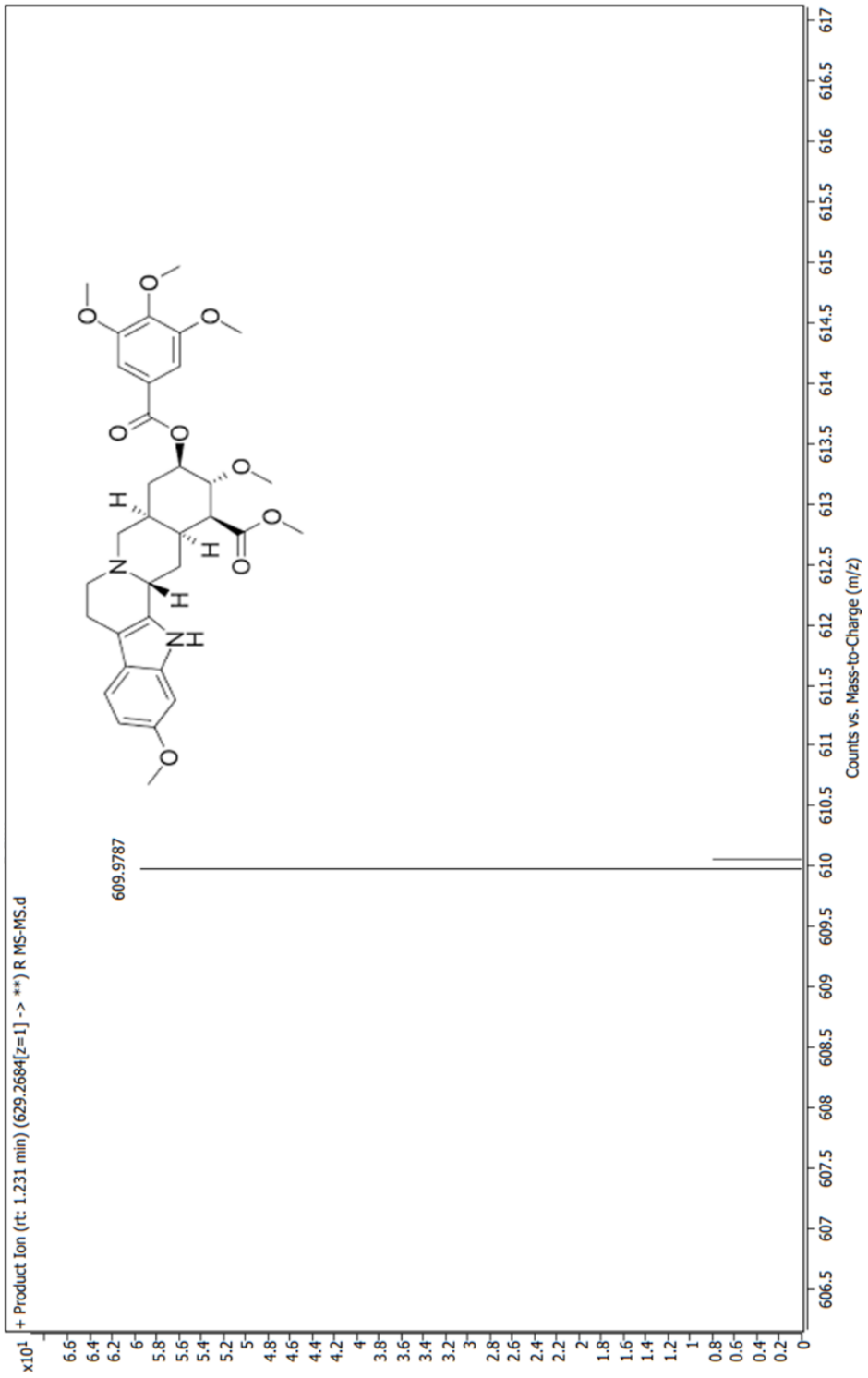

Fig. 17 Reserpine was detected in the crude extracts by LC–ESI – MS/MS analysis

Fig. 18 Column chromatography of methanolic leaf extract of *Rauvolfia tetraphylla* L.

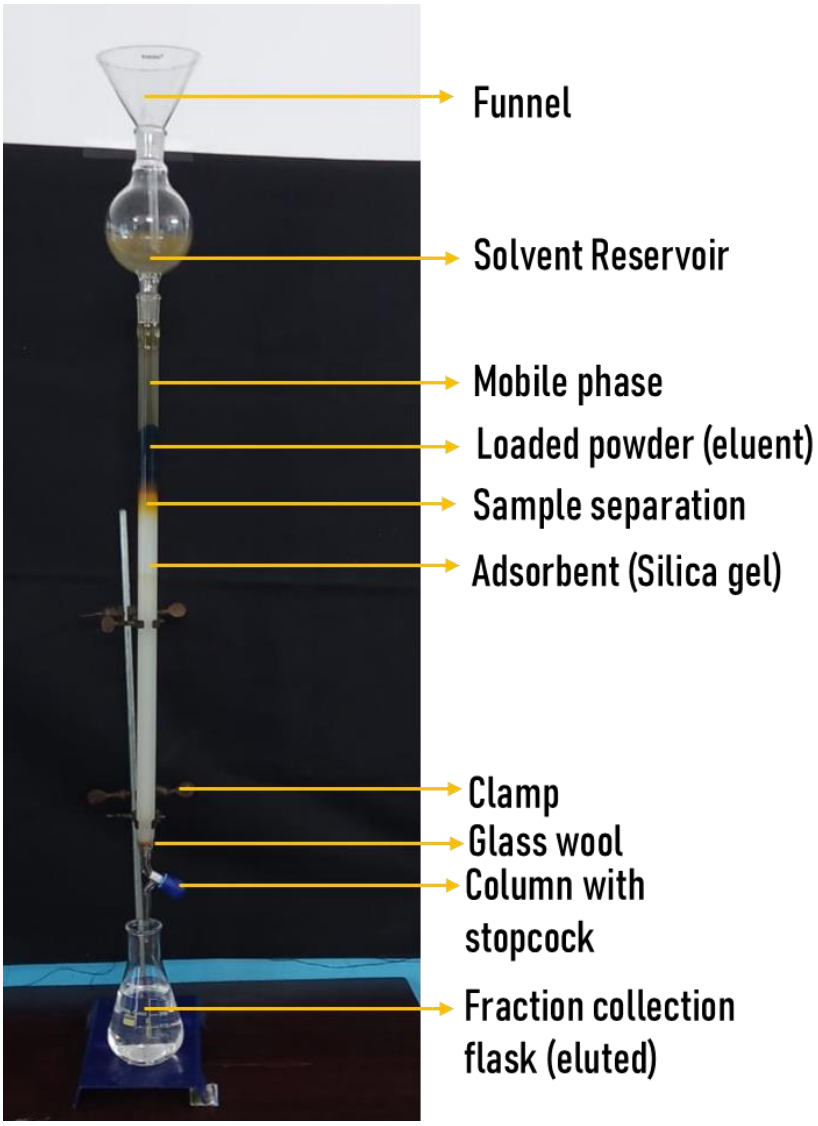

Fig. 19a TLC of isolated compound (fraction 1) from methanolic extract of *Rauvolfia tetraphylla* L.

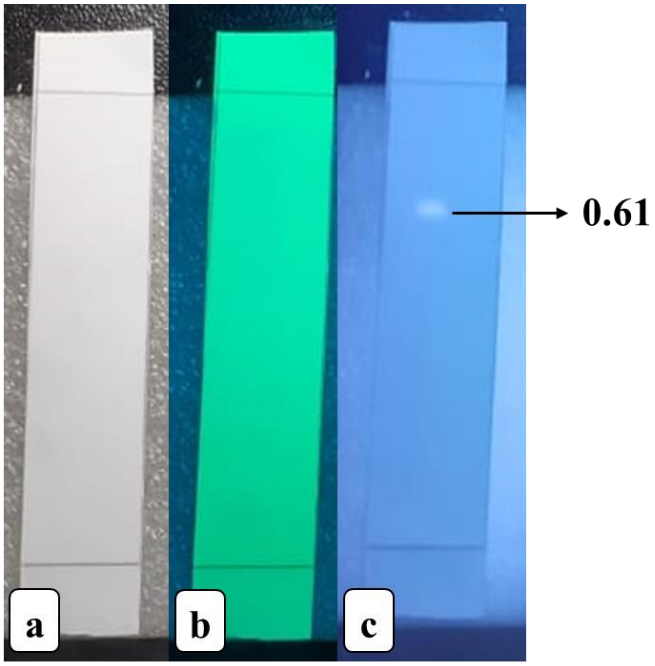

a. Visible light
b. Short UV
c. Long UV

Fig. 19b UV analysis of isolated compound (fraction 1) from methanolic extract of *Rauvolfia tetraphylla* L.

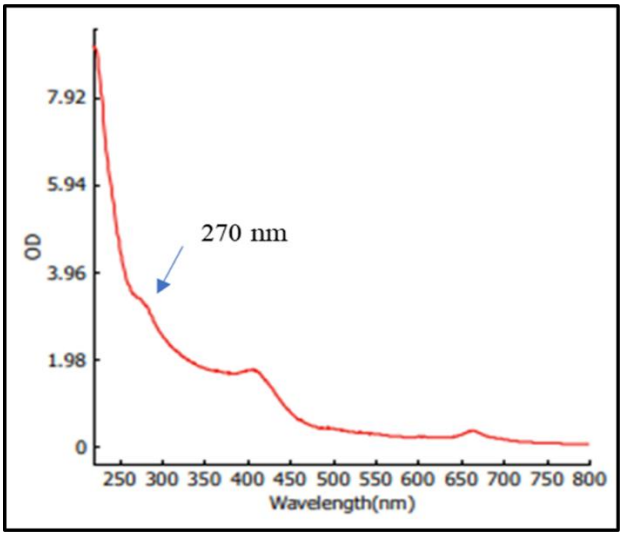

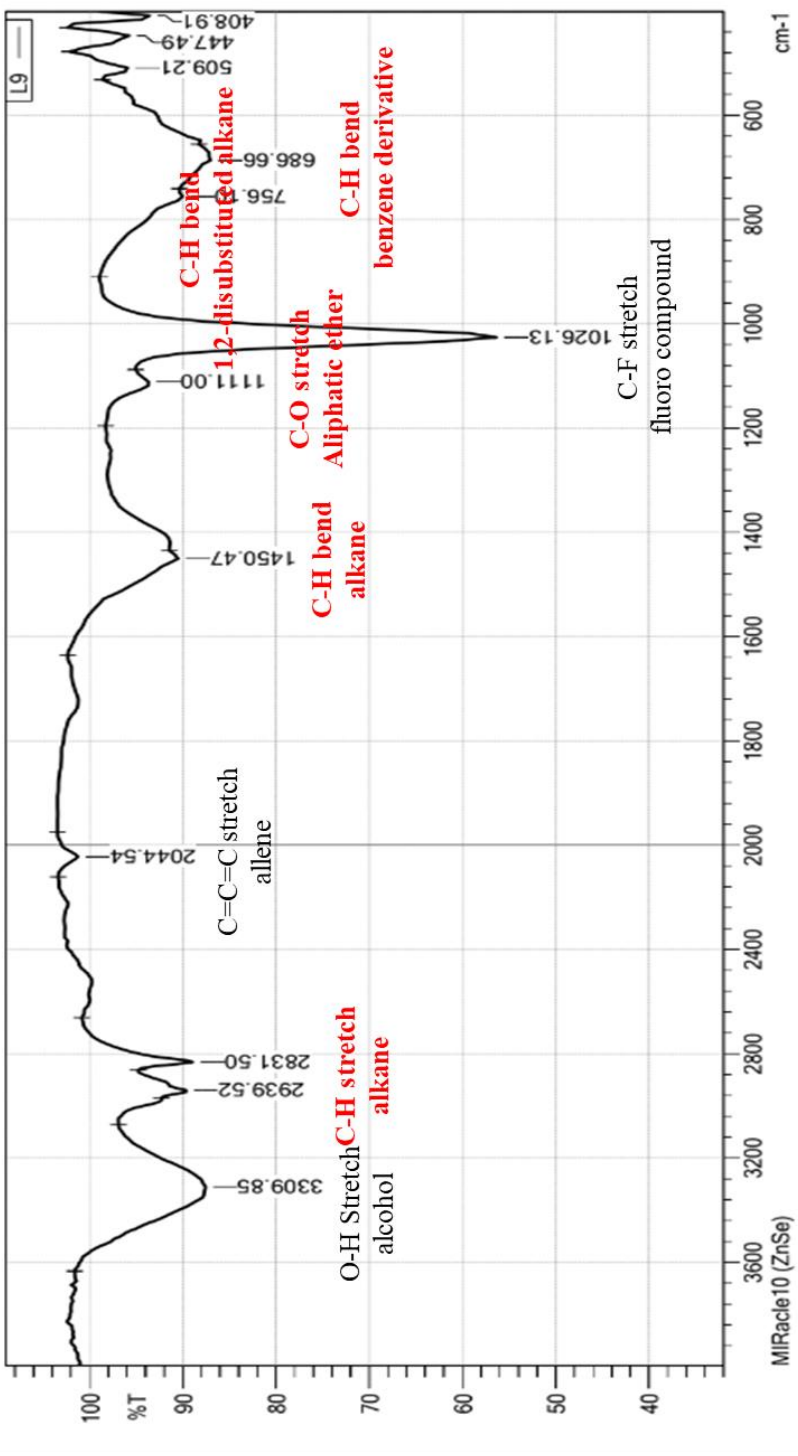

Fig. 19c FTIR analysis of isolated compound (fraction 1) from methanolic extract of *Rauvolfia tetraphylla* L.

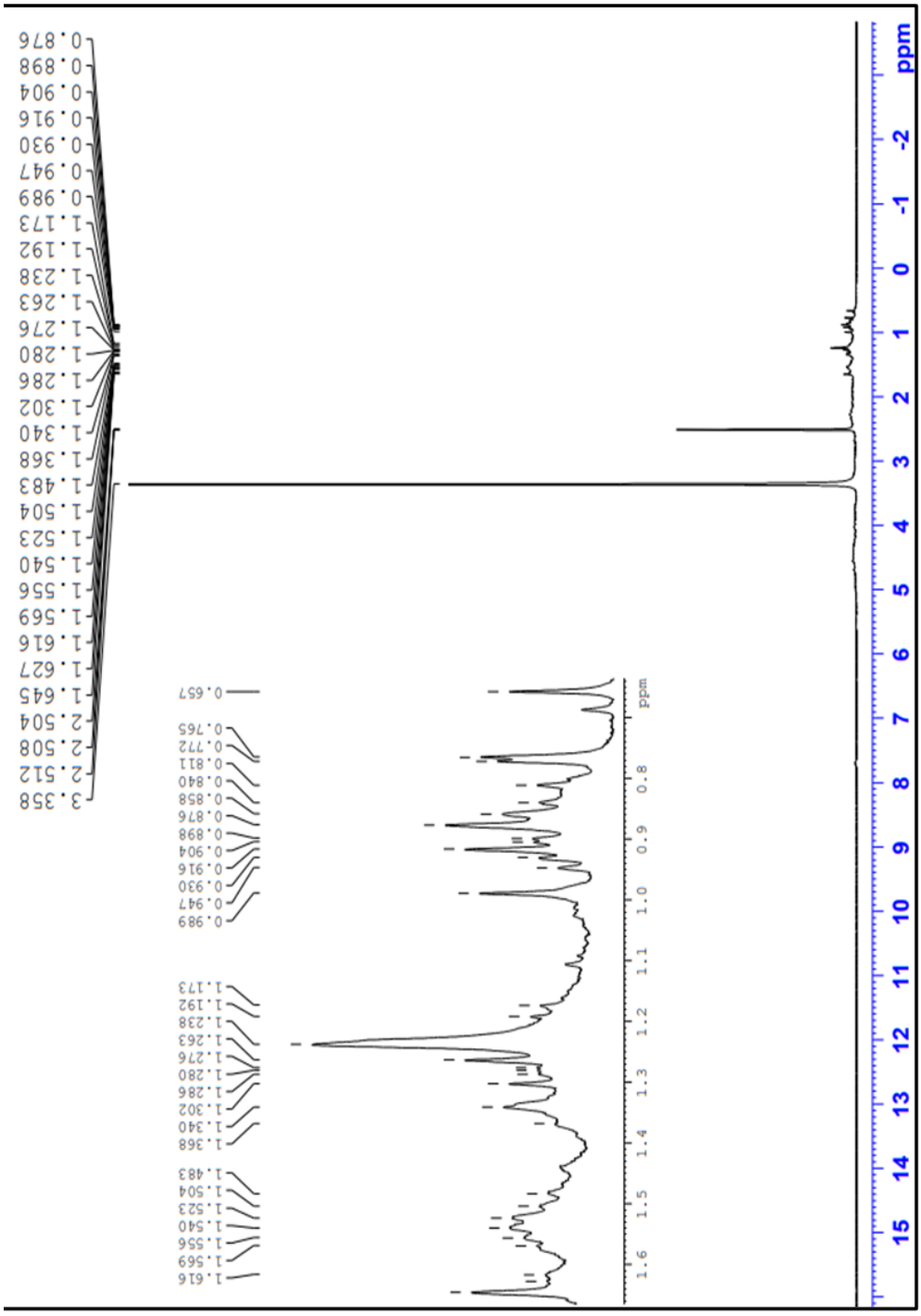

Fig. 19d ^{1}H NMR spectrum of isolated compound (fraction 1) from methanolic extract of of *Rauvolfia tetraphylla* L.

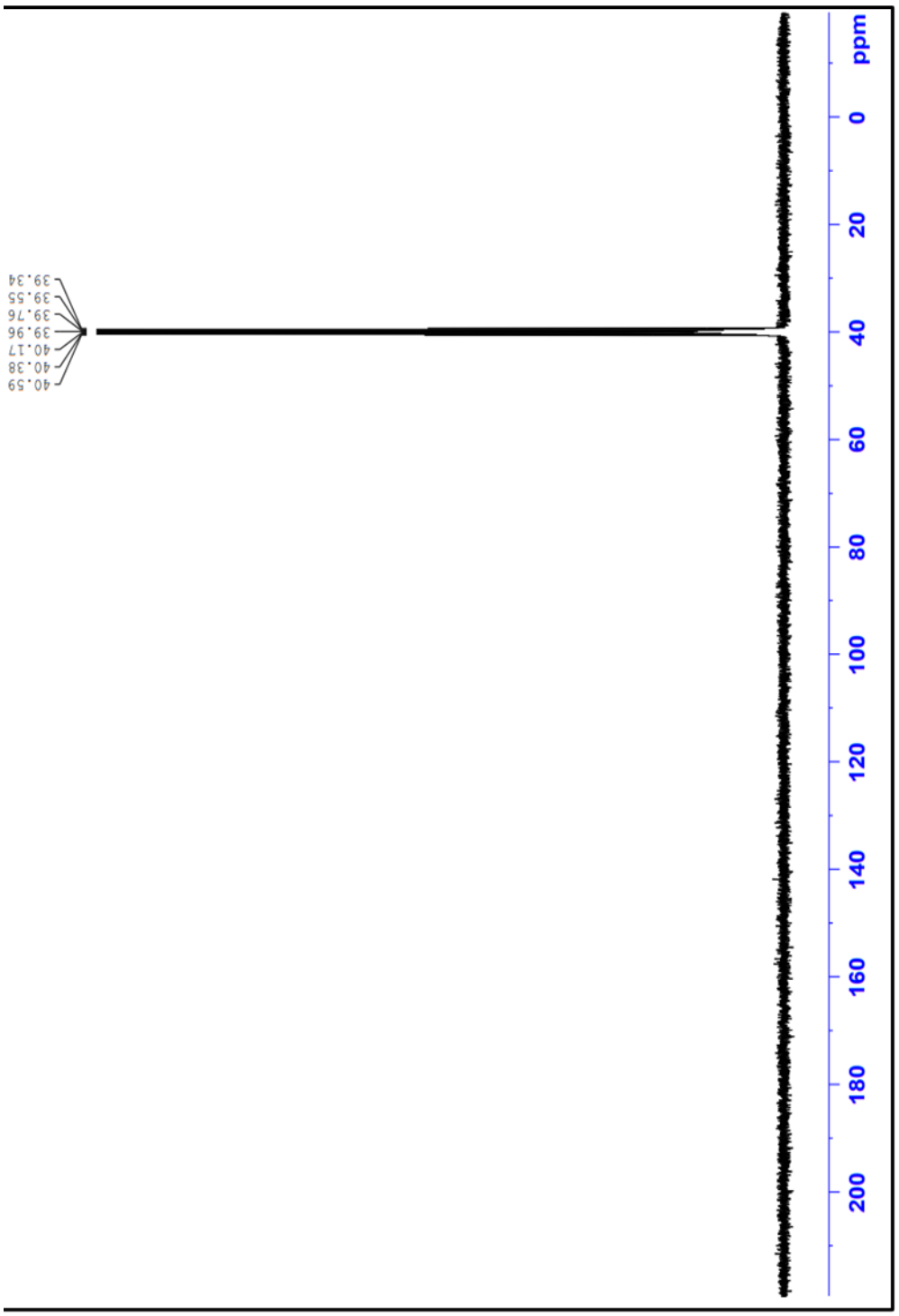

Fig. 19e ^{13}C NMR spectrum of isolated compound (fraction 1) from methanolic extract of *Rauvolfia tetraphylla* L.

Fig. 19f NIST Mass spectrum of isolated compound (fraction 1) from methanolic extract of *Rauvolfia tetraphylla* L.

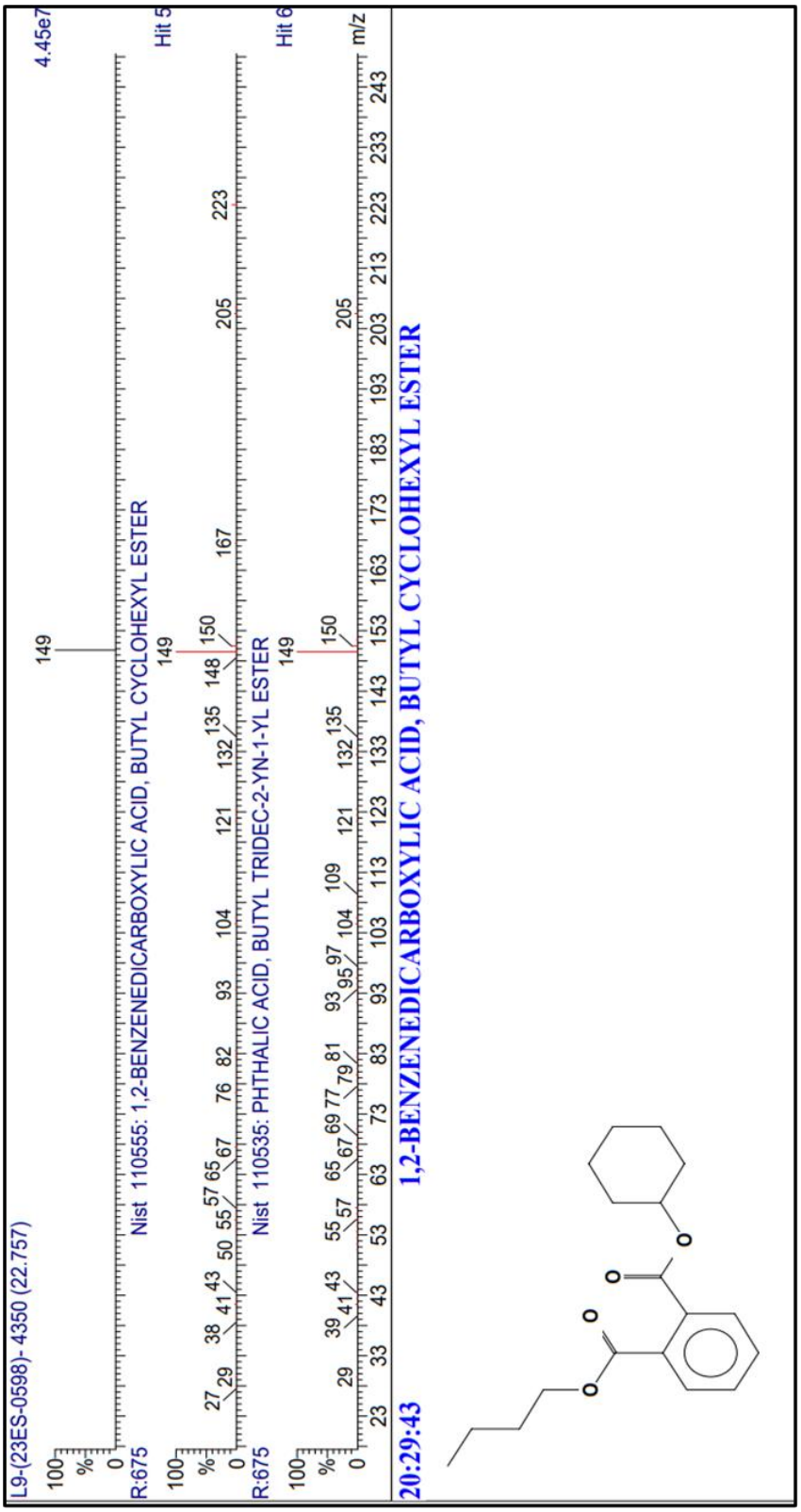

Fig. 20 Antibacterial activity of leaf extract of *Rauvolfia tetraphylla* L.

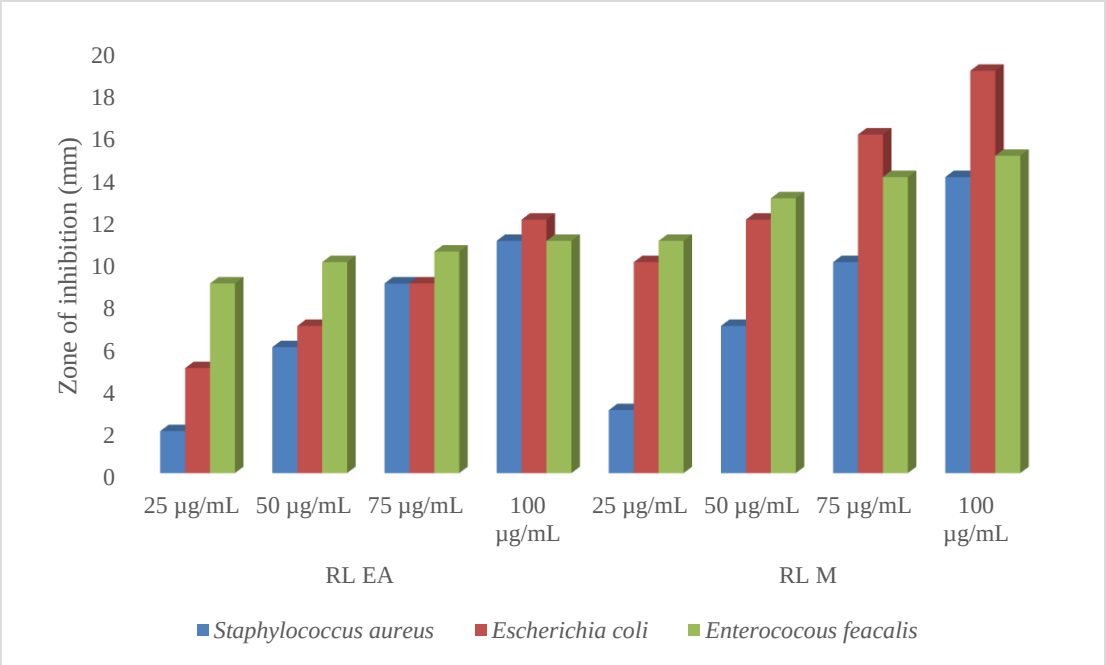

Fig. 21 Antibacterial activity of fruit extracts of *Rauvolfia tetraphylla* L.

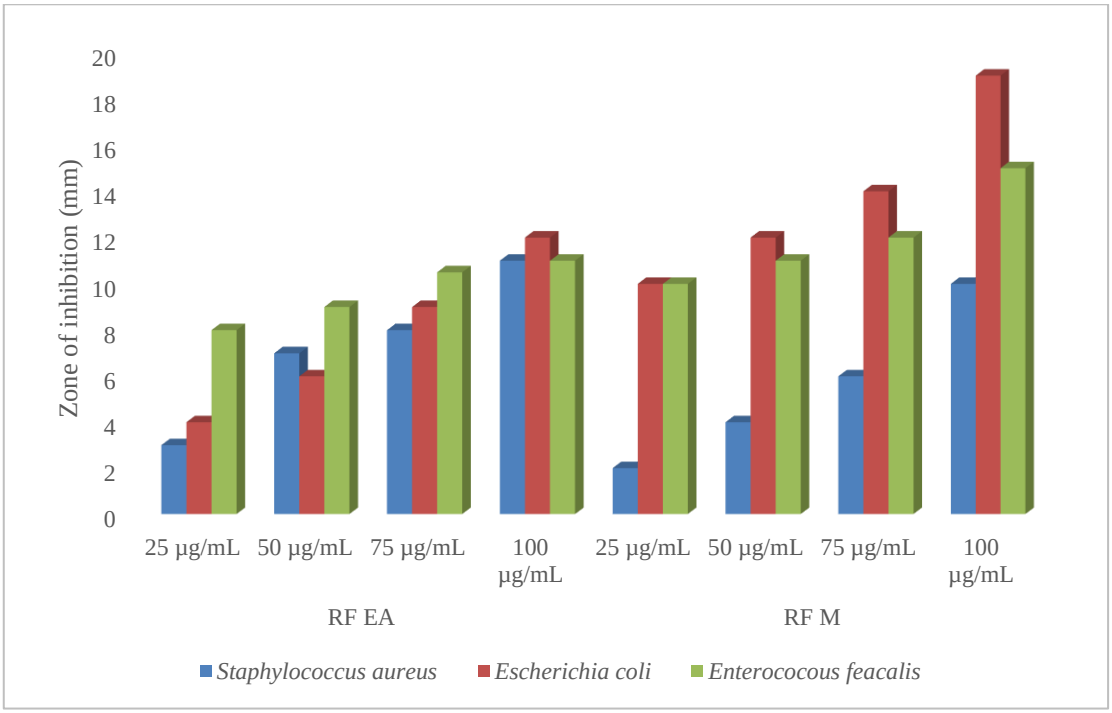

Fig. 22 DPPH radical scavenging activity of standard Ascorbic acid

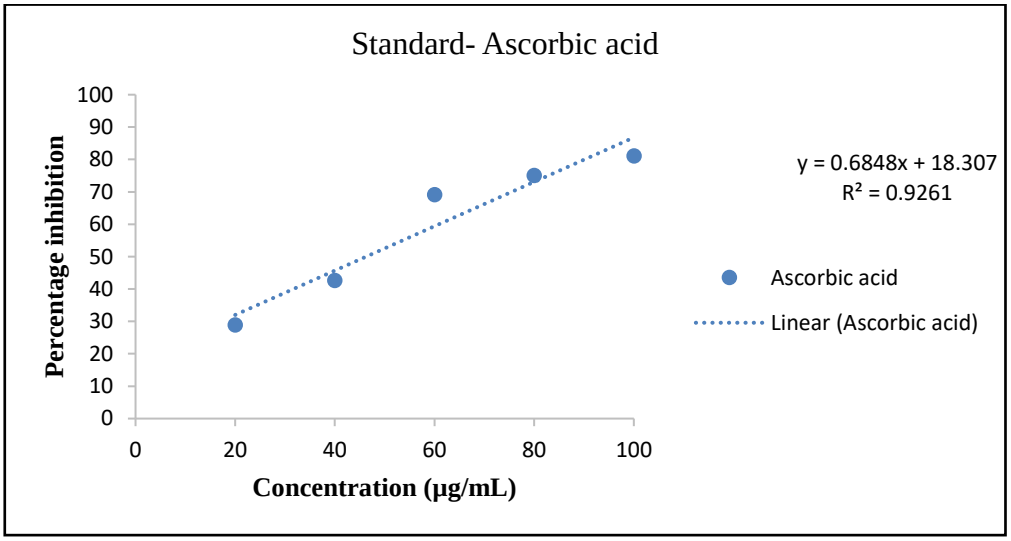

Fig. 23 DPPH radical scavenging activity of various crude extracts of fruit of *Rauvolfia tetraphylla* L.

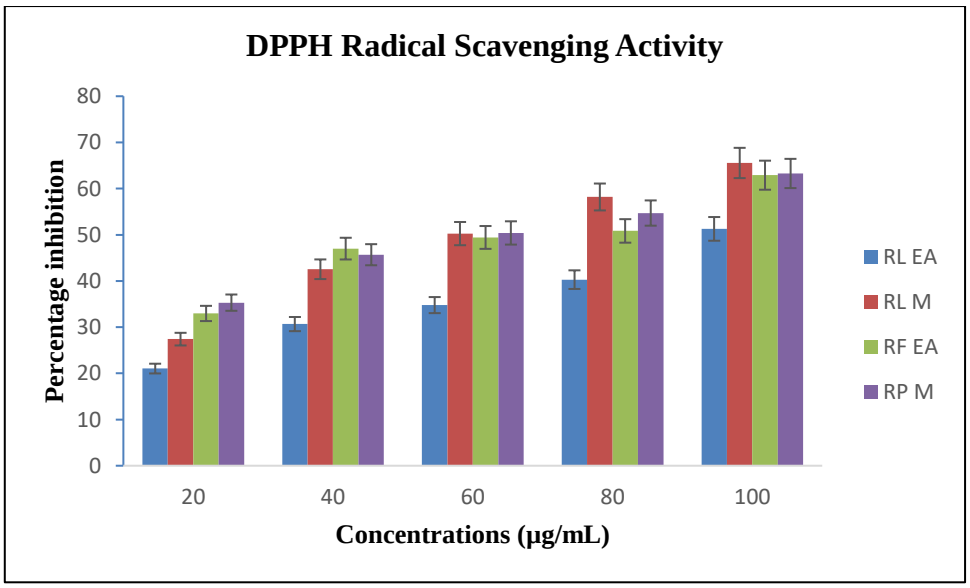

Fig. 24 Ferric Reducing Antioxidant Power (FRAP) Assay of *Rauvolfia tetraphylla* L.

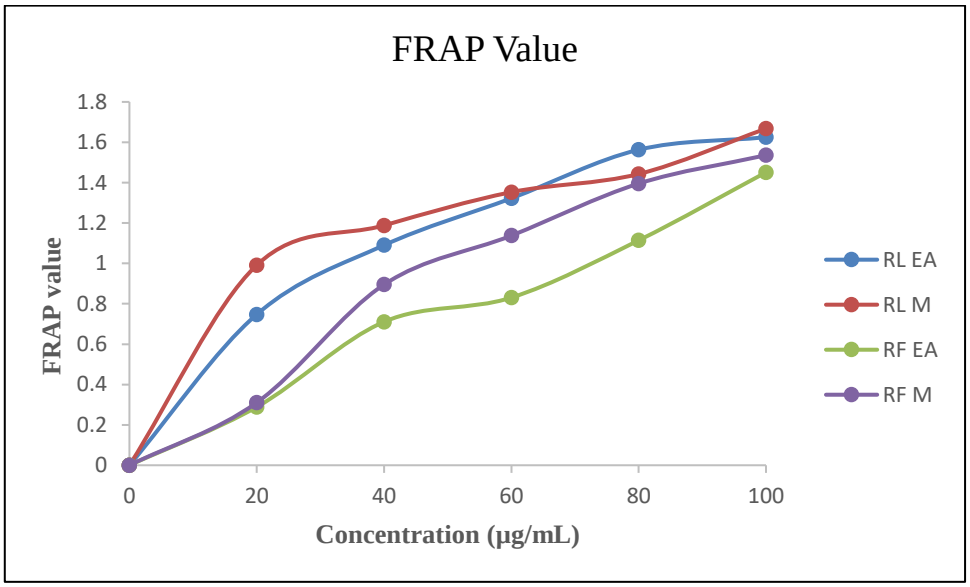

Fig. 25 Total antioxidant activity of standard Ascorbic acid

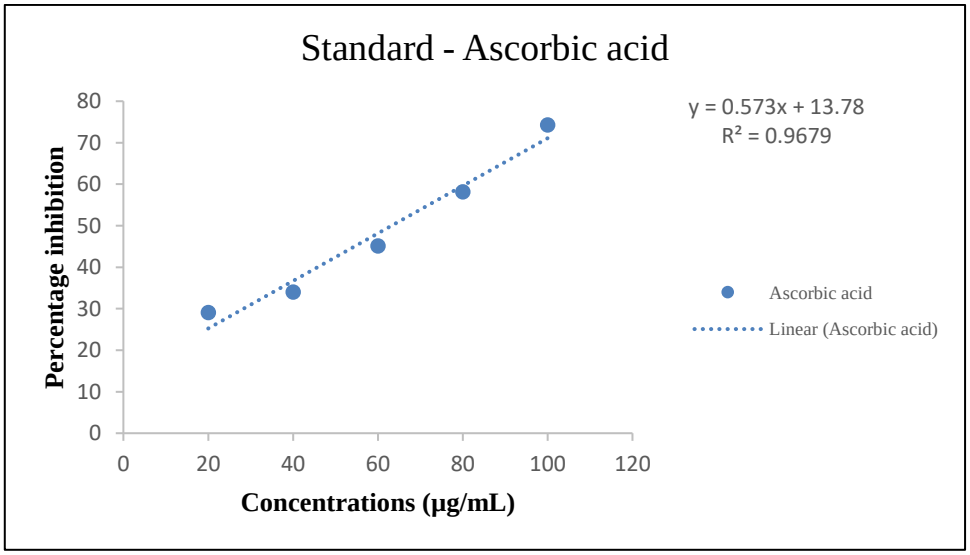

Fig. 26 Total antioxidant activity of various crude extracts of leaf and fruit of *Rauvolfia tetraphylla* L.

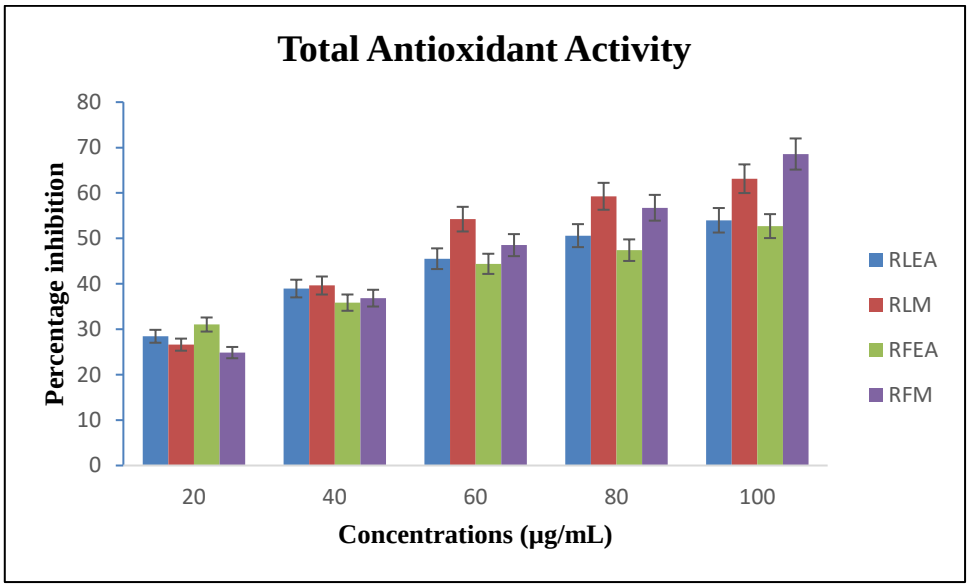

RL EA – Ethyl acetate extract of leaves; RL **M** – Methanol extracts of leaves

RF EA – Ethyl acetate extract of fruit; RF **M** – Methanol extract of fruit

Fig. 27 Anti-inflammatory activity of Diclofenac Sodium Standard

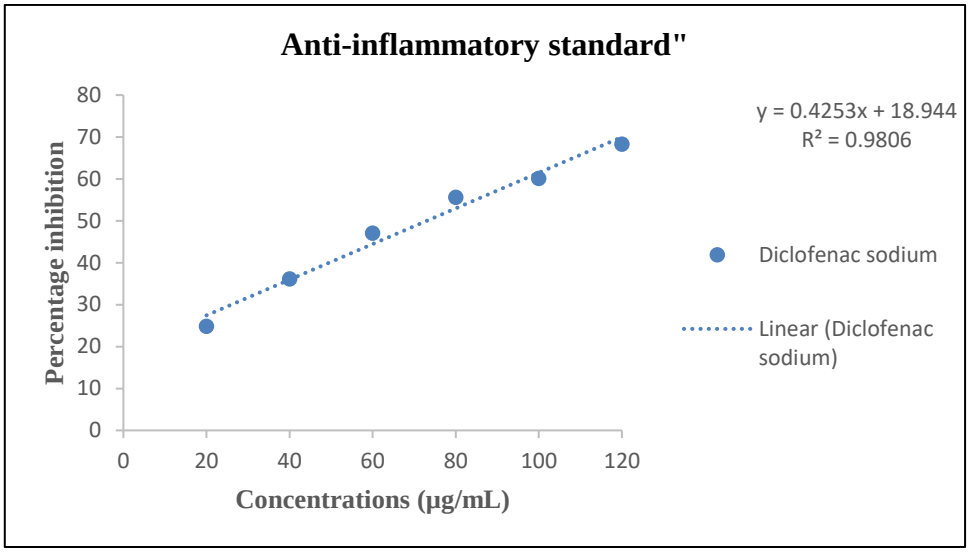

Fig. 28 Anti-inflammatory activity of various crude extracts of leaves and fruit of *Rauvolfia tetraphylla* L.

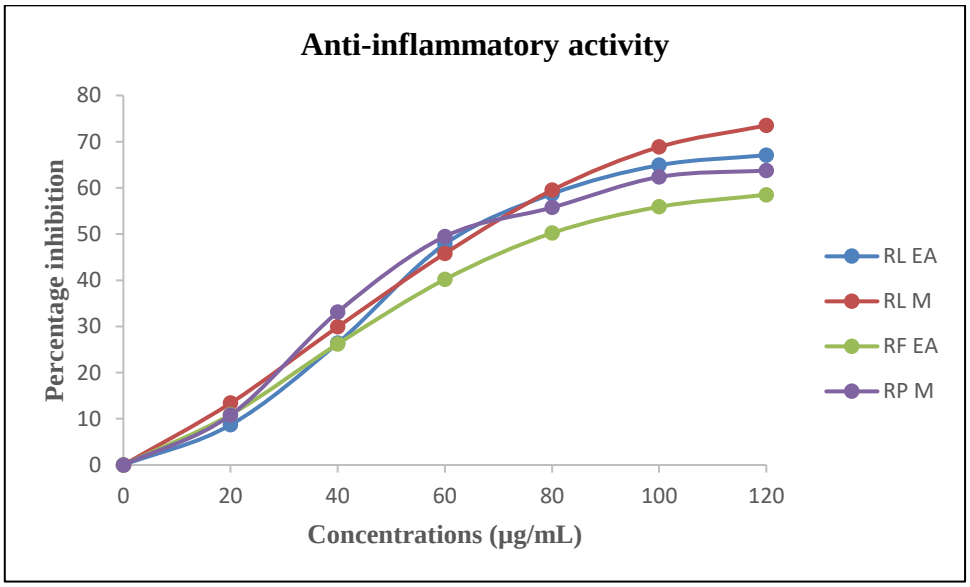

Fig. 29 Cytotoxicity activity of *Rauvolfia tetraphylla* extracts against Vero cells

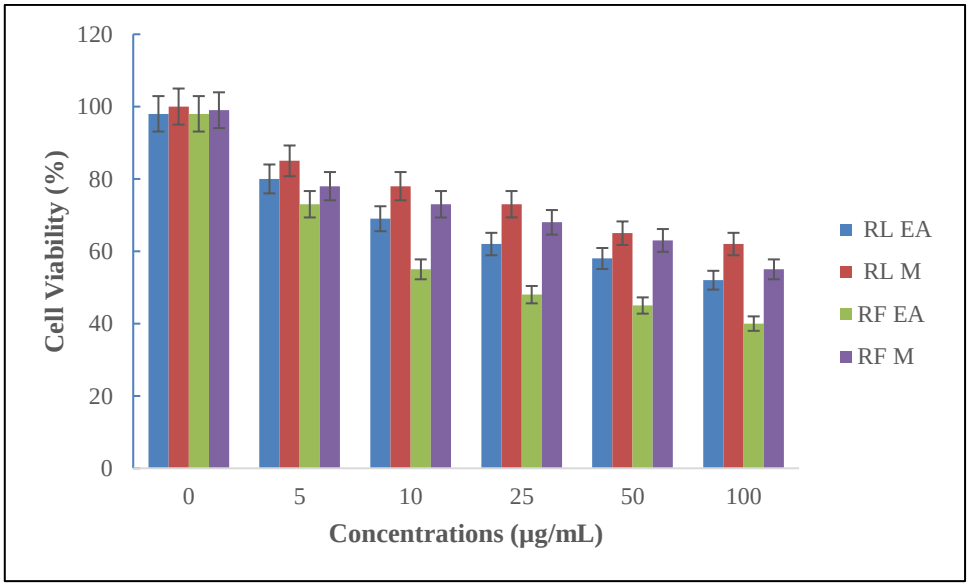

Fig. 30 Cytotoxicity activity of *Rauvolfia tetraphylla* extracts against 3T3 fibroblast cell line

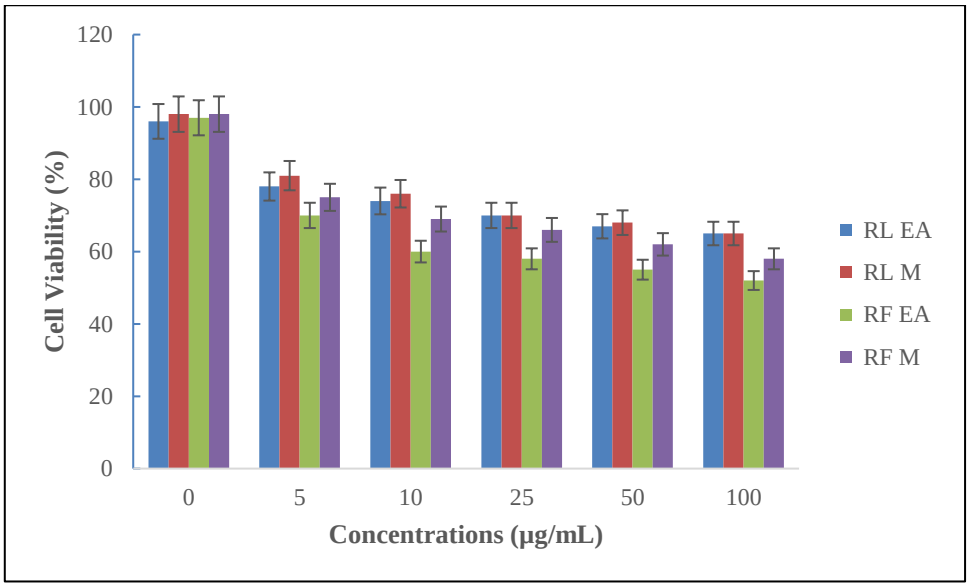

Fig. 31 Wound healing scratch assay using Vero cell line of *Rauvolfia tetraphylla* L.

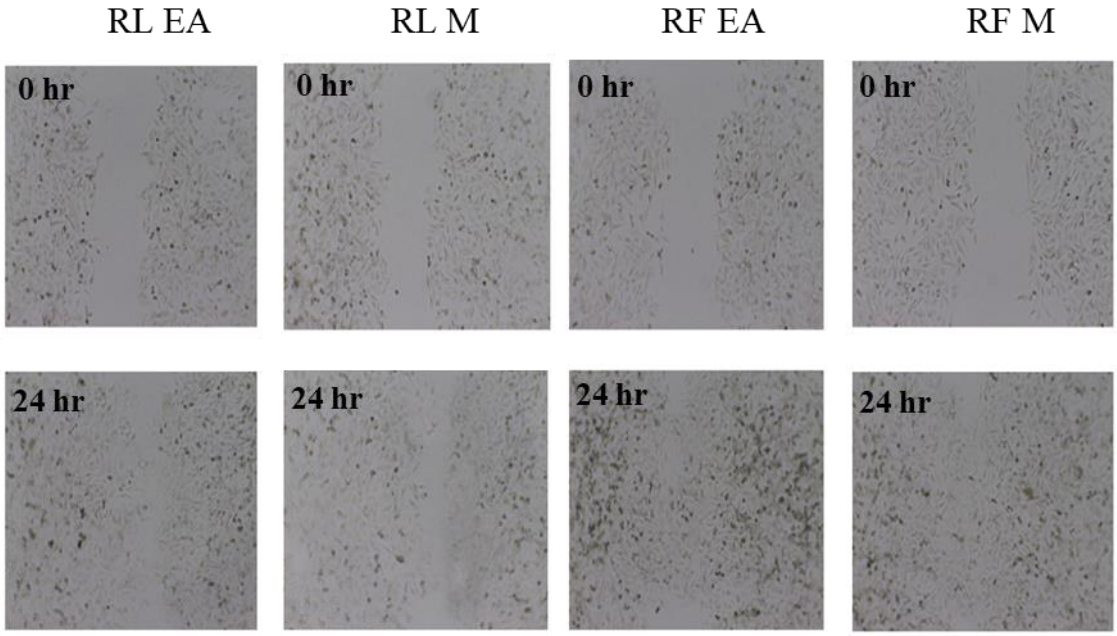

Fig. 32 Wound healing scratch assay using 3T3 fibroblast cells of *Rauvolfia tetraphylla* L.

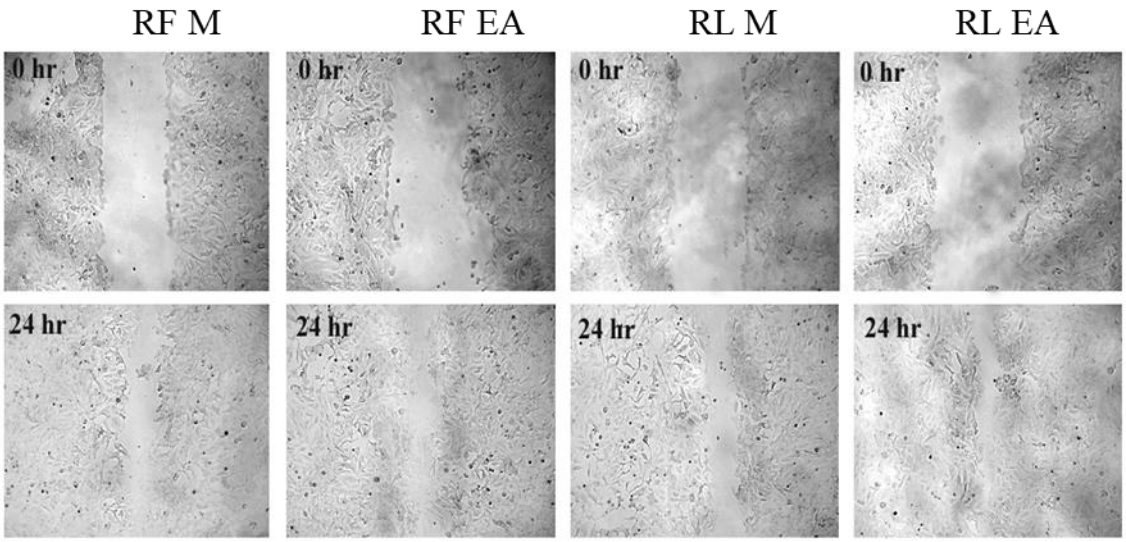

RL EA – Ethyl acetate extract of leaves; **RL M** – Methanol extracts of leaves

RF EA – Ethyl acetate extract of fruit; **RF M** – Methanol extract of fruit

Fig. 33 Chick Chorioallantoic Membrane (CAM) Assay of *Rauvolfia tetraphylla* L.

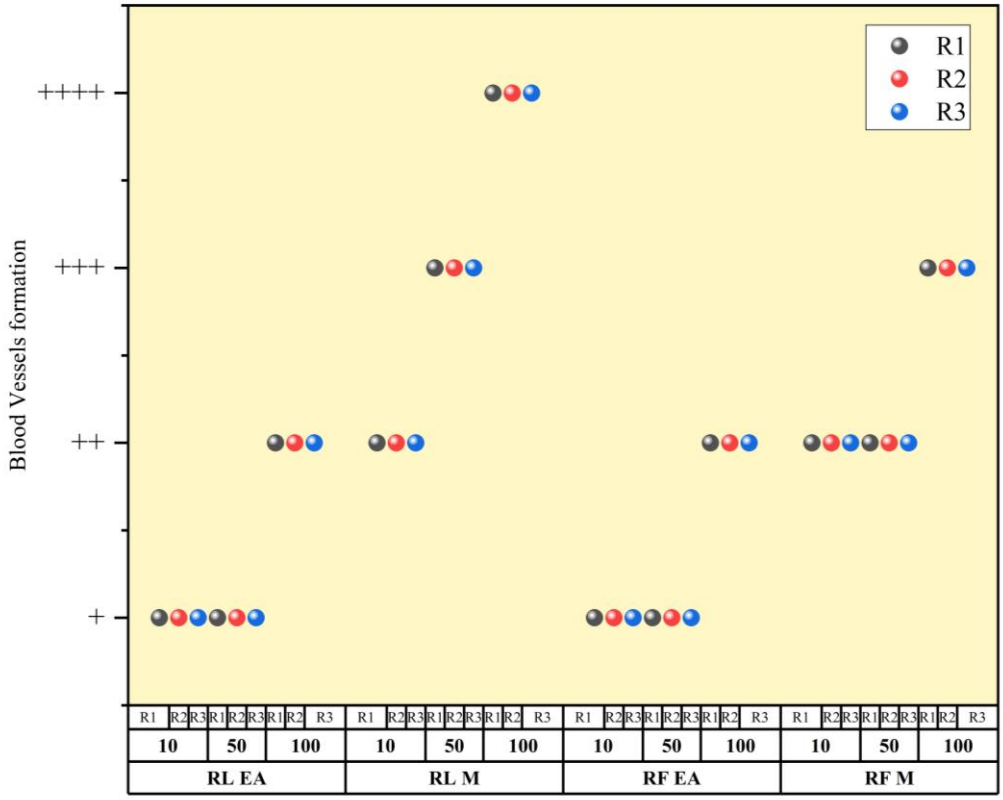

Blood vessels formation

'+' - weak

'++' - moderate

'+++' - strong

'++++' - very strong

RL EA – Ethyl acetate extract of leaves; **RL M** – Methanol extracts of leaves

RF EA – Ethyl acetate extract of fruit; **RF M** – Methanol extract of fruit

Fig. 34 Heat Stress Assay of *Rauvolfia tetraphylla* L. from leaf and fruit

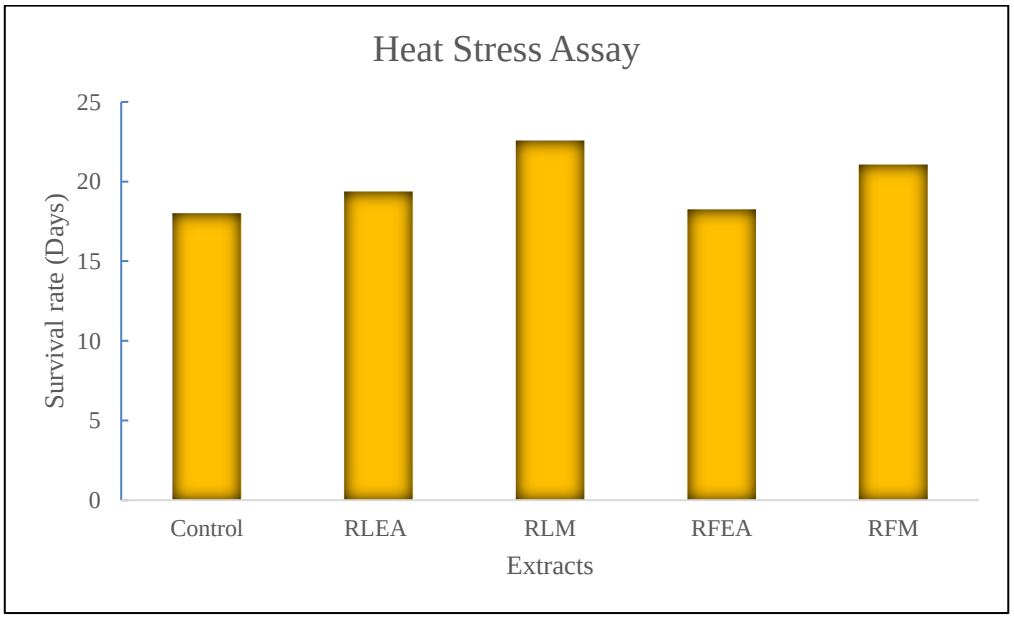

RL EA – Ethyl acetate extract of leaves; **RL M** – Methanol extracts of leaves

RF EA – Ethyl acetate extract of fruit; **RF M** – Methanol extract of fruit

Fig. 35 *In vivo* wound healing in Zebra fish model of *Rauvolfia tetraphylla* L.

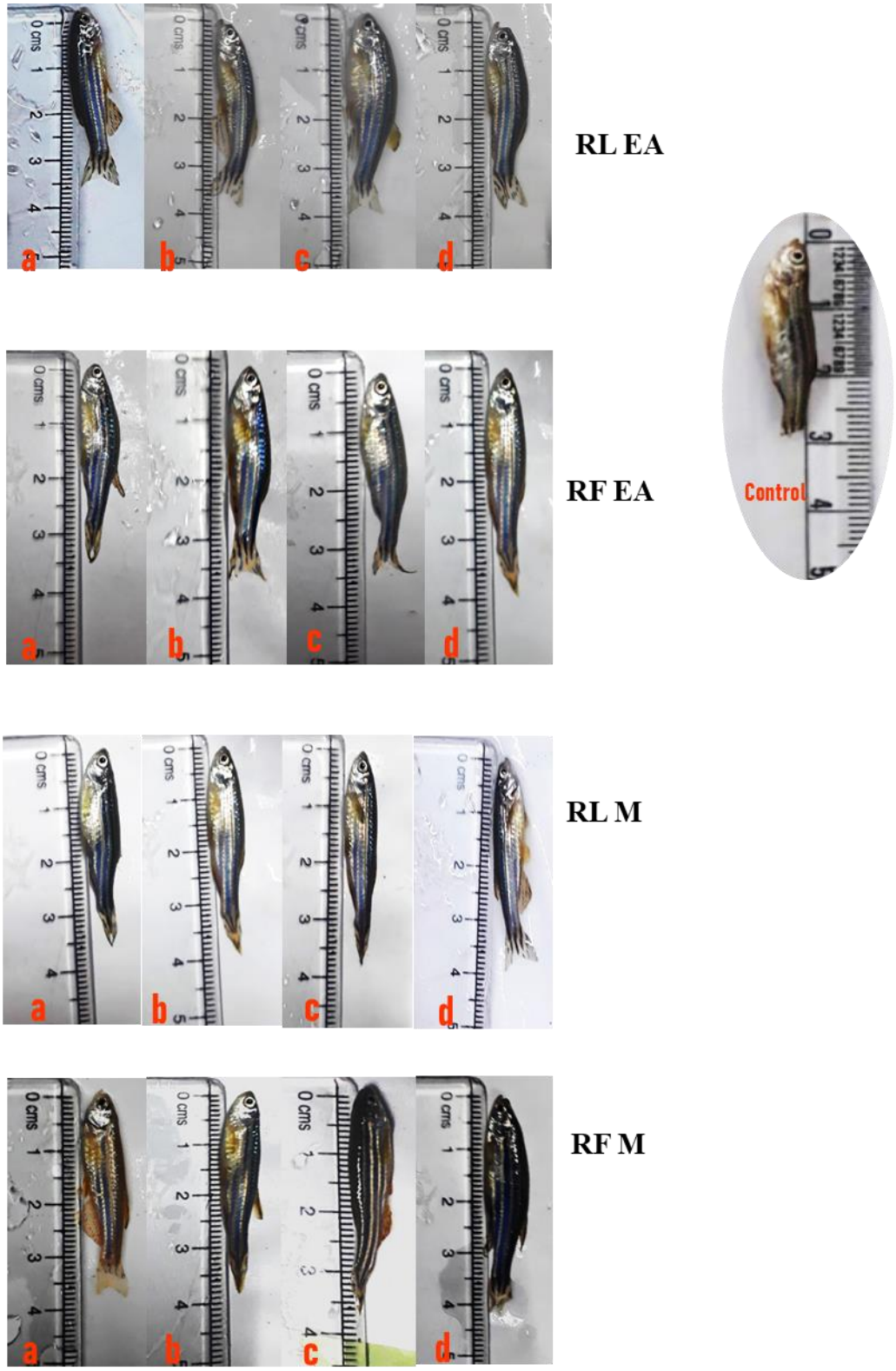

a) 25 µg/mL; (b) 50 µg/mL; (c) 75 µg/mL; (d) 100 µg/mL

Fig 36 Histological representation of zebrafish from leaf and fruit of *Rauvolfia tetraphylla* L.

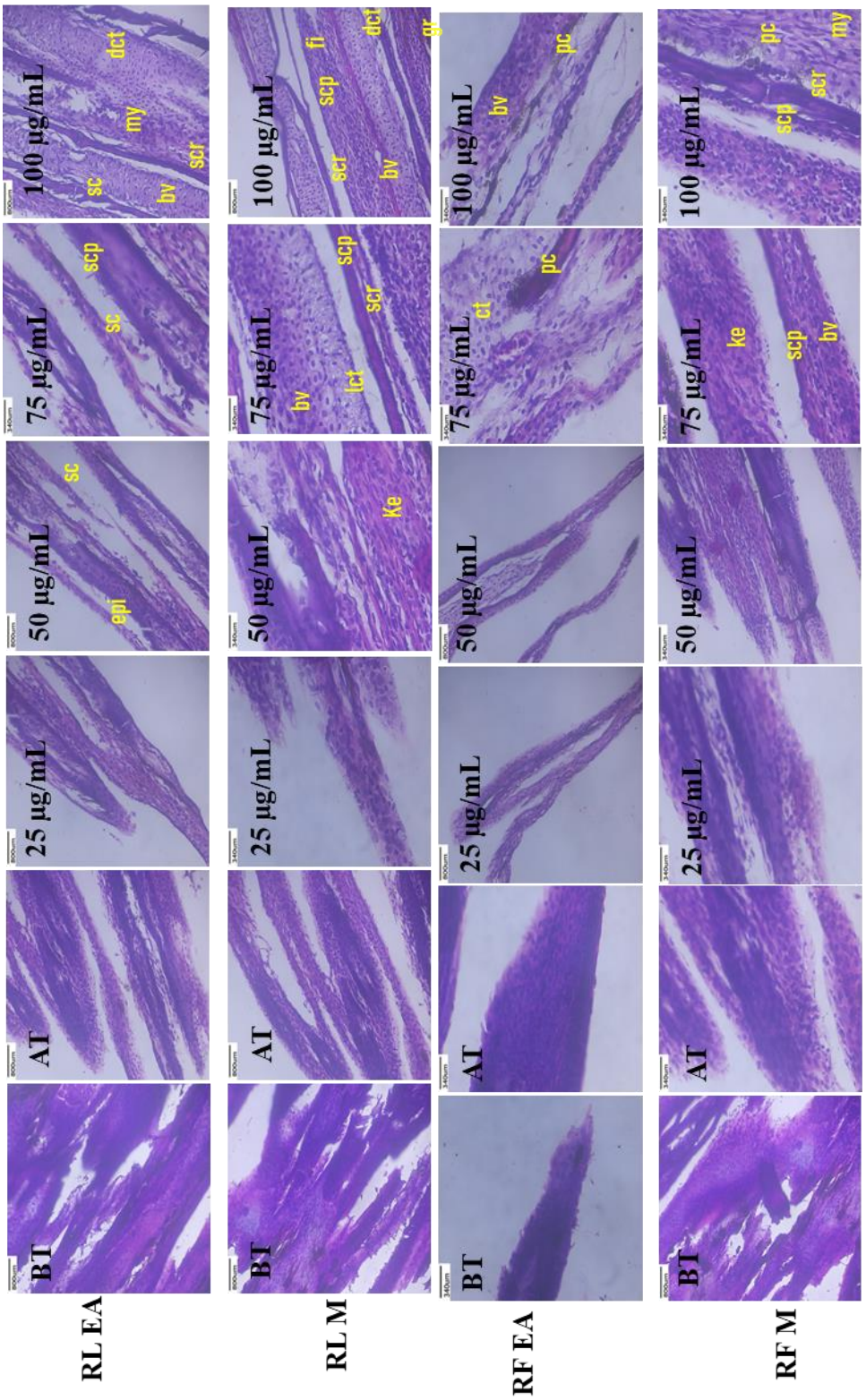

epidermis (epi); scale formation (sc); blood vessels (bv); separate scale pocket (scp); dense connective tissue (dct); loose connective tissues (lct); keratocytes (ke); pigment cells (pc); myofibroblast (my); fibroblast (fi); granulation tissue (gr)

Fig. 37 Isolation of Tryptophan decarboxylase from leaf of *Rauvolfia tetraphylla* L.

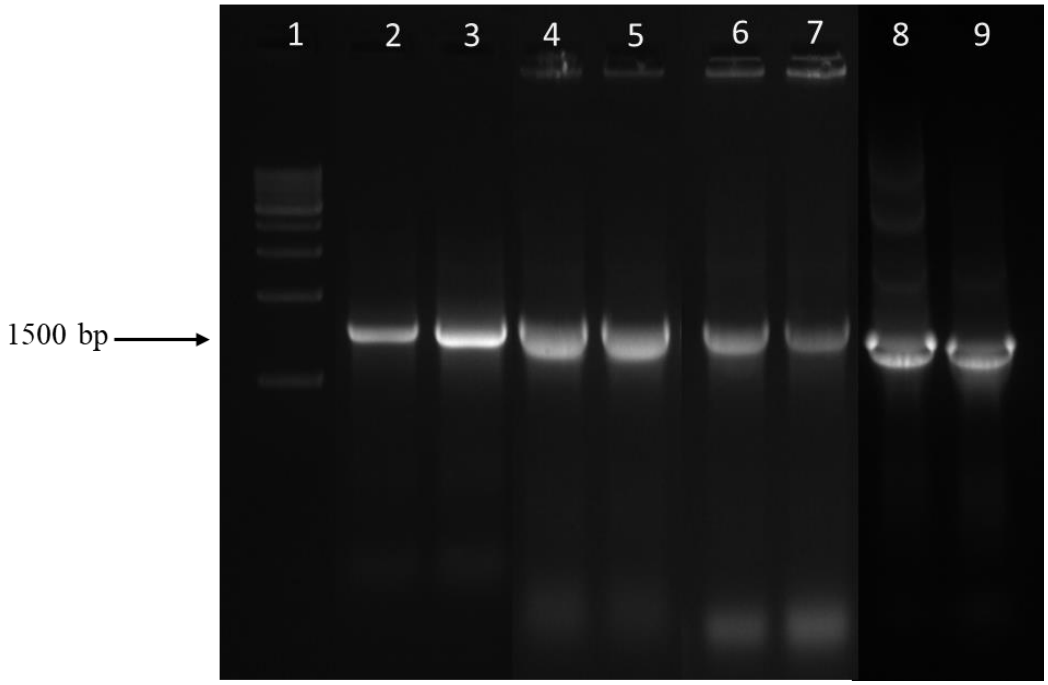

PCR products from genomic DNA on 1% agarose gel of known molecular weight.

Lane 1: DNA molecular weight marker (DNA ladder mix – 1kb ladder, Gene Ruler)

Lane 2&3: A total of 20 µL of PCR product amplification of TDC gene stained with ethidium bromide

Lane 4-7: Colony PCR for the confirmation of transformation;

Lane 8&9: Isolation of Plasmid after plasmid extraction process by QIAprep Spin Miniprep kit

Fig. 38 Ramachandran Plot

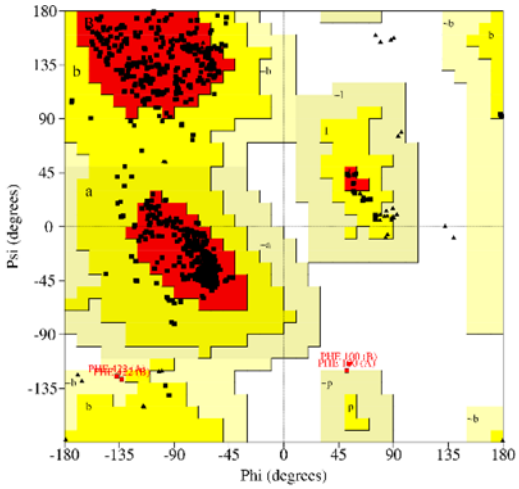

Fig. 39 Multiple sequence alignment

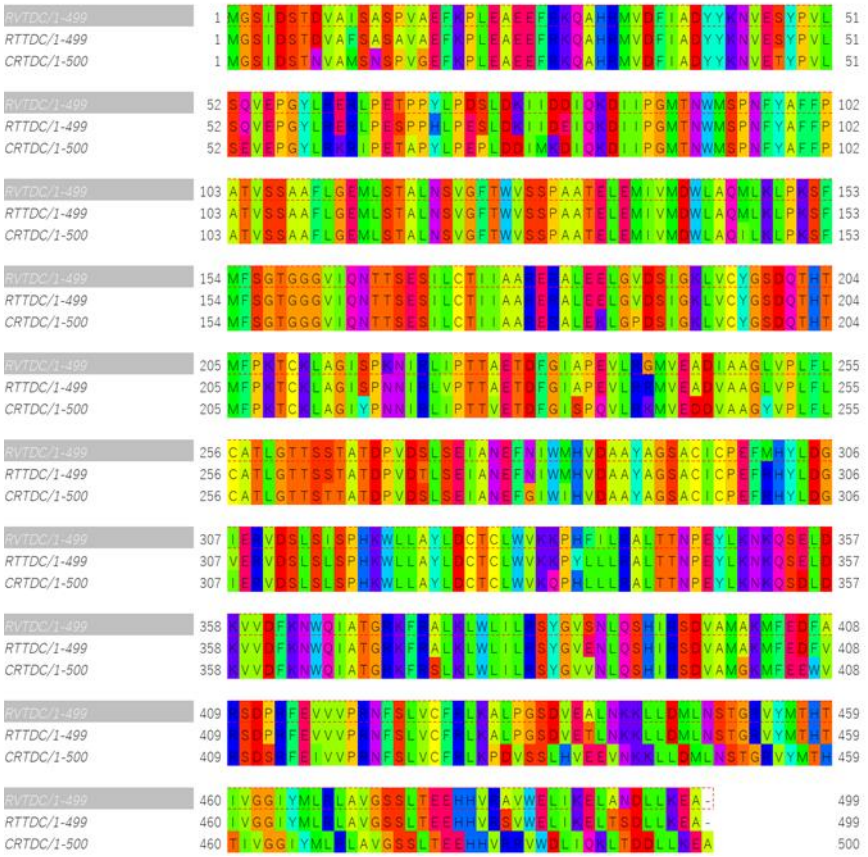

Fig. 40 Phylogenetic tree with related sequences

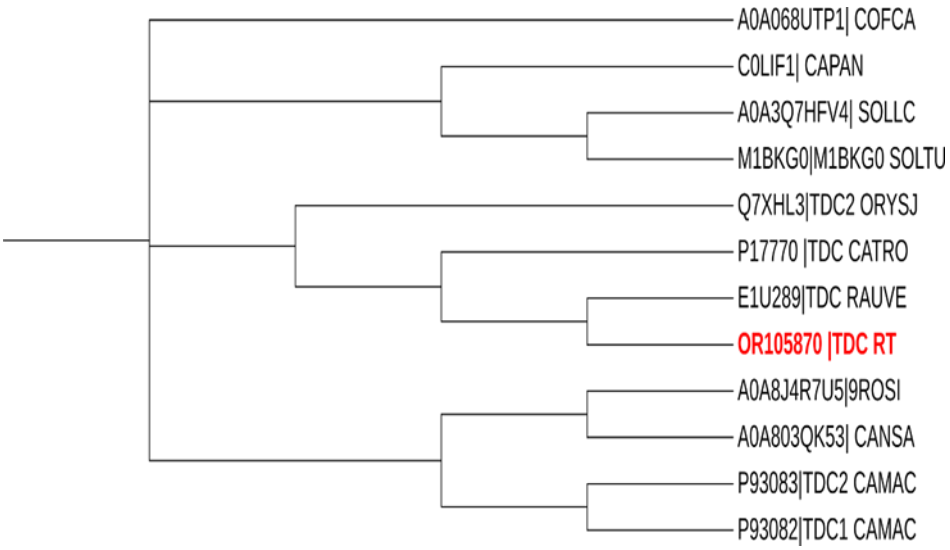

Bootstrap values are all above 95%. COFCA- *Coffea canephora*, CAPAN - *Capsicum annuum*, SOLLC - *Solanum lycopersicum*, SOLTU- *Solanum tuberosum*, ORYSJ- *Oryza sativa*, CATRO– *Catharanthus roseus*, RAUVE- *Rauvolfia verticilla*, TDC RT – *Rauvolfia tetraphylla*, 9ROSI - *Castanea mollissima*, CANSA - *Cannabis sativa*, CAMAC - *Camptotheca acuminata*.

Fig. 41 Hydropathy plot

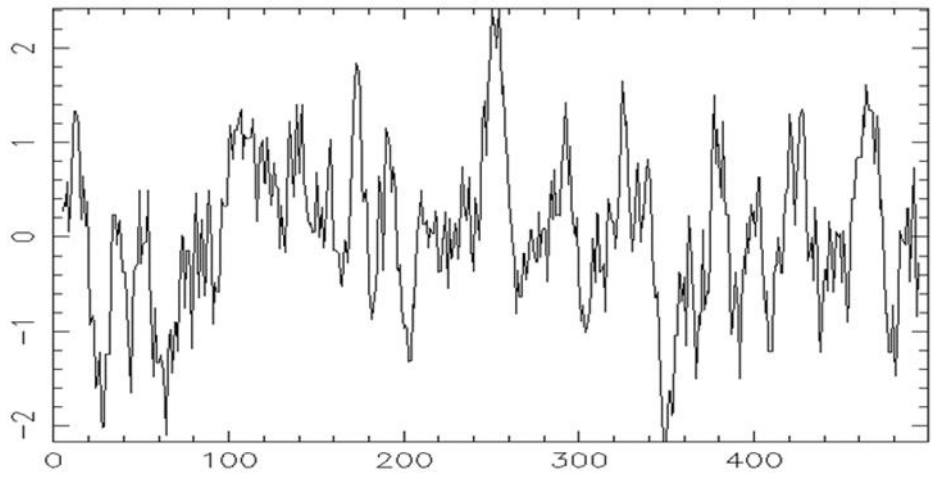

Fig. 42 Secondary Structure prediction of TDC

```
        10        20        30        40        50        60        70
         |         |         |         |         |         |         |
MGSIDSTDVAFSASAVAEFKPLEAEEFRKQAHRMVDFIADYYKNVESYPVLSQVEPGYLRERLPESPPHL
ccccccchchhehhhhhhhcccchhhhhhhhhhhhhhhhhhhhhcccccceeeecccccccccccccccc
PESLDKIIDEIQKDIIPGMTNWMSPNFYAFFPATVSSAAFLGEMLSTALNSVGFTWVSSPAATELEMIVM
chhhhhhhhhhhhhhhcccccccccchhhccccchchhhhhhhhhhhhhccceeeeecccchhhhhhhhh
DWLAQMLKLPKSFMFSGTGGGVIQNTTSESILCTIIAARERALEELGVDSIGKLVCYGSDQTHTMFPKTC
hhhhhhhhcccceeeecccceeeeecccchhhhhhhhhhhhhhhhhhhcccchceeeeecccccccccccc
KLAGISPNNIRLVPTTAETDFGIAPEVLRRMVEADVAAGLVPLFLCATLGTTSSTATDPVDTLSEIANEF
eeccccccceeeecccccccccchhhhhhhhhhhhhhhhhhhhheeecccccccccchhhhhhhhhhhh
NIWMHVDAAYAGSACICPEFRHYLDGVERVDSLSLSPHKWLLAYLDCTCLWVKKPYLLLRALTTNPEYLK
hhhhhhhhhhccccecccchhccccchhecccccccchhhhhhhhcccchhhhccchhhhhhhhcccccccc
NKQSELDKVVDFKNWQIATGRKFRALKLWLILRSYGVENLQSHIRSDVAMAKMFEDFVRSDPRFEVVVPR
cchhhhhhhhhccccchhhhhhhhhhhhhhhhhhhhccchhhhhhhhhhhhhhhhhhhhhccccceeeeecc
NFSLVCFRLKALPGSDVETLNKKLLDMLNSTGRVYMTHTIVGGIYMLRLAVGSSLTEEHHVRSVWELIKE
cceeeeeeecccccchhhhhhhhhhhhhccceeeeeeeechhheeeecccccchhhhhhhhhhhhhh
LTSDLLKEA
hhhhhhhcc
```

Fig 42 a) blue (h-Helix), orange (c-coil), red (e-sheet)

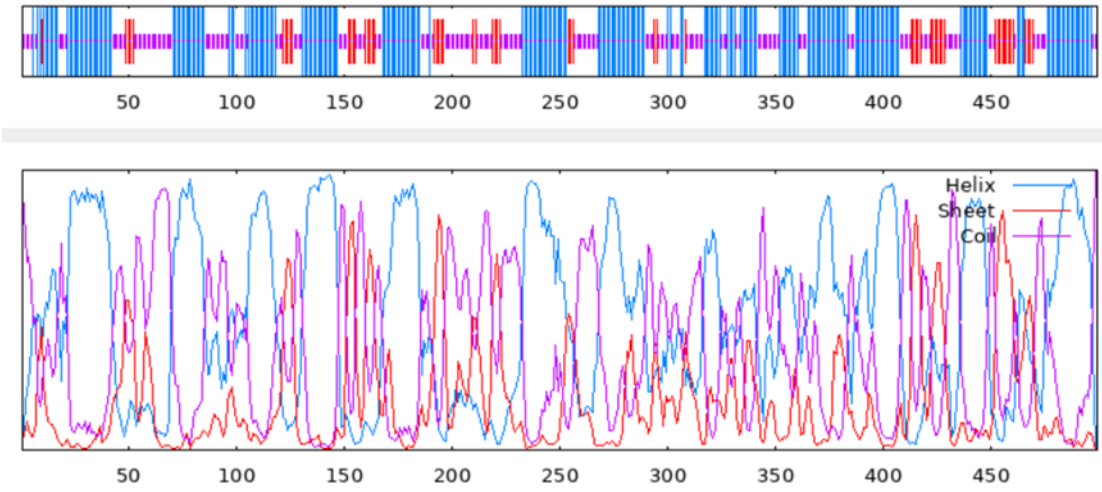

Fig. 42 b) Secondary Structure prediction of TDC *Rauvolfiate traphylla* protein sequence

Fig. 43 Pharmacophore model

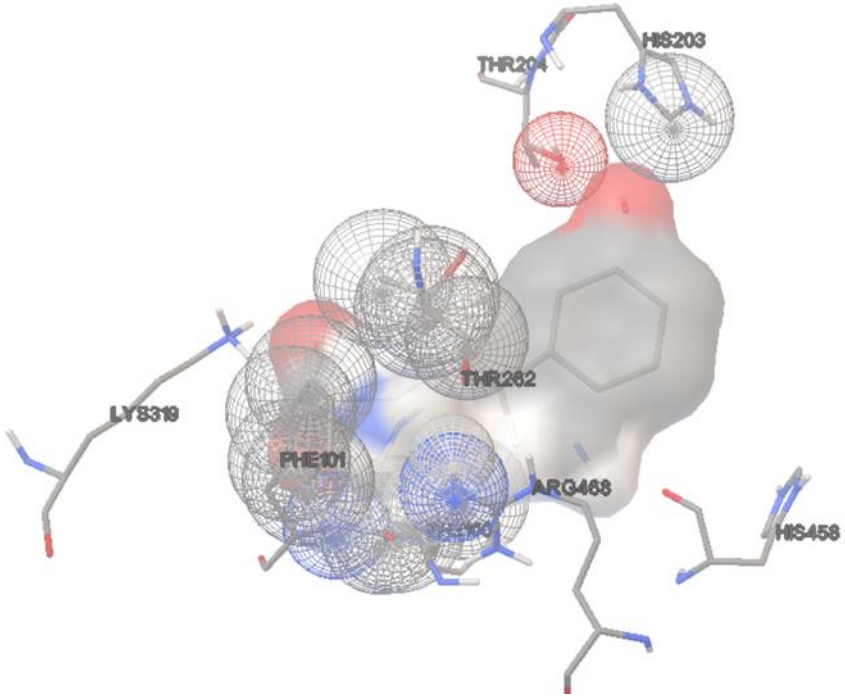

Fig. 44 Hydrogen Bond Interactions

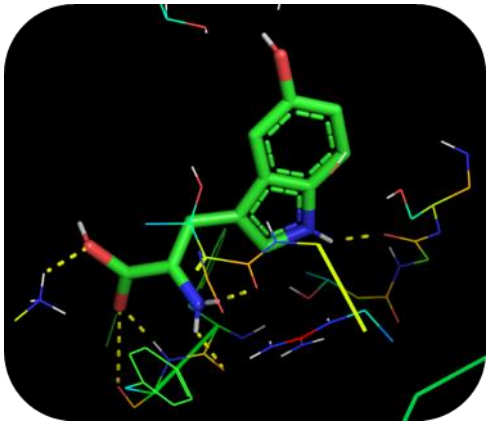

Fig. 45 Two-dimensional Analysis using Ligplot

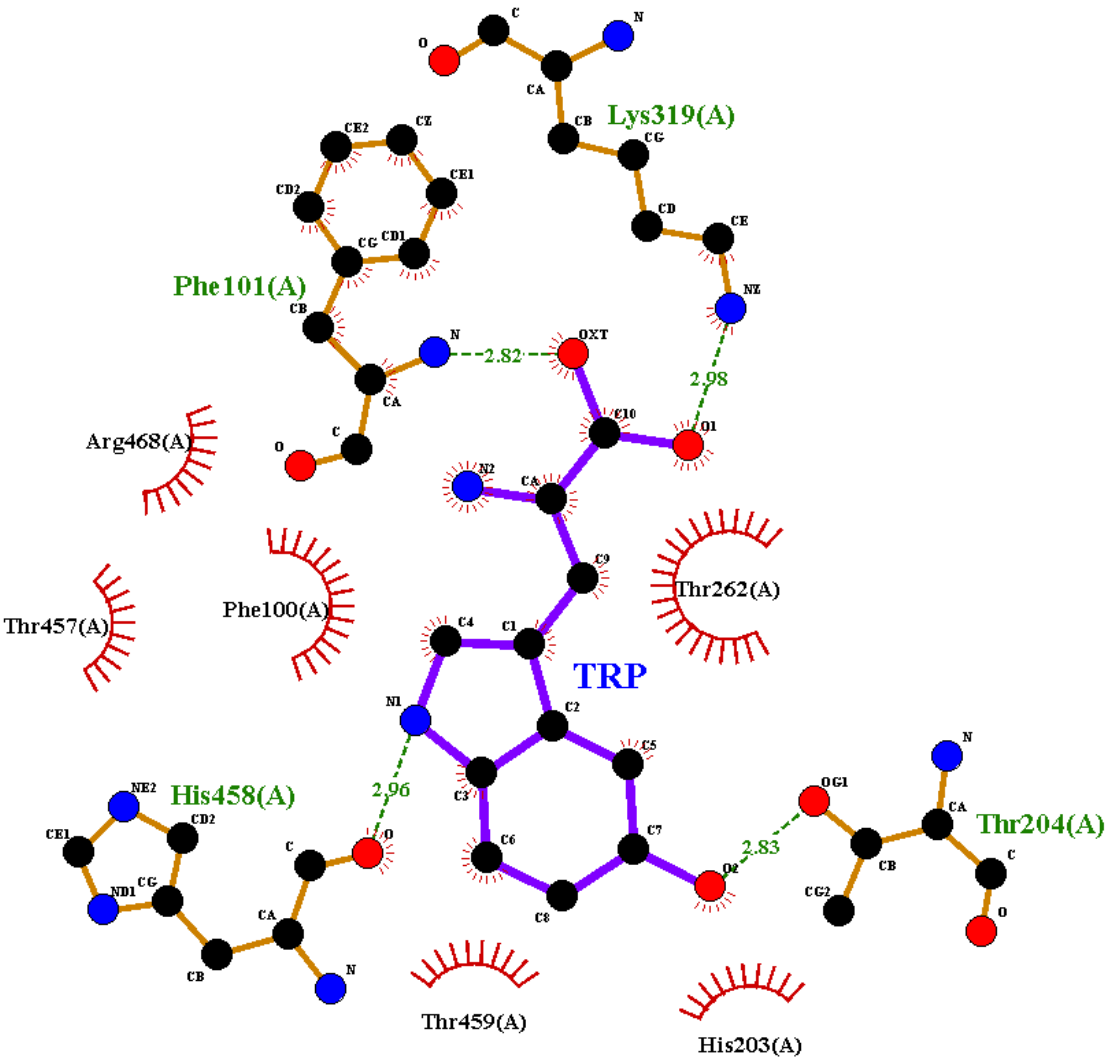

Ligand - blue-coloured, hydrogen-bonded residues from the protein -brown-coloured, Dashed lines - hydrogen bonds formed between the ligand and the protein, Hydrophobic contacts-spoked arcs pointing towards the ligand, corresponding spokes - which atoms are engaged in these contacts.

Fig. 46 Biosynthetic Pathway for Tryptophan

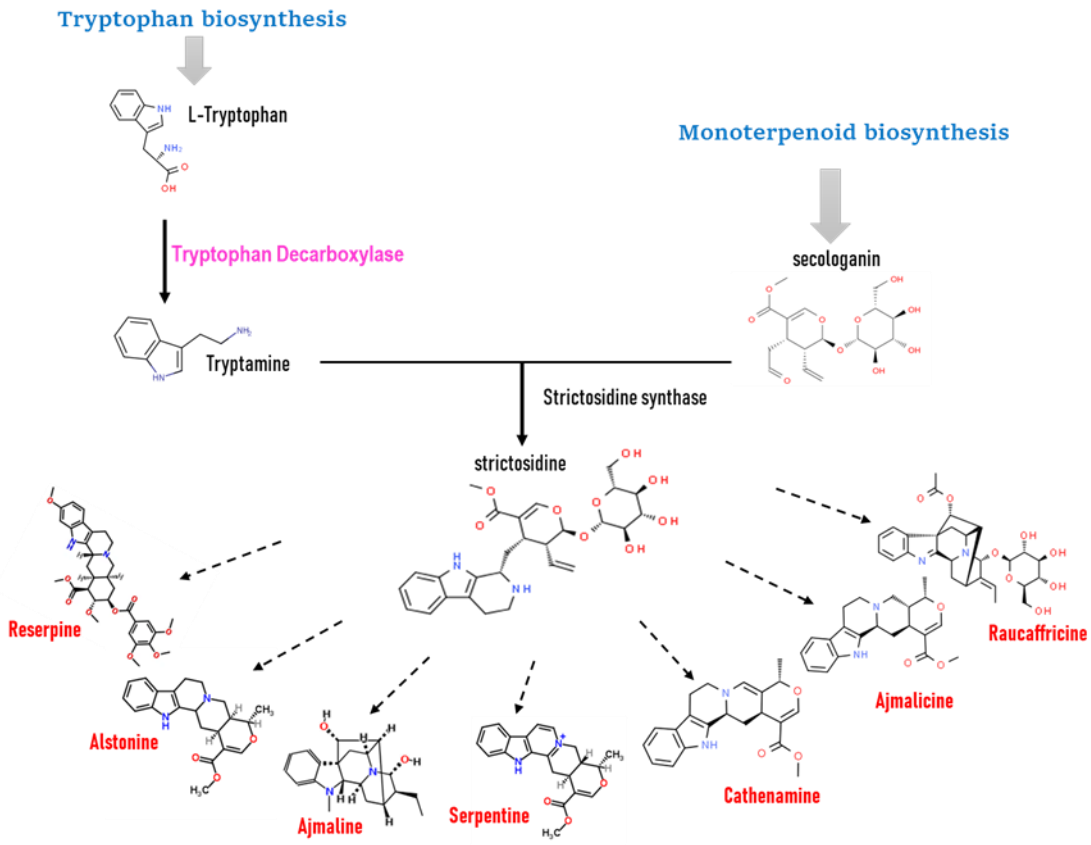

The biosynthetic pathway for indole alkaloids in *Rauvolfia tetraphylla* begins with the conversion of L-tryptophan, derived from tryptophan biosynthesis. In the presence of the enzyme tryptophan decarboxylase, L-tryptophan is transformed into tryptamine, ultimately leading to the production of alkaloids.

Fig. 47 High Pressure Liquid Chromatography analysis

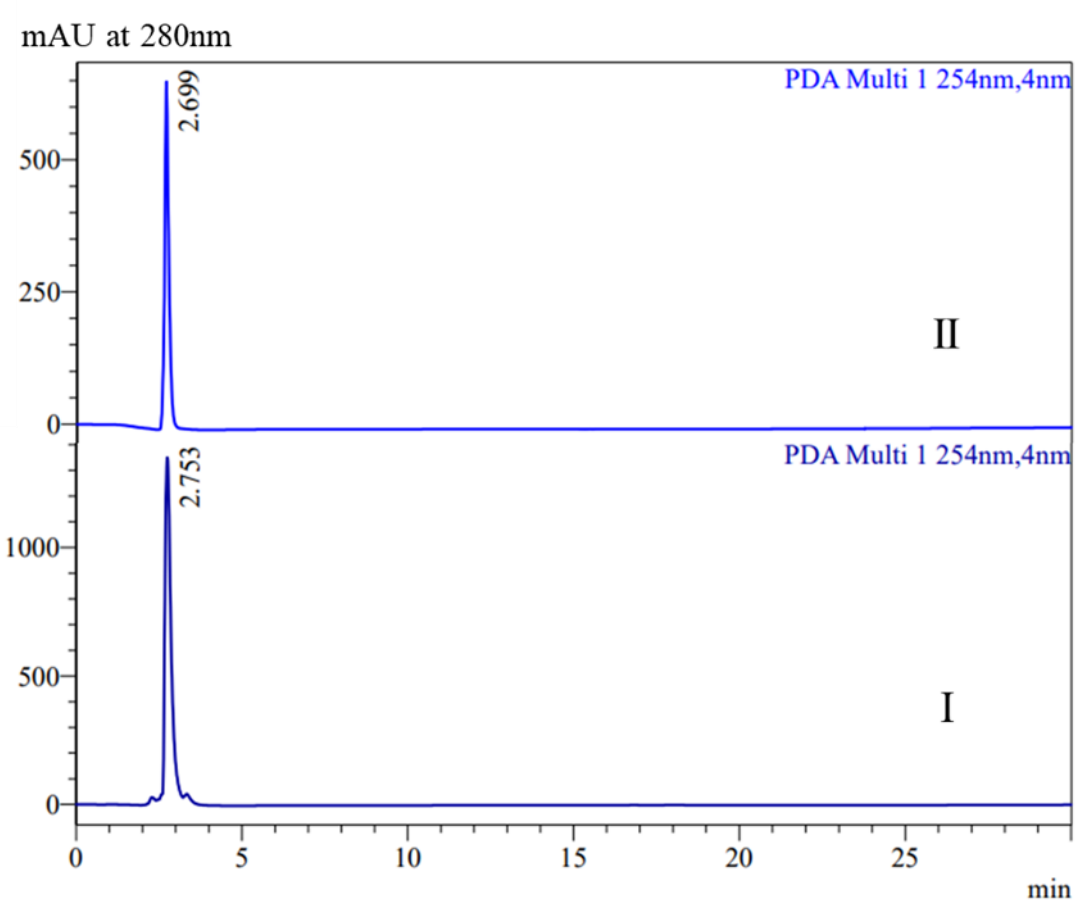

HPLC traces of decarboxylation reaction mixture catalyzed by *RtTDC* (panel I) and panel II represent standard tryptamine